

**DESIGN AND FABRICATION METHOD FOR A MICRONEEDLE  
ELECTRODE WITH FLEXIBLE BACKING FOR BIOSIGNALS  
MONITORING**

by

Jorge Luis Lozano Rodríguez

B.Sc., Instituto Tecnológico y de Estudios Superiores de Monterrey, 2013

A THESIS SUBMITTED IN PARTIAL FULFILLMENT OF  
THE REQUIREMENTS FOR THE DEGREE OF

MASTER OF APPLIED SCIENCE

in

THE FACULTY OF GRADUATE AND POSTDOCTORAL STUDIES  
(Electrical and Computer Engineering)

THE UNIVERSITY OF BRITISH COLUMBIA  
(Vancouver)

December 2020

© Jorge Luis Lozano Rodríguez, 2020

The following individuals certify that they have read, and recommend to the Faculty of Graduate and Postdoctoral Studies for acceptance, the thesis entitled:

DESIGN AND FABRICATION METHOD FOR A MICRONEEDLE ELECTRODE WITH FLEXIBLE BACKING FOR BIOSIGNALS MONITORING

submitted by Jorge Luis Lozano Rodríguez in partial fulfillment of the requirements for

the degree of Master of Applied Science

in Electrical and Computer Engineering

**Examining Committee:**

Boris Stoeber, Professor, Department of Mechanical Engineering, UBC  
Supervisor

Kenichi Takahata, Professor, Department of Electrical and Computer Engineering, UBC  
Supervisory Committee Member

Mu Chiao, Professor, Department of Mechanical Engineering, UBC  
Supervisory Committee Member

## **Abstract**

The conventional wet electrode still poses many inconveniences when recording biosignals, as it requires an electrolytic gel that dries over time, and the skin often needs to be abraded when the electrode is applied to record high-quality signals. Therefore, the wet electrode placement process often needs the assistance of trained personnel. Alternative electrode designs have been investigated to overcome the challenges of the wet electrode but most of them are not able to record small amplitude signals or their fabrication methods are complex and expensive.

This research thesis proposes a novel design and simple fabrication method for a dry microneedle electrode for biosignals monitoring. The electrode can record electroencephalogram and electrocardiogram signals from a human subject without electrolytic gel and it does not require skin preparation or abrasion. When applied to the skin of a human subject with an impact inserter, the electrode has a lower impedance at the skin-electrode interface yielding better signal recording compared to application by hand. The selection of the electrode materials provides microneedles stiff enough to cross the outmost layer of the skin, while the flexible backing of the electrode has been designed to improve the conformation of the electrode to the rounded shape of the body. The proposed fabrication method for the electrode is a simple mold casting process that enables batch production reducing the time spent in the cleanroom and the use of expensive machinery.

## **Lay Summary**

Biosignal monitoring is an essential procedure for medical diagnosis. The wet electrodes currently used in the clinical environment to record biosignals require the use of an electrolytic gel that dries over time and is uncomfortable to wear. The use of this gel makes the wet electrodes unsuitable for long-term applications like wearable devices or sleep disorder monitoring. Different dry electrode designs have been proposed to overcome the challenges of the wet electrodes but most of them require complicated or expensive fabrication methods and they often do not provide a comparable signal quality as the wet electrodes.

This project proposes a new microneedle dry electrode design with a simple fabrication method. We demonstrate that the fabricated electrode can record electroencephalogram and electrocardiogram signals without the use of an electrolytic gel or skin preparation and can achieve a comparable performance to the wet electrode.

## **Preface**

The research presented in this thesis was carried out at the University of British Columbia, Canada in the Stoeber Laboratory in the Department of Electrical and Computer Engineering, under the supervision of Prof. Boris Stoeber. The Clinical Research Ethics Board (CREB) at The University of British Columbia classified all the tests that involve human subjects as quality improvement and did not require ethics board review or approval.

A version of the fabrication methods presented in Chapter 2 and a portion of the results from the Chapter 4 were presented at a conference: J. Lozano and B. Stoeber, "Microspike Array Electrode with Flexible Backing for Biosignal Monitoring," *2019 IEEE SENSORS*, Montreal, QC, Canada, 2019, pp. 1-4, doi: 10.1109/SENSORS43011.2019.8956869. I designed the fabrication method for the device, performed all characterization tests and analyses, and wrote most of the manuscript. Dr. Boris Stoeber was a supervisor author on this project and was involved throughout the project in concept formation and manuscript edition.

## Table of Contents

<b>Abstract.....</b>	<b>iii</b>
<b>Lay Summary .....</b>	<b>iv</b>
<b>Preface.....</b>	<b>v</b>
<b>Table of Contents .....</b>	<b>vi</b>
<b>List of Tables .....</b>	<b>viii</b>
<b>List of Figures.....</b>	<b>ix</b>
<b>List of Symbols .....</b>	<b>xiv</b>
<b>List of Abbreviations .....</b>	<b>xvi</b>
<b>Acknowledgements .....</b>	<b>xvii</b>
<b>Dedication .....</b>	<b>xviii</b>
<b>Chapter 1: Introduction .....</b>	<b>1</b>
1.1    Motivation.....	1
1.2    Biosignals.....	2
1.3    Biosignal monitoring system .....	5
1.4    Electrode-Skin (body) interface .....	6
1.5    Types of electrodes .....	12
1.6    Research Objectives.....	23
<b>Chapter 2: Fabrication process .....</b>	<b>25</b>
2.1    Microneedle structures for master mold fabrication.....	27
2.2    Electrode casting with conductive polymers .....	39
2.3    Metal coating .....	45
<b>Chapter 3: Materials and methods.....</b>	<b>51</b>

3.1	Electrode structure materials.....	51
3.2	Electrode testing methods .....	65
3.3	Biosignal recordings .....	71
<b>Chapter 4: Results.....</b>		<b>78</b>
4.1	Skin insertion tests .....	78
4.2	Impedance tests on a human subject.....	82
4.3	Signal acquisition tests on a human subject.....	84
<b>Chapter 5: Conclusions and future work .....</b>		<b>90</b>
5.1	Conclusions.....	90
5.2	Suggested future work .....	94
5.3	Application of the research findings .....	96
<b>Bibliography .....</b>		<b>98</b>

## List of Tables

Table 1 Optimized exposure energy for different hole arrays of the microneedle matrix test mask. Straight structures for the 20 $\mu\text{m}$ hole diameter arrays were not achieved. ....	30
Table 2 Microneedle dimensions for different transparent features in the photolithography mask. The tip and base diameters are an average of the dimensions measured in 8 needles. For the transparency with 20 m diameter only 4 needles were sufficiently visible to measure the tip dimensions. ....	32
Table 3 Fresnel number for the different circular features of the mask for a 750 $\mu\text{m}$ separation between the mask and the SU-8 photoresist for a 356 nm wavelength. ....	37
Table 4 Calculated force to pierce the SC for the microneedles fabricated on SU-8 with a backside exposure lithography process. ....	38
Table 5 Resistivity measurement comparison with and without plasma etching .....	44
Table 6 Comparison between critical load for buckling of the microneedle structure and the force to pierce the skin for different microneedle shapes. ....	59
Table 7 Materials used in the backing of microneedle electrodes. ....	62
Table 8 Young's moduli comparison for the microneedle's material and the backing material. ....	64
Table 9 RMS Voltage for ECG signals recorded with wet electrode, microneedle electrode inserted with the pressure of the thumb and microneedle electrode inserted with high velocity impact ...	86
Table 10 ECG signal to noise ratio comparison between wet electrode, microneedle electrode inserted with the thumb pressure, microneedle electrode inserted with the high velocity impact inserter. ....	89
Table 11 Materials Young's modulus needed to fabricate microneedles with smaller radii. ....	93

## List of Figures

Figure 1 Normal morphology of the ECG signal.....	3
Figure 2 ECG electrode position for clinical recording.....	3
Figure 3 Normal morphology of EEG waves. ....	4
Figure 4 Tracing guidelines for EEG electrodes placement. (a) Anteroposterior mesial line (b) latero-lateral coronal line, (c) sagittal lateral longitudinal line. Figure 4.1 from © Mecarelli, O., (2019). Clinical Electroencephalography. Rome: Springer, Cham. Page 36. By permission from publisher. [9] .....	5
Figure 5 Biosignal monitoring system.....	6
Figure 6 Skin layers and elements Figure 7.3 from © Standring, S, (201). Gray’s Anatomy.: Springer. Page 141. By permission from publisher. [11].....	7
Figure 7 Simplified electrical model of the electrode-electrolyte interface. ....	9
Figure 8 Simple electrical model of the skin electrode interface electrode Figure 3.24 from © Kaniusas, E., (2019). Biomedical Signals and Sensors III. Vienna: Springer. Page 520. By permission from publisher. [3].....	10
Figure 9 electrical model of the skin Figure 3.2 from © Kaniusas, E., (2019). Biomedical Signals and Sensors III. Vienna: Springer. Page 408. By permission from publisher [3].....	11
Figure 10 Skin electrical model with sweat ducts included. $R_{subcor}$ is the resistance of the tissue under the stratum corneum. $R_{subcor}$ and $C_{subcor}$ are the stratum corneum resistance and capacitance respectively. $R_{elec}$ and $C_{elec}$ are the resistance and capacitance of the electrode respectively. $R_{sweat 1}..... R_{sweat n}$ are the switched bypass resistors representing the sweat ducts.....	12
Figure 11 Skin-electrode electrical model comparison between wet electrode (left) and microneedle electrode (right).....	18
Figure 12 General overview of the fabrication method for the microneedle electrode. ....	26
Figure 13 Microneedle structure created by the back-exposure photolithography process.....	28

Figure 14 Mask design for microneedle structures patterning on SU-8. The vertical axis on the left side of the wafer is the center-to-center distance between each hole in the array (pitch) in $\mu\text{m}$ . The horizontal axis at the top part of the wafer is the diameter of the holes in the array, also in $\mu\text{m}$ . The last row of the mask has the square shaped holes. A dark field mask is generated from this design. ....	29
Figure 15 Resulting microneedle structures with a 500 pitch for the different hole diameters of the mask using the exposure doses from Table 1. ....	31
Figure 16 Comparison of microneedles in arrays with different pitch. (a) Microneedles with a pitch of 300 $\mu\text{m}$ (b) Microneedles with a pitch of 400 $\mu\text{m}$ . ....	34
Figure 17 Fabricated needle arrays with a 1250 $\mu\text{m}$ gap between the mask and the SU-8 resists; (a) microneedle array with a pitch of 300 $\mu\text{m}$ , (b) array with apitch of 400 $\mu\text{m}$ . ....	35
Figure 18 Different diffraction effects when light passes through an aperture depending on the distance between the aperture and the projection screen or surface. Figure 10.54 from © Demtröder, W., (2019). Electrodynamics and Optics. Switzerland: Springer, Cham. Page 315. By permission from publisher [66]. ....	36
Figure 19 Process for microneedle casting with carbon black XCR72 and the biocompatible resin; (a) the cavities are filled with carbon black pressing the powder with a tongue suppresser and a cotton tip. (b) The biocompatible resin is spread over the mold cavities and it is let sit for 4 hours. (c) The excess of the resin is removed with a razor blade and by gently cleaning with a tissue soaked with acetone. (d) Expected result is a cavity filled with a high concentration of carbon black that the resin will paste together. ....	41
Figure 20 Structures cast with carbon black, biocompatible resin and polyurethane. ....	42
Figure 21 Microneedle cast with the conductive polymer using the proposed fabrication method. The red square shows an extreme case of a fabrication flaw where the microneedle tip is made only of biocompatible resin without carbon black. A probe tip is seen on the right of the microneedle. ....	43
Figure 22 (a) Shows the measurement points for the conductivity test. (b) depicts the placement of the microprobe tips for the tip to substrate measurement. ....	43

Figure 23 The silver film deposited by electroplating. The bright surface is the deposited silver film, while the black spots are the surface locations where the silver fell off or no deposition was achieved. ....	47
Figure 24 Light microscopy: (a) side view of two microneedles after silver deposition with electron beam evaporation; the microneedle highlighted with the red rectangle shows pour silver deposition on the microneedle body; (b) top view of the array with some spots not coated with silver at the base of some microneedles. ....	48
Figure 25 (a) Angled view of the microneedle array after silver deposition by sputtering; (b) top view of the array after silver deposition by sputtering; (c) light microscopy top view of the electrode after silver deposition by sputtering; (d) light microscopy side view of one microneedle after silver deposition by sputtering.....	49
Figure 26 Final prototype of the microneedle electrode. ....	50
Figure 27 Test sample dimensions for resistivity measurement of the carbon black polyurethane samples.....	54
Figure 28 Conductivity of the carbon black / hexane / polyurethane mixture as a function of the carbon black concentration in the polyurethane-carbon black mixture. ....	55
Figure 29 Resulting microneedle material with the proposed fabrication method. ....	57
Figure 30 Stress-strain curves for the biocompatible resin (dark green) and the carbon black/biocompatible resin mixture used to fabricate the microneedle structures (light green). The curves show the mean value from 4 different tests performed on different samples and the error bars correspond to the calculated standard error.....	58
Figure 31 (a) Microneedle insertion (b) Simplified model to approximate the critical load for the microneedle structure fabricated with the biocompatible resin and carbon black blend. ....	59
Figure 32 Stress-strain curves comparison for polyurethane, polyurethane with hexane and polyurethane with hexane and carbon black biocompatible mixture.....	61
Figure 33 Diagram of how a material sheet is bent around a body part. ....	62

Figure 34 Model used to approximate the critical load of the microneedle backing.....	63
Figure 35 Porcine skin stretched on the skin holder for insertion test.....	66
Figure 36 Insertion test set-up to apply the electrode by thumb pressure. ....	67
Figure 37 Experimental set-up for microneedle electrode insertion test with impact inserter. ....	68
Figure 38 Electrode placement for electrodes for short term impedance measurement. ....	70
Figure 39 Set up for EEG optically evoked potential test. ....	72
Figure 40 Frequency spectrum of the EEG signal recorded from the occipital area of a subject stimulated with video at 20 FPS. The red circle highlights the peak produced by the stimulus signal. ....	73
Figure 41 Electrodes placement for ECG recording.....	74
Figure 42 Five heart cycles from the cropped signal recorded with a wet electrode.....	75
Figure 43. Fifteen heart cycles superimposed and aligned by the R peak from the signal recorded with a wet electrode. ....	75
Figure 44 Average signal from 15 heart cycles recorded with a wet electrode.....	76
Figure 45 Example of noise extracted from one heart cycle signal recorded with a wet electrode. ....	76
Figure 46 Pig skin samples after insertion test pressing the microneedle electrode with the thumb. The blue dots dyed with the methylene blue are the areas where the microneedles crossed the skin (a) results with the electrode with 1000 $\mu\text{m}$ pitch (b) results with the electrode with 750 $\mu\text{m}$ pitch. ....	78
Figure 47 Pig skin samples after insertion tests using microneedle electrodes with the high velocity impact inserter. The blue dots are the areas where the microneedles crossed the skin (a) results with the electrode with 750 $\mu\text{m}$ pitch (b) results with the electrode with 1000 $\mu\text{m}$ pitch. ....	80

Figure 48 Curvature of the skin created by the 3D printed skin holder and the effect of it on the microneedle insertion test. .... 81

Figure 49 Short-term impedance measurement between a reference (wet) electrode placed on the right earlobe and a wet electrode (green line), a microneedle electrode pressed with the thumb (blue line) or a microneedle electrode inserted with a high velocity inserter (yellow line) placed in the Fp1 position (left side in the forehead). The curves show the mean value from 3 different measurements and the error bars correspond to the calculated standard error. .... 82

Figure 50 Long term impedance measurement at 40 Hz between a reference electrode placed on the right earlobe and a wet electrode (green line), a microneedle electrode pressed against the skin with the thumb (blue line) or a microneedle electrode inserted with a high velocity inserter (yellow line) placed in the Fp1 position (left side in the forehead). The curves show the mean value from 2 different measurements and the error bars correspond to the calculated standard error. .... 83

Figure 51 Signal to noise ratio for the EEG visually evoked potential test for videos with different frame rate. .... 85

Figure 52 ECG signal recording average (15 cycles) recorded with: (a) Microneedle electrode inserted with thumb pressure, (b) microneedle electrode inserted with high velocity inserter, (c) wet electrode. .... 87

## List of Symbols

$A_{\text{Average signal}}$	RMS voltage of ECG average signal.
$A_{MNtip}$	Area of the microneedle tip.
$A_{\text{noise}}$	RMS voltage of ECG average signal noise.
$b$	Radius of a circular aperture.
$C_{cor}$	Capacitance of the stratum corneum.
$C_d$	Capacitance at the electrode-tissue interface.
$C_{elec}$	Capacitance of the electrode.
$E_{hc}$	Half-cell potential.
$E_{R/Cb}$	Young's modulus of the biocompatible resin and Carbon black blend.
$E_{PU/Cb}$	Young's modulus of the Polyurethane and Carbon black blend.
$F_i$	Force applied on a single microneedle to pierce the skin.
$h$	Height.
$I$	Current.
$I_{Bck}$	Area moment of inertia of the electrode backing.
$I_{MN}$	Area moment of inertia of the microneedle structure.
$J$	Imaginary number.
$l$	Length.
$l_{Bck}$	Length of the electrode backing.
$l_{mn}$	Height of the microneedle.
$P_{cr}$	Critical load.
$R$	Resistance.

$R_{cor}$	Resistance of the stratum corneum.
$R_d$	Resistance at the electrode-tissue interface.
$R_{elec}$	Resistance of the electrode.
$R_{gel}$	Resistance of the electrolytic gel.
$R_s$	Resistance of the electrode materials.
$R_{sweat}$	Resistance along a sweat duct.
$U_s$	Voltage across the skin.
$V_{rms}$	Voltage Root mean square.
$w$	Width.
$wt$	Weight.
$z_0$	Separation between the mask and the photoresist.
$Z_s$	Impedance at the skin-electrode interface.

**List of Greek symbols**

$\lambda$	Wavelength.
$\rho$	Resistivity.
$\sigma$	Conductivity.
$\omega$	Angular frequency.

## List of Abbreviations

<b>3D</b>	Three dimensional.
<b>BCI</b>	Brain computer interface.
<b>CA</b>	Canada.
<b>CAD</b>	Canadian Dollars.
<b>CB</b>	Carbon black.
<b>CVD</b>	Chemical vapor deposition.
<b>ECG</b>	Electrocardiogram.
<b>EEG</b>	Electroencephalogram.
<b>EMG</b>	Electromyogram.
<b>FPS</b>	Frames per second
<b>HMDS</b>	Hexamethyldisilazane.
<b>LDW</b>	Laser direct writing.
<b>LPCVD</b>	Low pressure chemical vapor deposition.
<b>MN</b>	Microneedle.
<b>PDMS</b>	Polydimethylsiloxane.
<b>RMS</b>	Root mean square.
<b>RPM</b>	Revolutions per minute.
<b>SC</b>	Stratum Corneum.
<b>SNR</b>	Signal to noise ratio.
<b>UBC</b>	University of British Columbia.
<b>USA</b>	United States of America.

## **Acknowledgements**

I express my infinite gratitude to Dr. Boris Stoeber, for let me work in his lab, for his incredible commitment to this project, and for the time he invested to guide me and inspire me. I want to thank the faculty involved in Sensory Information Technologies and Implementation in Sleep Disorder Monitoring, in particular to Dr. Mu Chiao for taking the time to be part of my committee.

Special thanks are owed to Pranav Shrestha for helping me and instructing me with the skin insertion test, Carlos Gerardo for helping me with my first attempts in the cleanroom, Nabil Shalabi for his advice with the Omnicoat Photoresist, and Tan Nguyen for taking the time to help me to perform the impedance tests. I would like to thank all the Stoeber Lab members, Martina, Sam, Hamed, Sajana, Nicholas, Bryan, Crystal, Robin, Hatef, Farzad, and Nagesh for their positive feedback, advice, and encouragement.

I would like to extend my gratitude to Said Soltanian, Mario Beaudoin, and Kostis Michelakis for their support and training for the CEFT lab and Cleanroom equipment and Dr. John Madden for allowing me to use his equipment and lab facilities.

Special thanks are owed to my colleagues and friends at the Microfabrication, Nanotechnologies and MEMS Laboratories and the ECEGSA at UBC. Finally, I will like to thank my parents and siblings for their support and encouragement during this time.

This work was funded by the Natural Sciences and Engineering Research Council (NSERC) of Canada through the Strategic Partnership Grants project STPGP 493908 “Research in Sensory Information Technologies and Implementation in Sleep Disorder Monitoring.”

We would like to acknowledge CMC Microsystems for the provision of products and services that facilitated this research.

## **Dedication**

To my family and friends.

## **Chapter 1: Introduction**

This chapter contextualizes the research presented in this thesis, provides a brief explanation of the theory of biosignal recording and electrodes, describes the problem to solve, discusses previous electrode designs and fabrication methods presented by other researchers, and list the objectives for the thesis.

### **1.1 Motivation**

Biosignal recording and monitoring is an essential process for general medical diagnosis, as the continuous monitoring of electrical signals from different organs allows to have a better understanding of the body's wellbeing. Furthermore, in recent years the fast-growing market and the rapidly developing technology for wearable and smart devices has extended the analysis of biosignals from remote patient monitoring to personal use. Continuous and remote patient monitoring is of special interest for sleep disorders, cardiovascular diseases, diabetes and cancer.

The advancements of electronic technology allow us to record signals with high accuracy and to store long term measurements. However, a remaining challenge of the signal acquisition system for electric biosignals from the body is still the interface of these electronic systems and the body, where the electrode performance is a pivotal element. The impedance reduction without skin abrasion, high-quality signal acquisition and long-term stability to ensure continuous monitoring without signal degradation are some of the main limitations of the current devices.

Sleep disorder monitoring is one of the applications that requires comfort and long-term measurement performance of the biosignal electrodes. The general objective of this thesis is to develop an EEG electrode for sleep disorder monitoring as a contribution to a larger research project that aims to develop a better monitoring and diagnostic system for sleep disorders.

## **1.2 Biosignals**

Biosignals are signals that describe a physiological phenomenon [1]. These biosignals include acoustic, electrical, optical, thermal, magnetic and chemical signals. Electrical biosignals or bioelectrical signals are generated from the conduction of electric current, through body tissues, resulting from collections of electrogenic cells (cells that can produce electrical activity in the body) [2]; this includes electroencephalogram (EEG), electrocardiogram (ECG) and electromyogram (EMG) signals. EEG results from the electrical activity of a collective of neurons, ECG is the result of action potential of cardiac muscle cells and EMG reflects the potential from skeletal muscle.

### **1.2.1 Electrocardiogram**

An electrocardiogram is a visual representation of the recorded electrical activity of the heart over time, which is closely related to the mechanical activity of the heart.[3] The electrocardiogram is generated when the cardiac electrical impulse passes through the heart muscles. Electrical potential also spreads into the adjacent tissue and a portion spreads all the way to the surface of the body where the electrical potential can be recorded if electrodes are placed on limbs or body parts that are around the heart [4].

The normal morphology of the ECG wave is composed of a P wave, a QRS complex (composed by Q, R and S waves) and a T wave. This typical morphology is shown in Figure 1.

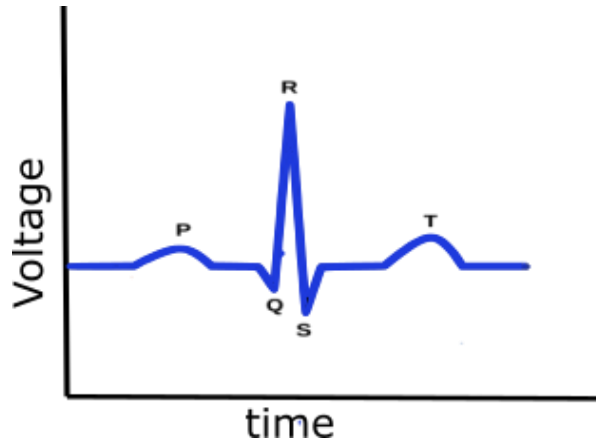


**Figure 1 Normal morphology of the ECG signal.**

For clinical applications, the usual way to record the potentials generated by the heart is with 12 standard ECG leads, often called derivations. Each of these derivations provides information of the electrical activity of different areas of the heart during the cardiac cycle. The 12 ECG derivations can be obtained with only six electrodes placed on the chest and 4 on the limbs. Figure 2 shows the position for all the electrodes, where the right leg functions solely as an electrical ground. [5]

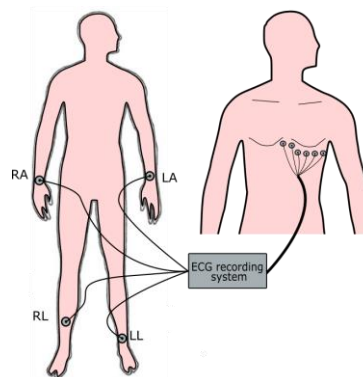


**Figure 2 ECG electrode position for clinical recording.**

### 1.2.2 Electroencephalogram (EEG)

There are approximately 100 billion neurons in the brain, and each neuron has approximately 10,000 connections with other neurons [6]. Neurons generate ionic currents flowing through the brain tissue that produce local field potentials [7]. The recorded electrical activity of these local field potentials is defined as electroencephalogram, an electrical signal with a morphology that has a wide diversity and depends among other things on the mental state of the subject. The electroencephalogram is recorded from the scalp by placing at least 3 electrodes and up to 128 electrodes on the scalp with a reference electrode on one of the earlobes. The signal has an amplitude ranging from a few microvolts to approximately 100 microvolts, and a frequency content ranging from 0.5 to 30-40 Hz [8]. EEG rhythms are conventionally classified into 4 frequency bands shown in Figure 3.

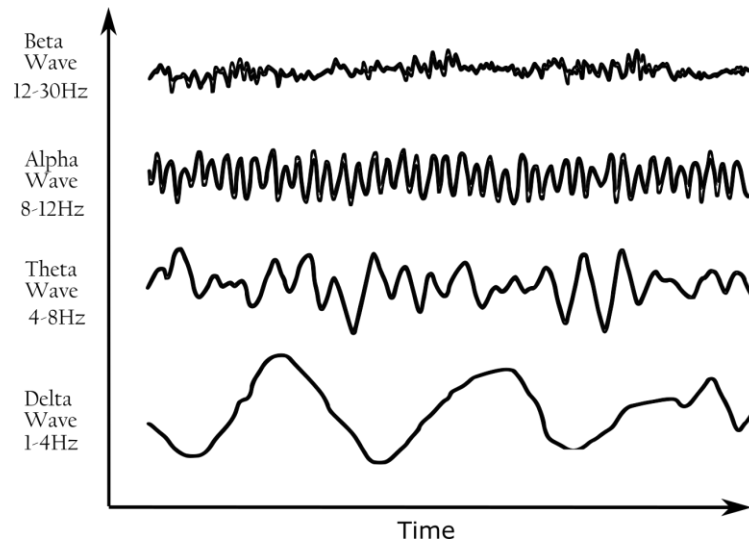


**Figure 3 Normal morphology of EEG waves.**

Electroencephalogram signals are most commonly recorded using electrodes placed on specific positions on the scalp, according to the standardized 10-20 system presented in Paris 1949 by the committee of International Federation of Societies for EEG and Clinical Neurophysiology.

The locations are chosen to ensure that the electrodes placement is as proportional as possible to the shape of the skull. The electrode distribution covers every part of the skull with an identifiable electrode location and identification of electrode positions underlying specific brain areas. The 10-20 position of the electrodes are achieved by tracing imaginary lines shown in Figure 4 starting from specific anatomical landmarks and measuring the skull dimensions along these imaginary lines[9]. The separation between electrodes is 20 percent the distance of this measurement, and the first and last electrodes are separated from the end and the beginning of the imaginary line by 10 percent of the measured distance.

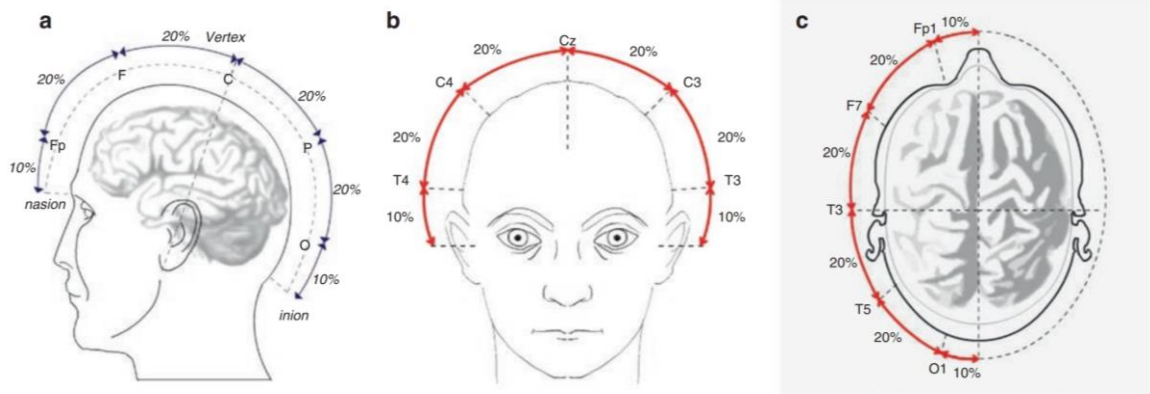


**Figure 4 Tracing guidelines for EEG electrodes placement. (a) Anteroposterior mesial line (b) latero-lateral coronal line, (c) sagittal lateral longitudinal line. Figure 4.1 from © Mecarelli, O., (2019). Clinical Electroencephalography. Rome: Springer, Cham. Page 36. By permission from publisher. [9]**

### 1.3 Biosignals monitoring system

Biosignal monitoring systems are composed of the following main elements: electrode, amplification, analog-to-digital conversion, and processing and visualization shown in Figure 5. Electronic systems today allow to record signals with high resolution and store long term measurements, but the main limitation to record quality biosignals is the interface of the electrode and the body.

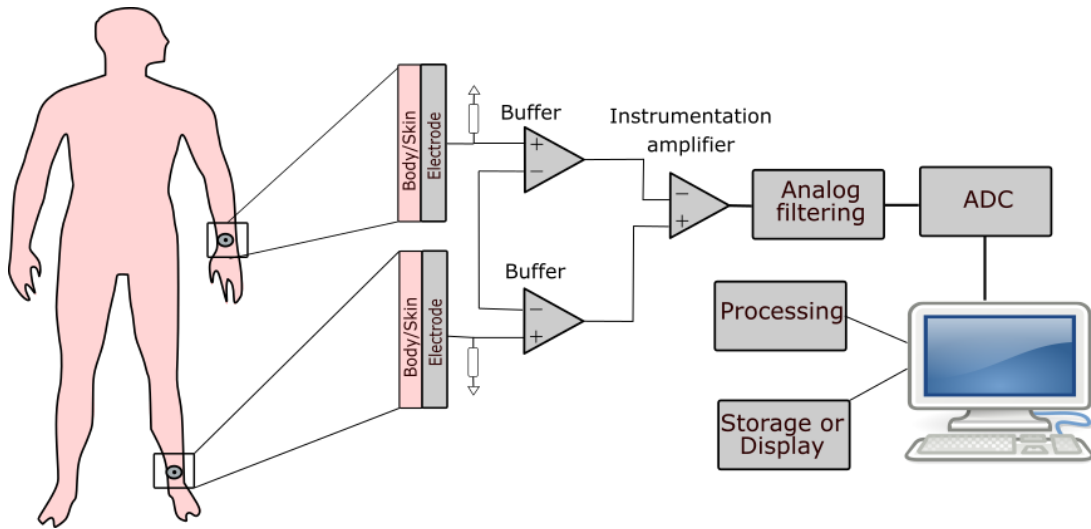


**Figure 5 Biosignal monitoring system.**

## **1.4 Electrode-Skin (body) interface**

As previously mentioned, the electrical signals generated by the brain, heart or muscles propagate through the surrounding tissue and can be recorded externally by placing electrodes on the skin. External electrodes, placed on the skin, are always preferred over invasive or implantable electrodes to avoid infection risks during implantation. At low frequencies, the skin impedance is very high compared with the polarization impedance of the wet electrodes and deeper tissue impedance [10]. Consequently, understanding the structure and electrical properties of the skin is of special interest.

### **1.4.1 Skin anatomy**

The skin is the largest organ on the human body, covering the entire external surface of the body. Its thickness varies from 1.5 mm to 5 mm depending on the location. The main function of the skin is to act as a barrier against microbial organisms and to protect against mechanical, osmotic (ions concentration inside the cells), thermal, chemical and ultraviolet damage. Other

important functions of the skin are temperature control, immune system surveillance and response initiation [11].

The general structure is divided in two main layers, the epidermis and the dermis as shown in Figure 6. The epidermis consists of 5 layers: the innermost basal layer (stratum basale), is succeeded by the spinous cell layer (stratum spinosum), the granular layer (stratum granulosum), the clear layer (stratum lucidum) and the cornified layer (stratum corneum). The three deepest layers of the epidermis are metabolically active compartments through which cells pass, change their morphology and undergo differentiation. The more superficial layer undergoes terminal cornification, a process that leads to skin cell's death and forms the mechanically tough stratum corneum.

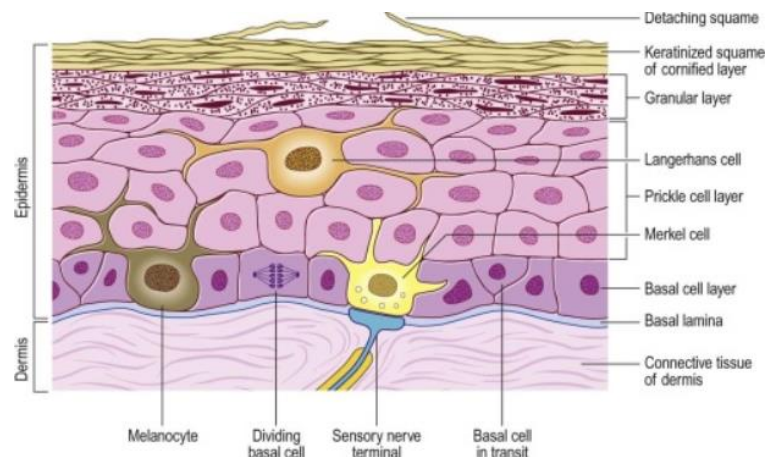


**Figure 6 Skin layers and elements Figure 7.3 from © Standring, S, (201). Gray's Anatomy.: Springer. Page 141. By permission from publisher. [11]**

Beneath the epidermis is the dermis, an irregular dense connective tissue composed of a collagenous and elastic network. This layer also contains nerves, blood vessels and lymphatic and epidermal appendages. The dermis can be divided into two zones the superficial papillary layer and the deeper reticular layer [11].

### 1.4.2 Electrical properties of the skin

From the electrical point of view, it is impossible to regard biological tissue as a homogenous material. In general, tissue is an anisotropic conductive medium because of the orientation of cells, organs and macromembranes that cover the organs (i.e. peritoneum, pleura, meninges, etc). Such anisotropy is present at low frequencies due to the membranes. The higher the concentration of cells in biological tissue the lower the tissue's low-frequency conductivity. Tooth, cartilage, the skin stratum corneum (SC), and connective tissue may contain many inorganic materials with low conductivity, but their electrical properties are very dependent on body liquid perfusion. Tabulation of tissue conductivity is challenging particularly for living tissue as the exact value depends on frequency, temperature, water content, blood perfusion and immunological status of the body, and even compression of the tissue can modify the electrical properties.[10]

Many electrical models have been proposed to describe in a simple manner the electrical properties of the different layers of the skin. Living tissue in general is often modeled as an electrolytic medium with a capacitive and resistive component and with a non-linear and current density dependent behavior [12]. Under low potentials and current conditions, the electrode-skin interface can be represented by linear models, such as the circuit shown in Figure 7 [13]. This model is often used to represent the electrode-tissue interface as living tissue is often considered to behave as a solid electrolyte. In this circuit  $R_d$  and  $C_d$  are the components associated with the electrode electrolyte interface. The capacitor  $C_d$  models the interaction between the electrode and skin, where one plate of the capacitor is the electrode, the stratum corneum is the insulator layer and the conductive tissue under the SC is the second plate of the capacitor. This model considers that a current can leak through the stratum corneum, so  $R_d$  models the resistance of this layer that

will vary depending on how moist it is.  $R_s$  is the series resistance associated to the electrode material and  $E_{hc}$  represents the half-cell potential of the electrode created by the charge distribution at the electrode surface on the interface [14]. Such potential is defined mainly by the material of the electrode and is the main cause of motion artifacts; when you move the electrode on the skin the distribution of the charges is disturbed.

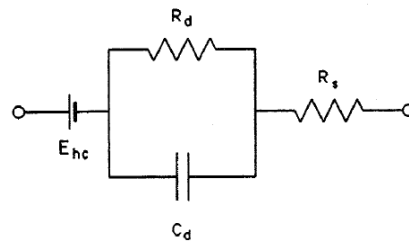


**Figure 7 Simplified electrical model of the electrode-electrolyte interface.**

A modified version of this model is commonly used to represent the skin-electrode interface, as shown in Figure 8 and have been analyzed by many authors [8][15][16][12]

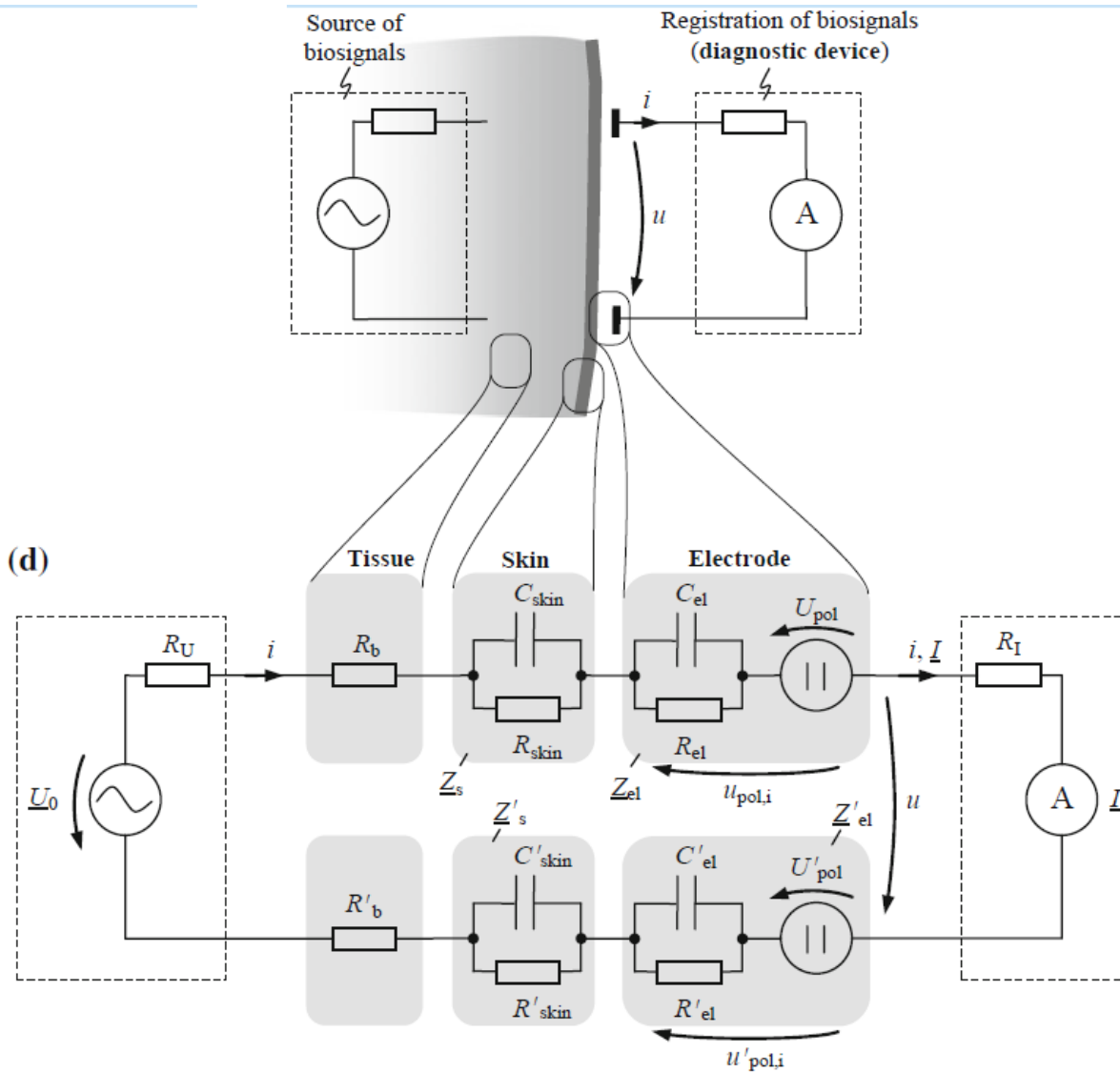


**Figure 8 Simple electrical model of the skin electrode interface electrode Figure 3.24 from © Kaniusas, E., (2019). Biomedical Signals and Sensors III. Vienna: Springer. Page 520. By permission from publisher. [3]**

The deeper layers of the skin are assumed to show electrolytic behavior as these layers consist of living cells, while the outmost layer of the skin, the stratum corneum with its total thickness of 10  $\mu\text{m}$  to 40  $\mu\text{m}$ , consists of dead cells and is therefore considered a poor conductor material when is dry [3]. When the stratum corneum is wet it still possesses a resistance in the order of tenths of kilohms, but even with this impedance reduction, abrasion may be required to

reduce this impedance more significantly before attaching the electrode. Figure 9 [3], shows the simple electrical model of the skin layers.

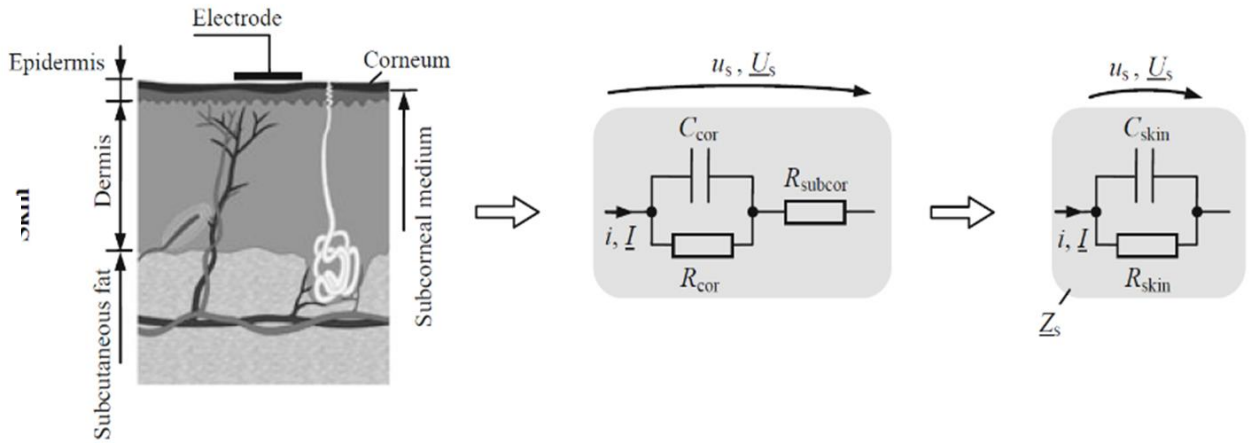


**Figure 9 electrical model of the skin Figure 3.2 from © Kaniusas, E., (2019). Biomedical Signals and Sensors III. Vienna: Springer. Page 408. By permission from publisher [3]**

The total impedance at the skin-electrode interface

$$Z_S = \frac{U_s}{I} = R_{subcor} + \frac{R_{cor}}{1+j\cdot\omega\cdot C_{cor}\cdot R_{cor}} + \frac{R_{elec}}{1+j\cdot\omega\cdot C_{elec}\cdot R_{elec}} \quad (1)$$

depends on the resistance of the tissue under the stratum corneum,  $R_{subcor}$ , the stratum corneum resistance and capacitance  $R_{cor}$  and  $C_{cor}$ , respectively and the resistance and capacitance of the electrode  $R_{elec}$  and  $C_{elec}$  respectively. One variation often considered is that the sweat ducts in the skin may act as a bypass resistor to the resistive and capacitive elements of the stratum corneum. The ducts are modeled as switched resistors in parallel to the resistance and capacitance of the SC as shown in Figure 10. The switch closed state is when sweating happens, the resistance along the sweat duct  $R_{sweat\ x}$  is very low compared to the stratum corneum resistance as the sweat has a high concentration of NaCl ions[17].

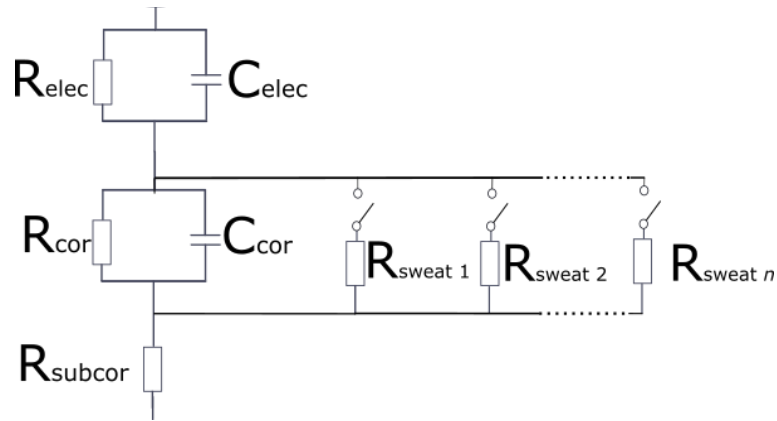


**Figure 10 Skin electrical model with sweat ducts included.  $R_{subcor}$  is the resistance of the tissue under the stratum corneum.  $R_{subcor}$  and  $C_{subcor}$  are the stratum corneum resistance and capacitance respectively.  $R_{elec}$  and  $C_{elec}$  are the resistance and capacitance of the electrode respectively.  $R_{sweat 1}, \dots, R_{sweat n}$  are the switched bypass resistors representing the sweat ducts.**

These models are a simple way to describe the electrode-skin interface and the transfer of electrical signals from the source organs to the skin. More realistic models of tissue conductivity taking in account the anisotropic tissue properties or the volume conductivity of the skull and tissues are challenging, as electrical properties of dead tissue are very different from living tissue. Similarly, testing in humans is not a reliable method to obtain realistic tissue electrical models as all the variables (hydration, temperature, cells density, tissue thickness etc.) are not controllable and vary significantly between individuals.

## 1.5 Types of electrodes

Electrodes are devices that transform ionic currents present in electrolytes in biological solutions or body tissues, product of biochemical activity of nerves and muscles, into electrical currents. The electrodes' function is to transfer charge between ionic solutions and metallic conductors [14]. The electrode is the first element in the signal acquisition chain and its properties determine the noise and amplitude quality of the acquired signal. Therefore, the electrode's design,

material selection and fabrication method are crucial to ensure the whole biosignal recording system performance.

In the literature the electrodes are classified in three main types, wet electrodes, contact electrodes and capacitive or non-contact electrodes.

### **1.5.1 Wet electrodes**

Conventionally in a clinical environment, wet electrodes are used to record EEG signals from the scalp. This electrode uses a metal cup, normally gold or silver plated, with an electrolyte paste that reduces the impedance of the skin electrode-interface which facilitates biosignal recordings.

The electrolytic paste applied between the electrode and the skin, penetrates the stratum corneum moistening it and creating an electrolytic path that allows charge conduction between the inner layers of the skin and the electrode. This reduces significantly the impedance of the electrode-skin interface.

This method often requires a laborious preparation procedure including skin abrasion to achieve the low impedance required to record quality biosignals and reduce motion artifact [18]. Moreover, it has been reported that for measurements that last more than one hour, the electrolyte gel tends to dry, increasing the impedance on the skin-electrode interface. Wang et al. [19] reported that the impedance can increase as soon as an hour after the electrode was applied. The change of the gel characteristics makes this type of electrodes unsuitable for long-term measurements as this may degrade the signal quality [10].

### **1.5.2 Wet electrodes variants**

To overcome the problem of the impedance variability on the skin-electrode interface produced by the gel drying during long-term measurements, wet electrode variants have been proposed. These electrodes aim to keep the skin-electrode impedance low, continuously supplying electrolytic solution to the skin by keeping it moist.

Alba et al. [20] propose a hydrogel swelled with NaCl solution embedded on a metal cup electrode, the hydrogel will act as a sponge that will keep the skin moist with electrolyte solution during a certain period of time. Electrodes with reservoirs for the electrolytic solution and long tips that dispense the solution have been also proposed [21][22]. These electrodes can potentially record signals on hairy parts of the scalp as the long tips get in between the hair and the dispensed electrolytic solution will keep the impedance at the skin low. These types of electrodes are quite bulky and pressing their stiff tips against the scalp or the body makes them uncomfortable to wear. X. Xing et al. [23] proposed flexible seepage tips to increase comfortability. However, these electrodes also have complex structures that are difficult to fabricate, and they still require preparation as you need to load the electrolytic solution into the reservoirs of all the electrodes.

### **1.5.3 Dry Electrodes**

Different dry electrode designs have been proposed in order to replace the wet electrodes with a simpler design that can allow easy attachment by the patient without the assistance from a technician, while providing the required signal quality for clinical evaluation of EEG signals [24].

### 1.5.3.1 Capacitive electrodes

Capacitive or non-contact electrodes can record signals from the body without direct contact with the skin. These devices use the capacitive coupling created between the skin and electrode plate to detect displacement currents inside the body. Capacitive recordings require time-varying behavior of the electrical bio signals, faster variation causes a lower capacitive impedance, leading to a stronger current displacement registered by the capacitive electrodes [3]. Capacitive electrodes are commonly used on wearable devices and one of the main advantages of these electrodes is that they can potentially record signals even over clothing up to a 3 mm separation distance between the skin surface and the electrode plate.

Biosignal sensing with capacitive electrodes has been studied for many years. One of the first approaches [25] was an aluminum plate with an aluminum oxide layer as a dielectric with a resistance greater than 4 G $\Omega$  at DC. A field effect transistor source follower circuit was used to match the high output impedance of the plate. Many different approaches have been proposed in order to improve the performance of these electrodes.

More recent designs include coin sized capacitive electrodes with onsite amplifiers, bias and common noise rejection circuits [26] [27], and electrodes with ceramic dielectric [28]. Another design uses clothing as an insulator and a conductive fabric as the capacitor plate [29].

These type of electrodes are considered active because they need ultrahigh input impedance amplifiers that need to be placed on the electrode itself to avoid powerline interference [30]. The need of an onsite shielded circuit to avoid parasitic capacitances, make these electrodes more expensive and bulkier as you need more cable lines to power the amplifier as well as difficult to fabricate as the circuitry is embedded in the electrode body.

### 1.5.3.2 Contact electrodes

Dry contact electrodes rely on their good electric contact with the skin and high input impedance of their amplifiers. Many of these have a design focused on improving comfortability, attachment and contact of the electrodes on the body specially on hairy areas. Flexible devices that can deform to adapt to the skin shape to improve contact with the skin and reduce motion artefacts have been developed: a simple approach presented by [31], that proposes a flexible PDMS piece coated with gold as an electrode, [32] proposes a flexible parylene based electrode with silver/silver chloride micropads that can bend, and [33] uses a foam electrode that can bend to the shape of the body and even penetrate into the space between the hairs. The main problem with contact electrodes is that even if they improve the contact with the skin, they still cannot reliably record small amplitude signals present in EEG as they do not solve the problem of the high impedance of the stratum corneum.

To overcome the problem of the electrode contact on hairy areas of the body, especially during EEG measurements, electrodes with metallic millimeter size tips have been proposed [34][35]. The hair gets in between the tips which then have good contact with the skin. An interesting design proposed by [36] has spring loaded tips that will contact the scalp. This electrode aims to ensure that the tips are always pressed against the skin. One of the main problems with this type of electrodes is that they are uncomfortable to wear specially when EEG signals are recorded during sleep. Other authors [37] [38] propose flexible tips that will get in between the hairs to increase the comfortability and contact area of the electrode. [34] demonstrated that their electrode has a similar impedance as the wet electrode without skin preparation, but their electrode still has a higher impedance than the wet electrode with skin preparation. [35] does not provide a fair comparison of the impedance of their electrodes with a wet electrode; while they reported a lower

impedance for their device they seem to have used multiple electrodes embedded in a headband on the forehead to measure the impedance and compare their result against a single wet electrode in Fp1 position. The chosen electrode materials of this last approach need a high contact area to achieve a lower or similar impedance to the wet electrode making it very bulky.

Another interesting similar approach is an electrode made of silver coated bristles [39], the authors reported good signal acquisition when the electrodes were well pressed against the scalp. The main problem with this design seems to be comfortability as many of the test subjects reported to have an uncomfortable feeling or prickling sensation while wearing the electrode for only one hour. Also, the authors reported that the silver coating is prone to peeling off over time.

### **1.5.3.3 Microneedle electrodes**

The stratum corneum is the layer of the skin with the highest impedance component, thus electrodes that can bypass or penetrate through this layer are able to record biosignals with a similar performance to wet electrode. Microneedles or micro spikes are structures with micrometer dimensions that are able to cross the stratum corneum without reaching the pain receptors in the skin [40], and have been widely studied as a potential solution for transdermal drug delivery [41] [42]. Microneedle electrodes for biosignal acquisition have been proposed as an alternative to the wet electrode and many different designs with different materials have been studied. Figure 11 shows a comparison of electrical models for the skin-electrode interface between the microneedle (MN) electrode and the wet electrode as described by [15][43].

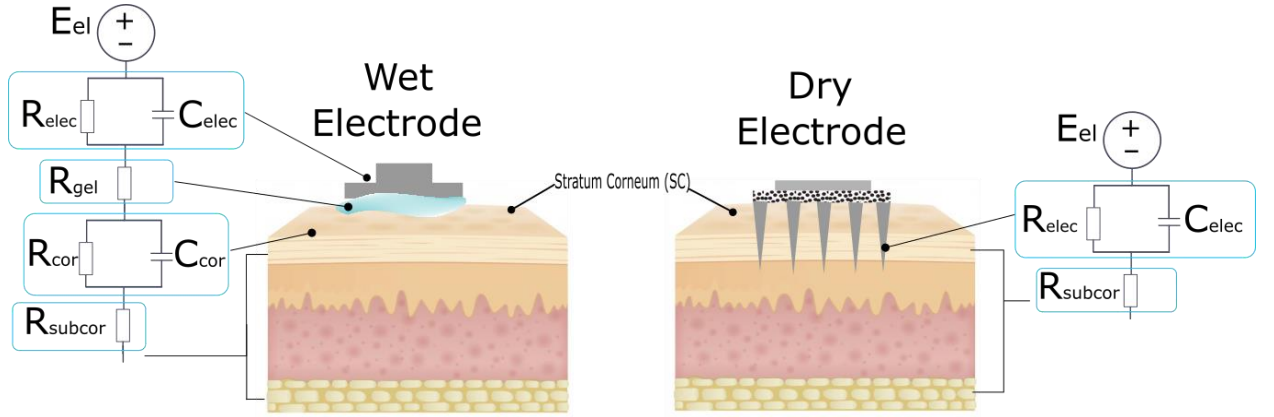


**Figure 11 Skin-electrode electrical model comparison between wet electrode (left) and microneedle electrode (right).**

The impedance for both, the wet electrode and the microneedle electrode, can be calculated following Equation 1 discussed in section 1.4.2. The electrical model of the skin-electrode interface for the wet electrode yields the impedance

$$Z_{wet\ electrode} = \frac{R_{subcor}}{1+j\cdot\omega\cdot C_{subcor}\cdot R_{subcor}} + \frac{R_{cor}}{1+j\cdot\omega\cdot C_{cor}\cdot R_{cor}} + R_{gel} + \frac{R_{elec}}{1+j\cdot\omega\cdot C_{elec}\cdot R_{elec}} \quad , \quad (2)$$

and this impedance reduces to the impedance for the microneedle electrode

$$Z_{microneedle\ electrode} = \frac{R_{subcor}}{1+j\cdot\omega\cdot C_{subcor}\cdot R_{subcor}} + \frac{R_{elec}}{1+j\cdot\omega\cdot C_{elec}\cdot R_{elec}} \quad (3)$$

according to the corresponding model in Figure 10.

The use of the electrolytic gel with the wet electrode induces moisture in the stratum corneum reducing the impedance of this layer by reducing  $R_{cor}$  and  $C_{cor}$  in Equation 2. The model presented here considers that the moist stratum corneum still has a small impedance component

and that the gel may also add some impedance to skin-electrode interface, represented as  $R_{\text{gel}}$  in equation 2.

As opposed to the wet electrode, a microneedle electrode does not use gel so this impedance component is not present at the skin-electrode interface. Similarly, the microneedles are physically crossing the stratum corneum and reaching the sub corneum tissue thus the impedance components of the stratum corneum  $R_{\text{cor}}$  and  $C_{\text{cor}}$  are not present in the electrical model.

The most used material for microneedle electrodes is silicon, because of the well-known micromachining techniques for this material. These electrodes are normally made from a silicon wafer using under etching of a mask, and they require a metal coating [44][45] [46] [47] [48] [49]. The connection between the backside of the electrode chip and the front side with the microneedles is often achieved with a through-silicon via using an etched hole.

Most of these silicon-based designs include electrodes with very sharp and robust needles that allow piercing through the stratum corneum. However, the entire electrode is normally made out of silicon and needs to be coated with a metal after patterning the microstructure for a sufficiently low impedance. The backing of these silicon electrodes is also not flexible and rather brittle, preventing the electrode from conforming to the round shapes of the body. This lack of flexibility can lead to an unstable attachment of the electrode on the body, making the signals prone to motion artifacts [50].

With the recent development of additive manufacturing technologies and the increase in resolution for prototype fabrication, an electrode using 3D printing techniques and coated with gold has been proposed [51]. For this electrode as for many other fields, 3D printing is a good option for prototyping but it is also a time consuming process not suitable for high volume device fabrication. Other miscellaneous approaches include an electrode with needles made of carbon

nanotubes [52], to study the performance of this material at the electrode skin interface, but carbon nanotube fabrication still expensive and time consuming. A microneedle electrode fabricated by magnetization [53], has been proposed; this method has the potential to produce microneedle structures in one step, although the microneedle dimensions are quite difficult to control. A different method for microneedle fabrication is laser micromachining [54], unfortunately this method is very time consuming and not suitable for batch production.

To overcome the problem of the flexibility of the backing of the electrode, [55] proposes an electrode made of PDMS (elastomer) coated with silver, but they found that even with the silver coating the needles made of PDMS will bend when the electrode was pressed against the skin. Additionally, the silver coating will easily peel off so a nanoporous parylene coating is needed to cover the silver layer. The authors only demonstrated the feasibility of the fabrication method to produce a microneedle electrode but they did not perform any kind of tests to evaluate the impedance of the device at the skin-electrode interface nor did they perform biosignal recording tests. The same group proposed a microneedle electrode made of SU-8 [56]. The authors demonstrated that this device can achieve a similar impedance to the wet electrode and was able to record biosignals, but as the whole device is made of SU-8, the backing of the electrode is not flexible.

A design with a flexible backing that conforms to the curved area of the skin and stiff silicon needles plated with gold was developed by [57], this design will allow to cross the stratum corneum and improve the attachment of the electrode to the body. However, the fabrication process of such an electrode requires several steps in a microfabrication cleanroom including the growth of an SiO<sub>2</sub> layer, photolithography processes, deep reactive ion etching, parylene layer deposition, an aluminum photoresist liftoff process and gold and platinum deposition and includes the

extensive use of expensive machinery such as thermal oxidation furnace, photolithography equipment, reactive ion etcher, sputtering and parylene deposition systems.

The same group also presented a simpler fabrication approach for a similar electrode design [58]. For this approach, the microneedles are made from silicon by using a diamond dicer but the fabrication process is still very complex requiring multiple wet etching and deposition processes.

An interesting approach to biosignal recording and monitoring has been demonstrated with tattoo like electrodes [59] that not only can bend to the round shape of the body but they can stretch and completely deform as the skin does when attached. Ren et al. [60] combined the concept of microneedle electrodes and flexible electronics printed on very thin and flexible substrate that can deform such as the skin does. This type of electrodes has a lot of potential, but the fabrication process based on laser-direct writing (LDW) and magneto-rheological drawing lithography is complex and difficult to scale to mass production.

One of the main challenges of microneedle electrodes is reaching the skin on hairy areas of the body as the hair diameter is about  $100\mu\text{m}$ , so if the needles are not long enough, they will not be able to reach the skin on hairy areas. Some authors have focused on solving this problem by fabricating pillars of millimetric size with microneedles on the tip of these pillars [61][62]. With these electrodes the hair will be placed in between the pillars letting the microneedles on their tips penetrate the skin. The fabrication process for these electrodes is based on casting polymer using elastomer molds that could be suitable for batch production at a low cost, nevertheless the electrode microneedles and backing is still made of the same material, not achieving the desired flexibility of the backing and the stiffness of the needles.

After reviewing the state of the art of dry electrodes and other alternatives to wet electrodes, the following conclusion can be drawn:

- Contact electrodes can record ECG signals and evoked EEG signals. Some of the proposed designs have a simple and inexpensive fabrication process. The main problem with contact electrodes is that they do not solve the problem of the high impedance of the stratum corneum at the skin-electrode interface. This drawback makes them not suitable to record the small-amplitude signals present in spontaneous EEG recordings needed in clinical assessments.
- Capacitive electrodes do not use electrolytic gel, such electrodes can record only high amplitude biosignals, and they could potentially record signals through layers of clothes. However, as the recording method of these electrodes is through polarization instead of electrolytic conduction, these types of electrodes are very prone to have noise and motion artifacts. Furthermore, these electrodes need an active high impedance input amplifier as close as possible to the electrode plates, making them very bulky.
- Microneedle electrodes seem to be the best alternative to solve the challenges of the wet electrodes as they can achieve a stable low impedance in the skin-electrode interface without the use of an electrolytic gel. This low impedance makes them suitable to record small-amplitude spontaneous signals. The design of the electrode can be optimized to reduce its size and have a flexible backing that will improve the attachment of the electrode to the body, reducing the presence of noise or motion artifact.

- Most of the proposed microneedle electrodes with the desired flexible backing and stiff needles have complex fabrication methods and often require expensive machinery that limits the use of these electrodes in clinical environments.

Therefore, this thesis focuses on the design of an electrode with a simple fabrication method that will allow having a stiff material for the microneedle structures and a flexible backing while minimizing the use of expensive manufacturing equipment.

## **1.6 Research Objectives**

1.- Design of a microneedle electrode with the following requirements:

- The electrode should be able to record EEG signals without any significant impedance variation during at least 8 hours as this is the time required to perform a sleep disorder evaluation.
- The electrode design should allow conforming to the round shape of the body to decrease the chances of presenting motion artefacts.
- The electrode should be built with materials that will not produce an allergic reaction in the skin.

2.- Propose a simple fabrication method for a microneedle electrode with the following requirements:

- The fabrication method should be easy to implement and involve inexpensive processes.
- The fabrication process should allow batch fabrication of the device.
- The fabrication method should allow to produce an electrode with a stiff material for the microneedle structures and a flexible material for the backing.

3.- Characterize the performance of the microneedle electrode and compare its performance with a wet electrode.

### **1.6.1 Thesis outline**

Chapter 1 provides an introduction, including a brief explanation of the biosignal recording process, and describes the current challenges with wet and dry electrodes. Chapter 2 describes the proposed fabrication method for the microneedle electrode. Chapter 3 explains the materials selection and mechanical properties characterization of the microneedle electrode as well as the microneedle testing methods. Chapter 4 describes the experimental results. Chapter 5 provides the conclusions and outlines potential future work.

## Chapter 2: Fabrication process

This chapter describes the proposed fabrication method and processes followed to produce a microneedle electrode. First, an overview of the complete fabrication method is presented, followed by a detailed explanation of each step.

The selection of the electrode materials is determined by two main factors. The first one is the electrode performance, for which the desired characteristics are high conductivity, good performance at the electrode-skin interface (low impedance at the interface), stiffness for the needle material (material hard enough to penetrate the skin), flexibility for the backing material (sufficient flexibility to adapt to the rounded shapes of the body when the electrode is applied with the hand) and biocompatibility of the materials, especially for the microneedle structures. The second factor is the fabrication method as the selected materials will dictate the fabrication process to follow. This process shall minimize the use of expensive materials and equipment, reduce the amount of time spent inside a cleanroom and involve processes that allow batch production.

There are several approaches to microneedle fabrication depending on the materials, the desired geometry and final application of the device, most of the microneedles developed are intended to be used for drug delivery [63]. Microneedle fabrication for electrodes do not need to be hollow and are often fabricated from silicon through a wet etching process [64]. When the fabrication of the whole electrode (microneedles and backing) is made from the same material, either by etching or machining from the bulk, it is challenging to achieve the desired flexible characteristic of the backing and the high stiffness of the microneedles simultaneously. The present work proposes a method based on casting of conductive polymers, that allows to have a flexible material for the backing and a stiff material for the microneedles.

A general overview of the fabrication process is shown in Figure 12. First, an array of microneedle structures is fabricated by a photolithography process, using a glass wafer coated with a thick layer of a negative photoresist and a back-exposure procedure followed by conventional development and baking steps. Once the microstructures are patterned, PDMS is poured onto the wafer to create a negative mold of the structures. This PDMS mold is used to replicate the microneedles with a conductive polymer formed by mixing carbon black powder with a biocompatible resin, and the backing consists of a mixture of carbon black and polyurethane. Finally, the polymer-carbon black composite chip with the microneedle array is coated with silver by a sputtering process. The fabrication steps are described in detail in the following sections.

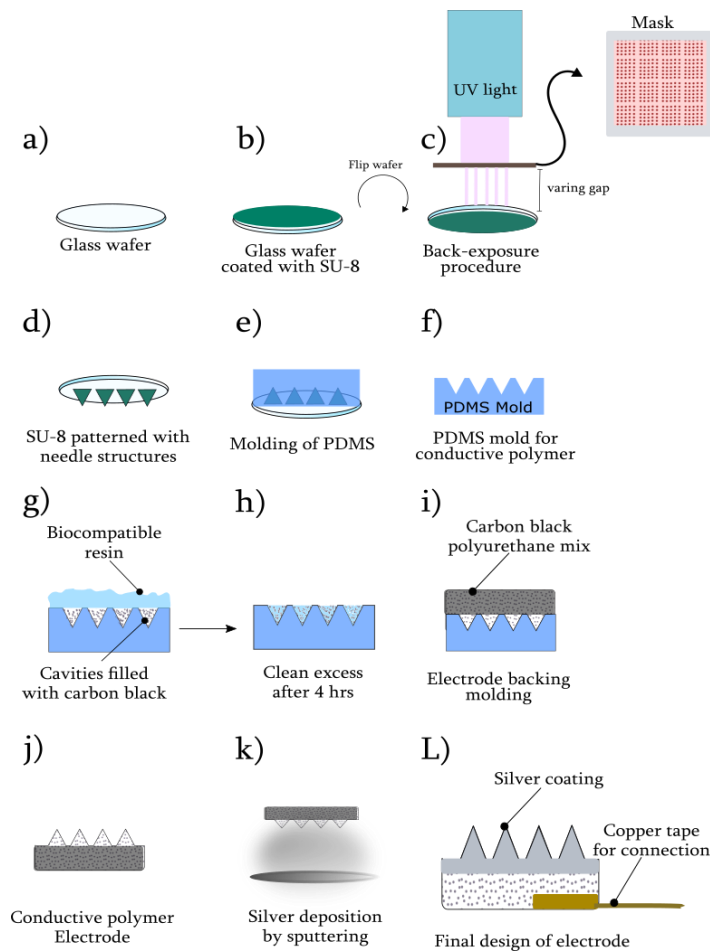


**Figure 12 General overview of the fabrication method for the microneedle electrode.**

## **2.1 Microneedle structures for master mold fabrication**

### **2.1.1 Master mold fabrication**

The first step of the fabrication process is to fabricate the microneedles as a positive master mold; these microstructures will be replicated with a conductive polymer using a second flexible mold made from PDMS. The fabrication of the master mold with the microstructures is based on a back exposure photolithography process similar to the one employed by Kim et al. [65]. A glass wafer is coated with a thick layer of SU-8 photoresist, then the photoresist is exposed with UV light through the wafer and a mask patterned with transparent holes. The microneedle structure is created by the light diffraction due to the separation of the photoresist and the mask created by the glass wafer in between, as shown in Figure 13. This separation can be increased by creating a gap between the mask and the glass wafer. The UV exposure system of the mask aligner is highly collimated; as a result, the UV light beam that passes straight through the transparent holes has a high light intensity such that it will be able to penetrate through the whole photoresist. On the other hand, the diffracted light that separates from this beam is less intense, such that it penetrates less far into the photoresist, creating the tapered structure. The diameter of the microneedle tip is controlled by the diameter of the hole in the mask, the height is controlled by the thickness of the deposited photoresist and the tapered shape of the structure can be modified by increasing the separation between the photoresist and the mask.

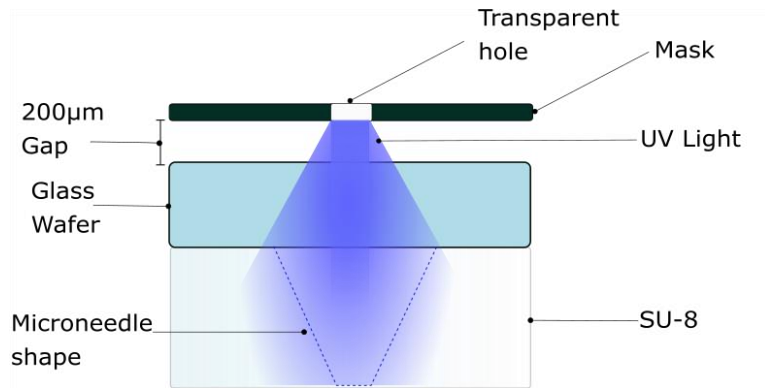


**Figure 13 Microneedle structure created by the back-exposure photolithography process.**

For this work, a 100 mm-diameter soda lime glass wafer with a 550 µm thickness (University Wafer, Inc., USA) is first cleaned with acetone, isopropanol, and deionized water. Then it is left to dehydrate in a convection oven at 153 C° for at least 45 minutes. The wafer is then cleaned by an oxygen plasma treatment for 1 minute, at a 100 W, 15 sccm oxygen flow rate and a pressure of 79.5 mTorr using a PE-50 plasma etching system (Plasma Etch, USA). This step removes organic residues on the wafer and improves adhesion of the photoresist to be coated on the wafer.

Direct adhesion of SU-8 to soda lime glass is not strong and the structures may detach during the developing process or later over time. To improve the adhesion, Omnicoat (Microchem, USA) is dispensed over the wafer and spin coated at 3000 rpm for 30 seconds and then heated at 200°C for 1 minute before dispensing the photoresist. Omnicoat should be neither developed nor should a hard-bake be performed as this will detach the Omnicoat layer, detaching the photoresist microstructures from the wafer. The wafer is then coated with a 600 micron thick layer of SU-8 2100 (Microchem, USA) using a spin-coater at 500 rpms for 10 seconds with a ramp of 100 rpm/s followed by a 750 rpm/s spin for 30 seconds. The photoresist is then soft-baked on a hot plate at

65°C for 30 minutes and at 95°C for 2 ½ hours, followed by a back-exposure procedure using a dark-field mask with a matrix of arrays of transparent holes with different diameters and pitches shown in Figure 14. The test mask has a matrix of transparent hole arrays, each of these arrays has structures with 20, 30, 40, 50, 60 or 100 micron diameters and a center-to-center distance between the holes (pitch) of 300, 400, 500, 750, 1000 or 1250 microns leading to a total of 36 different arrays with the combination of different pitches and diameters. As a test, an array with square shaped transparent features with a center-to-center distance of 500 microns were included in the mask to observe the difference in shape with respect to the circular shaped holes.

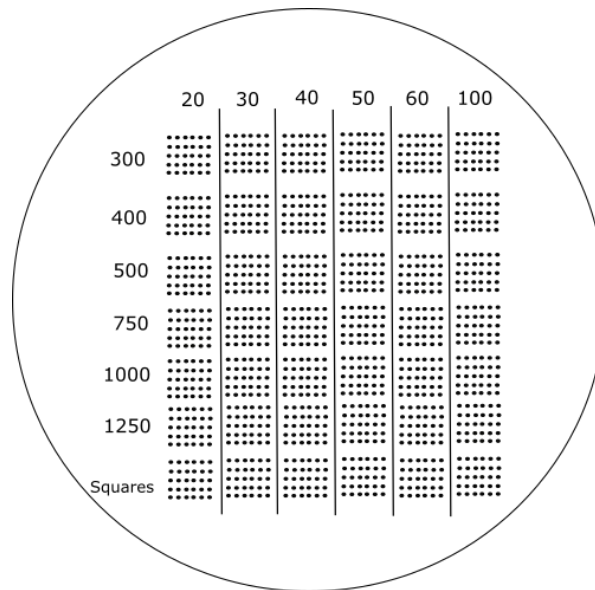


**Figure 14 Mask design for microneedle structures patterning on SU-8. The vertical axis on the left side of the wafer is the center-to-center distance between each hole in the array (pitch) in  $\mu\text{m}$ . The horizontal axis at the top part of the wafer is the diameter of the holes in the array, also in  $\mu\text{m}$ . The last row of the mask has the square shaped holes. A dark field mask is generated from this design.**

The back-exposure lithography process to pattern the SU-8 on the wafer is performed using an NxQ4006 mask aligner (Neutronix-Quintel, USA), with a 350 nm UV lamp. Microscope glass covers (Fisher Scientific, USA) of 200  $\mu\text{m}$  thickness are used to create a gap between the mask and the wafer, yielding a total of 750  $\mu\text{m}$  separation between the mask and the photoresist (550

microns thickness of the wafer + 200 microns from the microscope glass cover). Different exposure times, shown in Table 1, are needed to successfully fabricate all the structures with different diameters, since it was observed that for holes with a smaller diameter a higher dose of UV light was needed for sufficient exposure; only the holes of 20  $\mu\text{m}$  diameter on the mask did not yield microneedles even when increasing the exposure dose by a large amount, as the resulting structures will not stay straight by the end of the process.

**Table 1 Optimized exposure energy for different hole arrays of the microneedle matrix test mask. Straight structures for the 20  $\mu\text{m}$  hole diameter arrays were not achieved.**

<b>Hole diameter (<math>\mu\text{m}</math>)</b>	<b>UV exposure energy dose used (<math>\text{mJ}/\text{cm}^2</math>)</b>
60, 100	4,800
30 ,40, 50	7,200
20	9,600 (maximum attempted dose)

The back-exposure procedure is followed by a post-exposure backing process for 5 minutes at 65°C and 30 minutes at 95°C on a hot plate. The photoresist is developed using SU-8 developer (Microchem, USA) for 30 minutes. Figure 15 shows the resulting structures after developing the SU-8 using the exposure times described in Table 1.

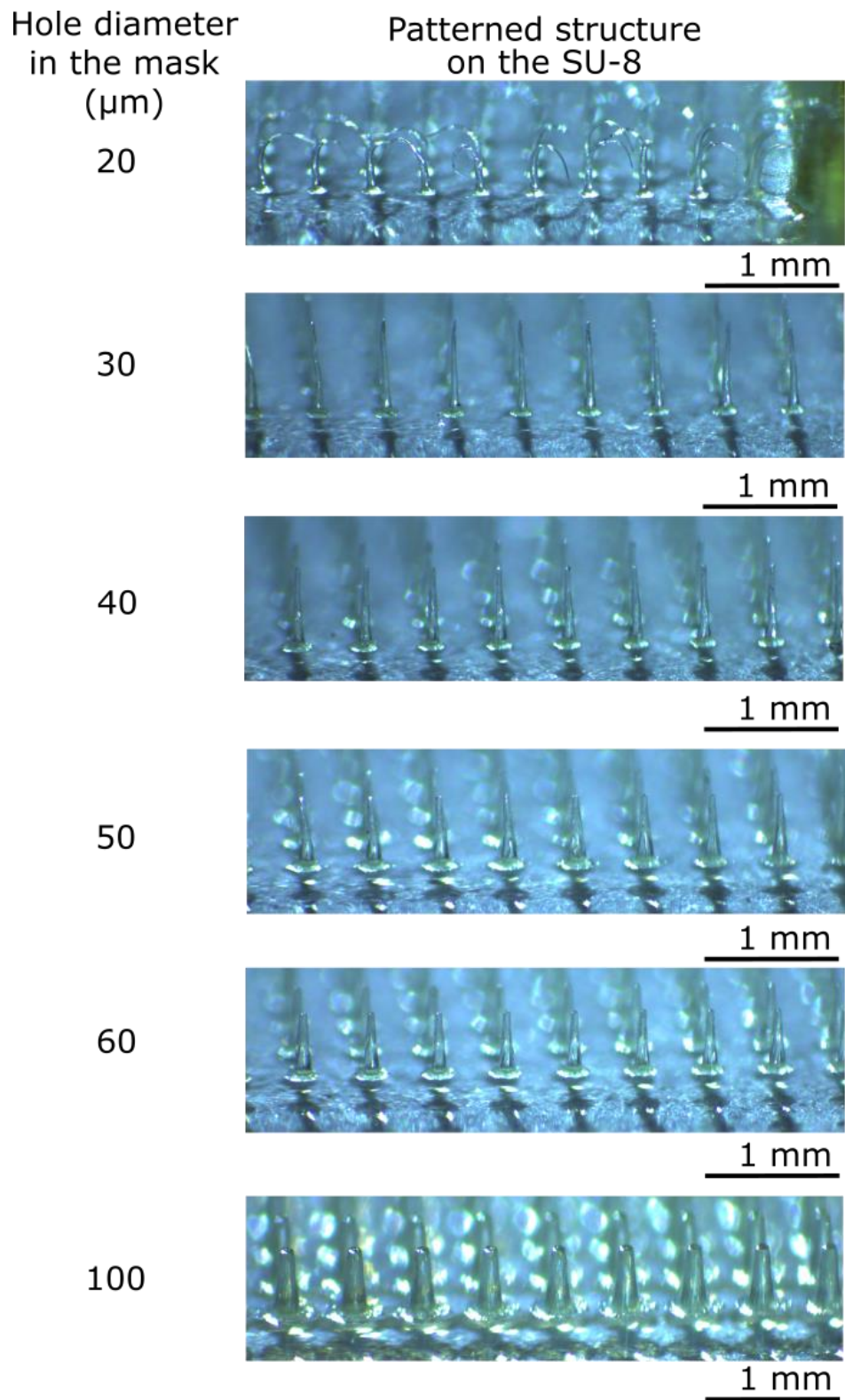


**Figure 15** Resulting microneedle structures with a 500 pitch for the different hole diameters of the mask using the exposure doses from Table 1.

The different transparent features in the darkfield mask used to pattern the SU-8 yield microneedle structures with the dimensions listed in Table 2.

**Table 2 Microneedle dimensions for different transparent features in the photolithography mask. The tip and base diameters are an average of the dimensions measured in 8 needles. For the transparency with 20 m diameter only 4 needles were sufficiently visible to measure the tip dimensions.**

<b>Diameter of circular transparent mask features (<math>\mu\text{m}</math>)</b>	<b>MN Tip Diameter (<math>\mu\text{m}</math>)</b>	<b>MN Base Diameter (<math>\mu\text{m}</math>)</b>	<b>MN Height (<math>\mu\text{m}</math>)</b>
20	9 (bent tips)	82	N/A
30	26	91	580
40	38	111	575
50	44	125	563
60	53	128	565
100	110	203	579

Excluding the case of the structures created from transparent circles with a 20  $\mu\text{m}$  diameter that did not result in upright pillars, the resulting microneedle shapes produced with this fabrication method show that the diameter of the tip of the microneedle is just slightly different from the desired dimensions of the mask. The microneedle tip diameters have a maximum deviation of 10  $\mu\text{m}$  and a minimum deviation of 2  $\mu\text{m}$  for needles made with the 100  $\mu\text{m}$  diameter and the 40  $\mu\text{m}$  diameter mask features, respectively.

The diameter of the base of the microneedles on the other hand, is more than double the diameter of the transparent mask features as expected. For the microneedles fabricated with a UV exposure energy dose of 4,800  $\text{mJ}/\text{cm}^2$  the diameter of the base of the needle is almost exactly 2 times larger than the diameter of the mask feature. The microneedles fabricated with a UV exposure energy dose of 7,200  $\text{mJ}/\text{cm}^2$  have a diameter 2.5 times larger than the diameter of the

mask feature. This is expected as the increase of energy dose increase the chances of the SU-8 to be cured by the diffracted light.

The needle heights are defined by the SU-8 thickness from spin coating. The variation in the height of the microneedles is due to the non-uniform thickness of the SU-8, this problem is created due to the leveling of the wafer during the soft baking step. Additionally, any movement that tilts the wafer (i.e. when the wafer is removed from the spin coater) will contribute to the microneedle height variation, as the SU-8 coating is very thick,

The microneedle center to center distance does not seem to significantly modify the microneedle shape, when the gap between the mask and the SU-8 is 750 $\mu\text{m}$ . Figure 16 shows an example comparison of microneedles made with mask feature diameters of 60  $\mu\text{m}$  and a pitch of 300  $\mu\text{m}$  or 400  $\mu\text{m}$ . The needles in the array with a 300  $\mu\text{m}$  pitch have an average tip diameter, base diameter and height of 56  $\mu\text{m}$ , 128  $\mu\text{m}$  and 291  $\mu\text{m}$  respectively, while the needles in the array with a 400  $\mu\text{m}$  pitch have an average tip diameter, base diameter and height of 53  $\mu\text{m}$ , 128  $\mu\text{m}$  and 289  $\mu\text{m}$  respectively, which is very similar.

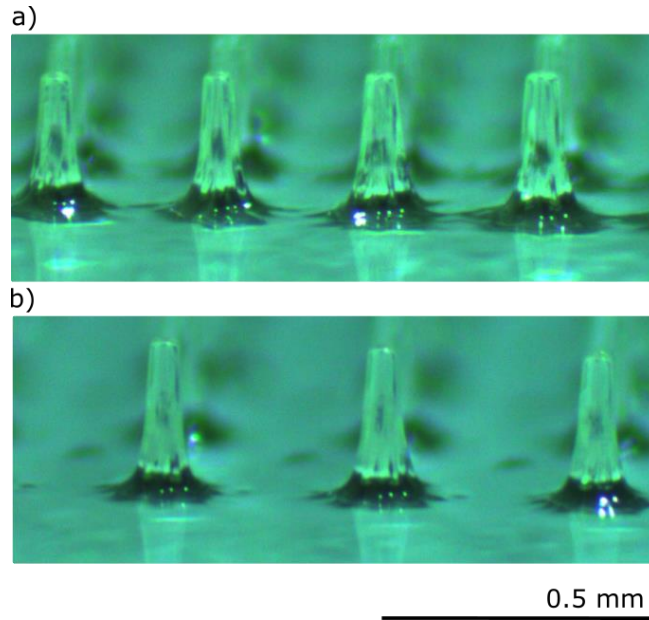


**Figure 16 Comparison of microneedles in arrays with different pitch. (a) Microneedles with a pitch of 300  $\mu\text{m}$  (b) Microneedles with a pitch of 400  $\mu\text{m}$ .**

However, when the gap between the mask and the SU8- resists is increased, the diameter of the base of the microneedle tends to increase due to diffraction of the UV light. This will have a negative impact for the arrays with small center to center distance and large diameter transparent features, as if the base radius of the needle is larger than the microneedle center to center distance, the structures will overlap. Figure 17, shows an example of this effect for microneedle arrays made from mask features with a diameter of 60  $\mu\text{m}$  and center to center distance of 300  $\mu\text{m}$  and 400  $\mu\text{m}$  when the separation between the mask and the SU-8 is 1250  $\mu\text{m}$ . This separation was not optimized as the mask aligner used for UV light exposure does not readily allow to modify the gap between the wafer and the mask. The gap variation for this test was performed by stacking glass wafers or placing glass slides covers between the mask and the wafer. Both the wafer and the slides have defined thicknesses that make it difficult to choose arbitrary gap dimensions to find the optimum gap size.

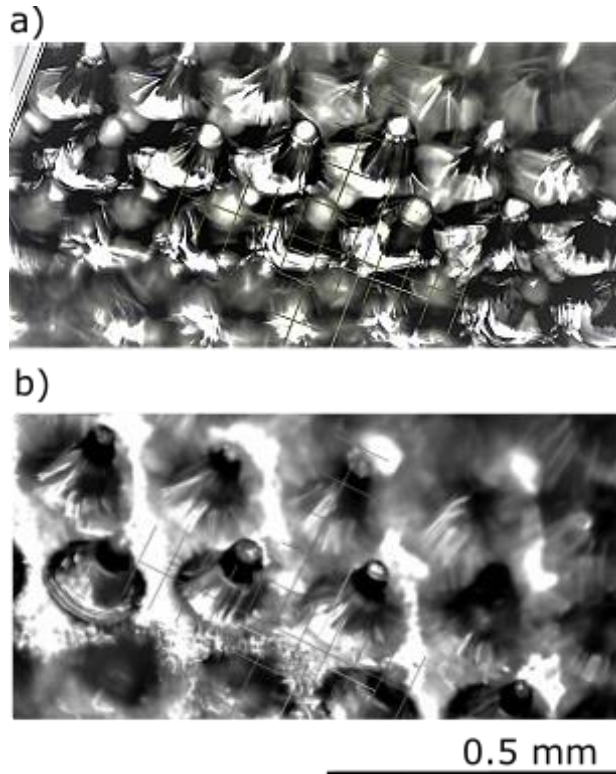


**Figure 17 Fabricated needle arrays with a 1250  $\mu\text{m}$  gap between the mask and the SU-8 resists; (a) microneedle array with a pitch of 300  $\mu\text{m}$ , (b) array with a pitch of 400  $\mu\text{m}$ .**

The diffraction pattern created in the photoresist by the UV light and the mask depends on three main factors: the wavelength used for exposure, the separation between the mask and the photoresist, and the circular aperture of the mask. The wavelength required to cure SU-8 photoresist is 365 nm, so this variable should not be modified. When the size of the diameter of the circular feature in the mask is comparable to the mask-photoresist separation, a near-field diffraction (Fresnel effect) will take place, producing a structure with a less pronounced difference between the diameter of base and the tip of the microneedle, thus the shape of the structure will be closer to a column. If the diameter of the transparent feature in the mask is significantly smaller than the mask-photoresist separation a far-field diffraction (Fraunhofer effect) will be produced, creating a larger difference between the tip and the base diameters on the SU-8 structure, yielding

a sharper microneedle shape. Figure 18 shows the intensity profile for both near- and far-field diffraction effects when light passes through an aperture and is projected on a surface.

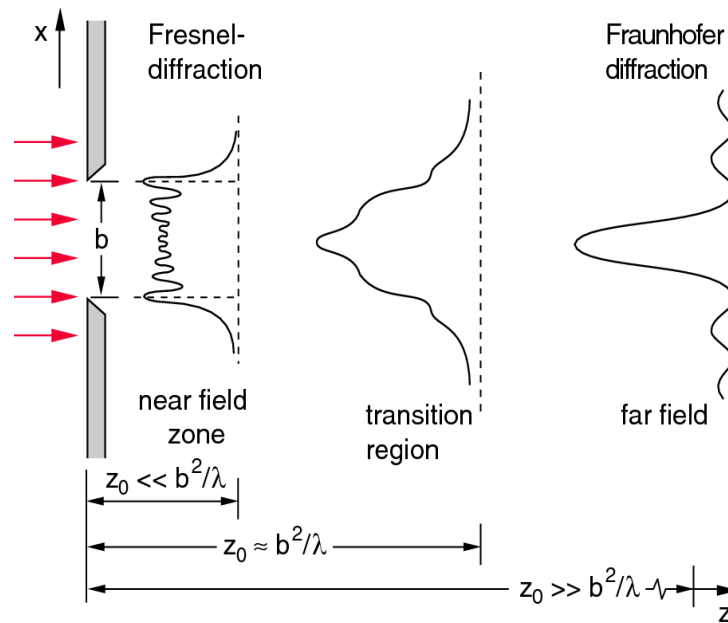


**Figure 18** Different diffraction effects when light passes through an aperture depending on the distance between the aperture and the projection screen or surface. Figure 10.54 from © Demtröder, W., (2019). *Electrodynamics and Optics*. Switzerland: Springer, Cham. Page 315. By permission from publisher [66]

The Fresnel number

$$F = \frac{b^2}{z_0 \lambda} \quad (4)$$

is used to determine whether a near-field effect ( $F > 1$ ) or a far-field effect ( $F < 1$ ) is expected. This number is calculated with the radius of the circular aperture  $b$ , the distance between the mask and the photoresist  $Z_0$ , and the wavelength  $\lambda$  used to expose the resist. The ratio of the based-tip diameter of the fabricated structures in SU-8 and the Fresnel number calculated for the different apertures of the mask and the mask-resist separation of 750  $\mu\text{m}$  are shown in Table 3. As shown by this table, a circular feature with a small diameter of 20  $\mu\text{m}$  will produce an effect similar to

far-field diffraction and thus the difference between the diameter of the tip and the base increases. If we increase the diameter of the circular the feature to 100  $\mu\text{m}$ , which is closer to the 750  $\mu\text{m}$  of the gap, we will have an effect similar to near-field diffraction resulting in a smaller difference between the tip and the base diameter of the structure. The Fresnel number calculated with the dimensions of the gap and our mask are not significantly larger or smaller compared to 1, so the effect that will pattern our structures is most likely a combination of both near and far field effects.

**Table 3 Fresnel number for the different circular features of the mask for a 750  $\mu\text{m}$  separation between the mask and the SU-8 photoresist for a 356 nm wavelength.**

<b>Diameter of circular transparent mask features (<math>\mu\text{m}</math>)</b>	<b>Fresnel number (For a 750 <math>\mu\text{m}</math> gap)</b>	<b>Base/tip diameter ratio</b>
20	0.365	9.1
30	0.821	3.5
40	1.461	2.9
50	2.283	2.8
60	3.287	2.4
100	9.132	1.8

Yang et al. [67] performed an analysis to understand the diffraction pattern created when the mask-photoresist separation and the diameter of the circular transparency are modified, taking into account the significant attenuation of the UV light when it passes through the SU-8 photoresist. The results of their work showed that for a separation between the mask and the resist of close to a 1000  $\mu\text{m}$  and an SU-8 thickness of around 400  $\mu\text{m}$  the diffraction effect on the resist will be a combination of both near- and far-field effect as the Fresnel number for circular apertures with a diameter of 5  $\mu\text{m}$  to 95  $\mu\text{m}$  are close to one.

Davis et al.[68] and Park et al. [69] demonstrated that the force needed to pierce the SC with a single microneedle is proportional to its tip cross-sectional area. Such force is determined by both groups using linear functions derived empirically from a series of microneedle insertion tests. The proposed approach by [68] only applies to microneedles with a tip diameter of 120  $\mu\text{m}$  to 320  $\mu\text{m}$ , while the function proposed by [69] can be used for microneedles with a 20  $\mu\text{m}$ -80  $\mu\text{m}$  tip diameter. Since the needles fabricated here have tip diameters between 26 and 110  $\mu\text{m}$ , this last approach is used to calculate the force needed to pierce the skin for the microneedles of the SU-8 master mold. The force (in N) to cross the skin

$$F_i = 0.00012 \times A_{tip} \quad (5)$$

is calculated using the tip area  $A_{tip}$  (in  $\mu\text{m}^2$ ) computed with dimensions listed in Table 2. The calculated force results are shown in Table 4.

**Table 4** Calculated force to pierce the SC for the microneedles fabricated on SU-8 with a backside exposure lithography process.

Diameter of circular transparency in the mask ( $\mu\text{m}$ )	MN Diameter ( $\mu\text{m}$ )	Force needed to pierce the skin (N)
20	9	0.03
30	26	0.08
40	38	0.15
50	44	0.23
60	53	0.33
100	110	0.94

The piercing force needed to cross the SC with the tip areas of the fabricated needles is relatively low considering that in average, the maximum force that humans can apply between the index and thumb fingers is 80 N for males and 55 N for females[70]. However, to ensure that the microneedles will cross the stratum corneum, the critical load, considering all the dimensions of the fabricated microneedles and final material of the electrode, needs to be lower than the calculated piercing force. This will be discussed in Chapter 3.

## **2.2 Electrode casting with conductive polymers**

In order to have a simple low-cost fabrication process for microstructures, we chose a soft lithography casting process with a PDMS mold. This process is widely used for rapid prototyping of microfluidic channels and microstructure patterning [71][72][73] since PDMS molds can achieve nanoscale resolution, are reusable, and allow to create multiple devices simultaneously.

Once the microneedle SU-8 master mold was fabricated, the wafer is fixed to a polystyrene petri dish using double sided adhesive tape. A silanization process is performed on the wafer with the SU-8 microneedle structures to reduce its adhesion to PDMS by pouring hexamethyldisilane (HMDS) onto the wafer with a pipette and letting it evaporate in a fume hood for 45 minutes at room temperature. Then, PDMS at a 10: 1 resin : hardener mixture ratio is poured in the petri dish letting it cure at room temperature for 48 hrs.

The PDMS mold now has the negative pattern of the microneedle structure, and it is removed from the wafer. A silanization process is then performed on the PDMS mold as well to reduce its adhesion with the electrode polymer materials and to facilitate the release of the cast electrode from the PDMS mold. For this step, HMDS is poured into the mold with a pipette covering all the areas that are going to be used for casting. The HMDS is left to evaporate in a

fume hood for 45 minutes at room temperature. Following the silanization process, the conductive polymer composites are molded following two steps, one for the microneedle structures and another one for the backing.

### **2.2.1 Microneedle casting**

The casting process for the microneedle structures with the carbon black and the biocompatible resin, was based on a procedure used to fabricate electrodes in microfluidic channels presented by Mustin et al. [74]. The cone shaped cavities are filled with carbon black XC72R (Cabot, USA) by pushing the powder with a tongue suppressor and a cotton swab into it. Next, the biocompatible resin (Epoxies, USA) at a 100 : 35 resin : hardener mixture ratio is spread over the cavities filled with carbon black. The resin is left on the mold for 4 hours to penetrate the cavities and fill the spaces between the carbon black particles. The excess resin is then cleaned with a razor blade and gently wiped with a tissue soaked with acetone. Figure 19 shows the steps of this process.

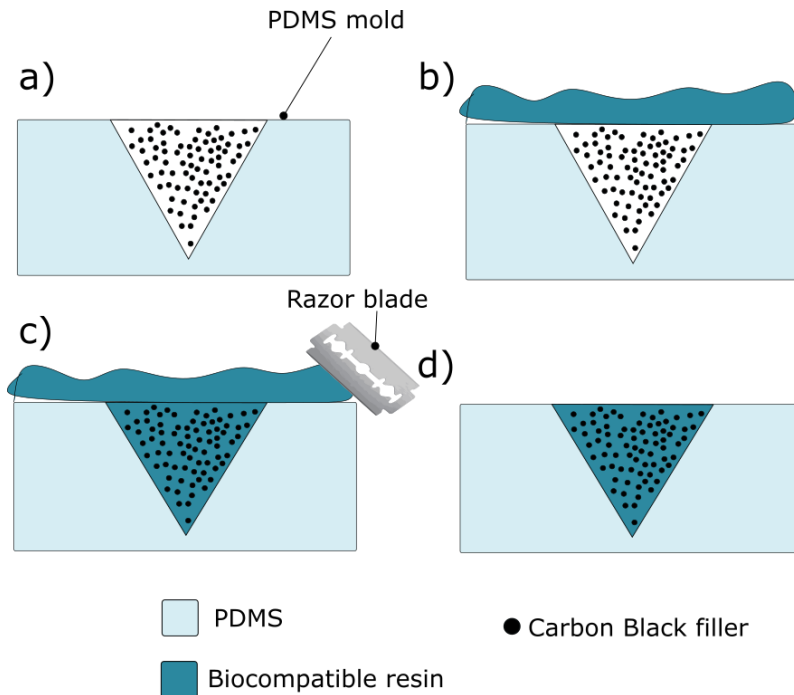


**Figure 19** Process for microneedle casting with carbon black XCR72 and the biocompatible resin; (a) the cavities are filled with carbon black pressing the powder with a tongue suppressor and a cotton tip. (b) The biocompatible resin is spread over the mold cavities and it is let sit for 4 hours. (c) The excess of the resin is removed with a razor blade and by gently cleaning with a tissue soaked with acetone. (d) Expected result is a cavity filled with a high concentration of carbon black that the resin will paste together.

### 2.2.2 Polyurethane backing

Once the excess of the biocompatible resin is cleaned from the mold, the polyurethane mixed with carbon black at 15% weight concentration is spread over the needle structures with a tongue suppressor and the excess is cleaned with a razor blade. Masking tape around the edges of the electrode is used to control the 400  $\mu\text{m}$  thickness of the polyurethane backing. Finally, both mixtures are left to cure in the mold for 48 hours at room temperature before releasing the electrode from the mold, the result is shown in Figure 20.

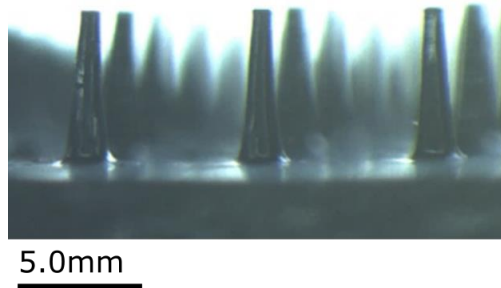


**Figure 20 Structures cast with carbon black, biocompatible resin and polyurethane.**

The arrays were visually inspected using a stereomicroscope and it was found that for some microneedle structures the tip was apparently made only of biocompatible resin, an extreme case of this flaw is shown in Figure 21. This meant that when filling the cavities, the carbon black was not going deep enough and thus the filling of the cavities needs to be done more cautiously. This issue raised some concerns about the conductivity at the surface of the microneedle structure. Evaluation of the surface conductivity, was performed using a microprobe station and measuring the resistance between the tip of the needle and the substrate surface and between the tip of needle and a piece of aluminum foil attached to the backing for the electrode; this piece of aluminum contacts the whole 1 cm<sup>2</sup> area of the backing. The probe contact points are showed in Figure 22.

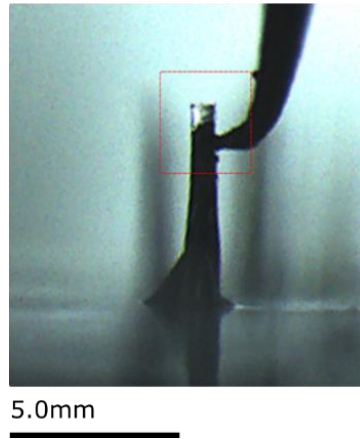


**Figure 21** Microneedle cast with the conductive polymer using the proposed fabrication method. The red square shows an extreme case of a fabrication flaw where the microneedle tip is made only of biocompatible resin without carbon black. A probe tip is seen on the right of the microneedle.

This measurement showed that the tips of the microneedles and the surface of the electrode at the base of the needles was not as conductive as the bulk of the material, tested with four-point measurements.

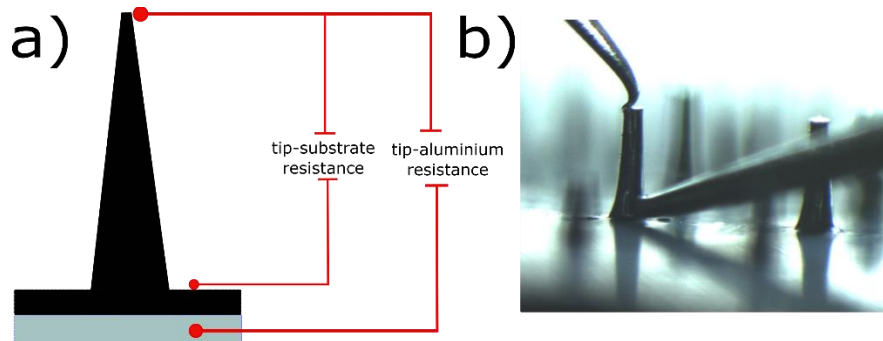


**Figure 22 (a)** Shows the measurement points for the conductivity test. **(b)** depicts the placement of the microprobe tips for the tip to substrate measurement.

To improve the conductivity on the surface of the polymer electrode, the device was treated with a plasma etching process using a PE-50 (PlasmaEtch, USA) plasma etcher, with a 15 sccm oxygen flow rate, at a 79 mTorr vacuum pressure and 100 W power for 60 minutes. This step removes some biocompatible resin and polyurethane from the surface, exposing more carbon black

particles. The previously mentioned resistivity measurements tip with substrate and tip with aluminum backing was repeated after the plasma process. Results and comparison between the measurements before and after the plasma etching treatment shown in Table 5 indicate that the plasma treatment provides better electrical contact with the conductive phase of the conductive polymers. This will also enhance the conductivity of the final device by creating a better contact between the carbon black and the metal coating.

**Table 5 Resistivity measurement comparison with and without plasma etching**

<b>Resistivity measurement points</b>	<b>Resistance without plasma etching (k<math>\Omega</math>)</b>	<b>Resistance with plasma etching (k<math>\Omega</math>)</b>
Substrate to tip	5,203	24.4
Aluminum backing to tip	820	12.1

Once the electrode frontside is coated with silver, the resistance between its backside and any point of the surface of the microneedles is expected to be lower than the 12 k $\Omega$  measured between the tip and the backside of the electrode. Thus, theoretically, the total impedance between the interface with the tissue below the stratum corneum and the cable of the electrode is expected to be lower than 12 k $\Omega$ .

From all the different arrays, only the 100 microns tip diameter needles, 600 microns height with a pitch of 750 and 1000 microns were used for the tests described in Chapter 4. These microneedle arrays structures were the first ones to be successfully fabricated in SU-8. So, in order to advance the project these arrays were used to optimize the further fabrication steps and to start

testing while working in parallel on the lithography process to fabricate microneedles with the other dimensions.

### **2.3 Metal coating**

Once the conductive polymer structure with the microneedle structures is released from the PDMS mold a thin layer of silver is deposited over the microneedle structures to provide a continuous conducting surface of the electrode. This layer helps to increase the biocompatibility of the electrode as it prevents the detachment of carbon black particles from the etched surface that could potentially remain in the skin after the electrode insertion.

There are many methods to deposit metal layers, including chemical vapor deposition (CVD), physical vapor deposition by sputtering or evaporation, electroplating and electroless plating just to name a few. CVD processes either at low or high pressure or plasma enhanced were discarded as any of these methods typically need a high temperature environment ( $>300^{\circ}\text{C}$ ) [75] the fabricated electrode is made of a conductive polymer with a low glass transition temperature, where a rubbery behavior was observed at around  $100^{\circ}\text{C}$ . Thus, at the high temperatures needed for CVD the device could melt completely or degrade, leading additionally to a possible contamination of the equipment.

Electroless plating was one of the most promising methods as the it is an inexpensive process and does not require any type of complex equipment, but no commercial ready-to-use plating solutions were found for silver deposition or a viable biocompatible metal. Most of the available plating solutions found were highly toxic metals like cobalt and cooper or metals that potentially could trigger allergy reactions such as nickel. Nevertheless, this method still has

potential as a nickel deposition could be used as a seed layer for a subsequent silver or gold deposition step.

Taking into account the aforementioned points and given that silver electroplating materials are low-cost of around 179 CAD for the plating materials that could potentially plate 1.7 million devices with a 100 nm layer and that the silver sputter deposition equipment access is relatively inexpensive at the UBC microfabrication facilities, the following three options were explored.

### **2.3.1 Electroplating**

Electroplating is a simple low-cost metal deposition method making it ideal for the batch fabrication of the microneedle electrode. Mansoor et al. [76] have demonstrated a successful deposition of nickel on conductive polymer constituted of carbon black and PMMA by electroplating. Silver electroplating was performed on the polyurethane/biocompatible resin and carbon black electrode. The electrode was prepared by pasting copper tape on the backing of the electrode to ensure that an uniform distribution of the current on the whole surface of the electrode, silicon glue was used to only expose the side with microstructures to the plating solution (Krhon industries, USA). The electroplating solution was left at room temperature and currents from 0.5 mA to 50 mA were attempted. The best deposition was achieved at high current 50 mA and room temperature, but the deposited film was still not uniform, and the adhesion of the film to the substrate was low, such that the silver created flakes on the surface and fell off when the device was cleaned with deionized water. The resulting film deposited by electroplating is shown in Figure 23. This nonuniform deposition could be explained by an inhomogeneous distribution of carbon black in the bulk material of the microneedle and the backing, where spots with high carbon

black concentration have silver deposition while silver will not deposit on electrode parts with low carbon black concentration or a poor electrical connectivity to the bulk.

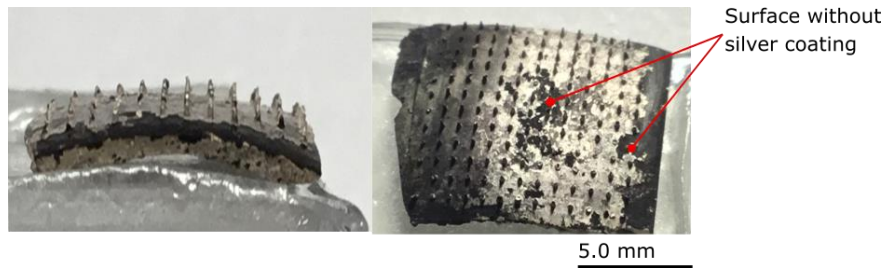


**Figure 23** The silver film deposited by electroplating. The bright surface is the deposited silver film, while the black spots are the surface locations where the silver fell off or no deposition was achieved.

### 2.3.2 Evaporation

A thermal evaporation process was performed using an in-house electron beam evaporation system at the UBC Nanofabrication Facility. The deposition rate of  $2000 \text{ \AA}/\text{min}$  was used to deposit a layer with 100 nm thickness, and the result is shown in Figure 24. The main problem with this method is that it is a directional deposition that will not cover the whole surface of the microneedle as depicted in Figure 24a. Here the red rectangle shows a microneedle with no silver coating on some parts of the needle body. Also, the silver layer easily falls off when the surface is touched.

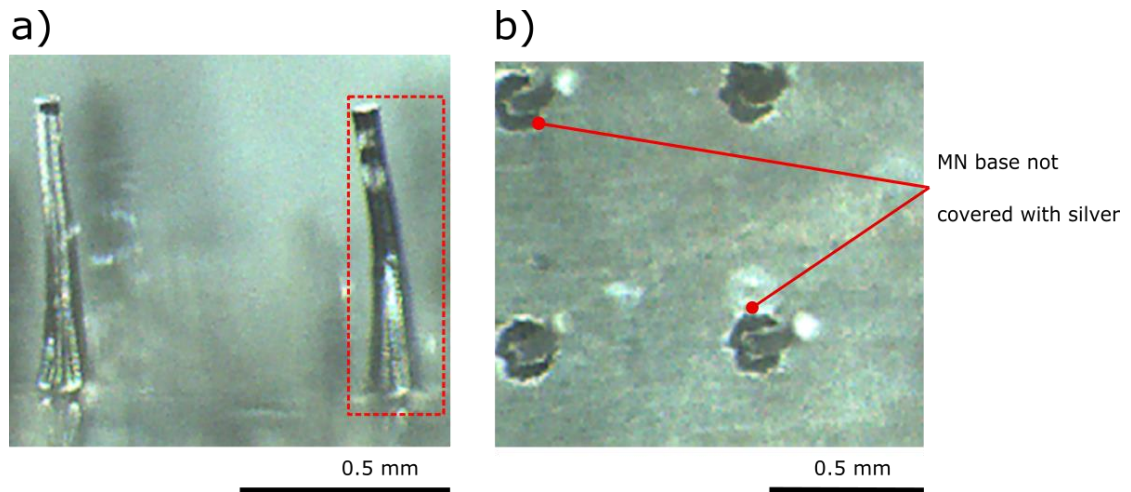


**Figure 24** Light microscopy: (a) side view of two microneedles after silver deposition with electron beam evaporation; the microneedle highlighted with the red rectangle shows pour silver deposition on the microneedle body; (b) top view of the array with some spots not coated with silver at the base of some microneedles.

### 2.3.3 Sputtering

The most successful deposition on the conductive polymer electrode was achieved by a sputter deposition process resulting in a deposition of 100 nm of silver at a 2 nm/s deposition rate using a Nexdep sputtering tool (Angstrom Engineering, CA). The coated electrodes after silver deposition are shown in Figure 25. After this process the back part of the electrode was sanded with sandpaper to expose more carbon black and a piece of cooper tape (3M, USA) was attached instead of the previously used aluminum foil, to electrically connect the backing of the electrode with the leads of a biosignal acquisition board.

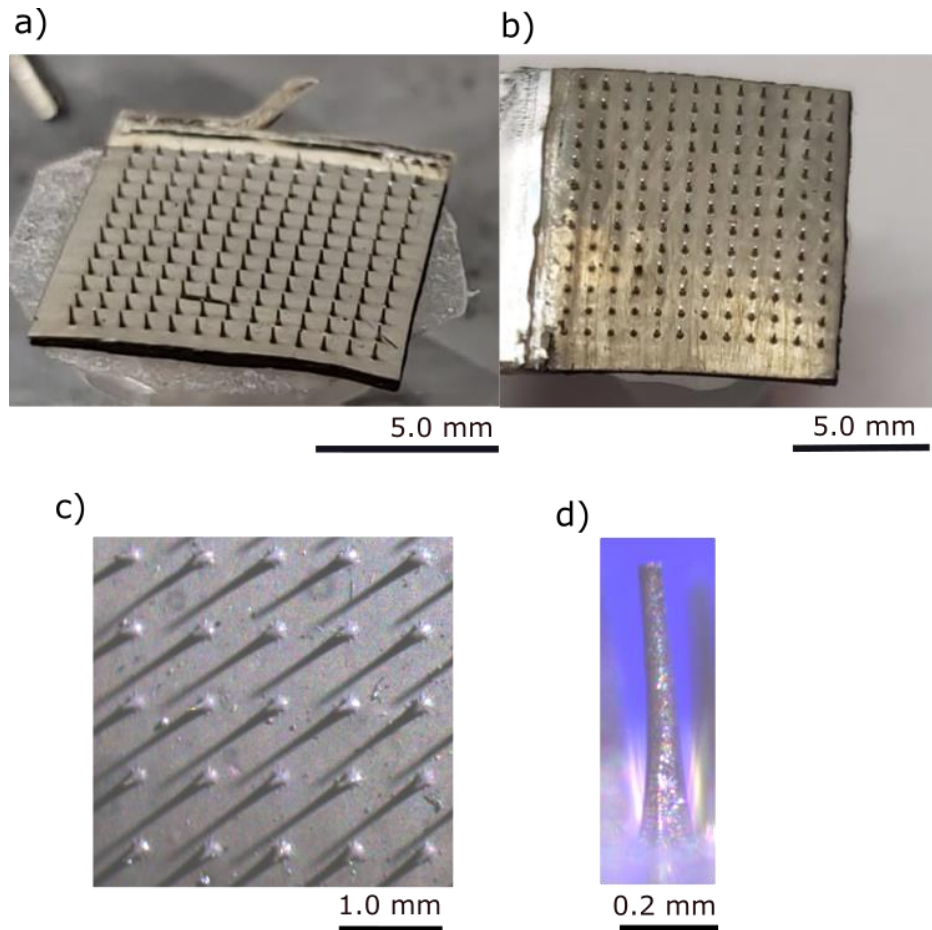


**Figure 25 (a) Angled view of the microneedle array after silver deposition by sputtering; (b) top view of the array after silver deposition by sputtering; (c) light microscopy top view of the electrode after silver deposition by sputtering; (d) light microscopy side view of one microneedle after silver deposition by sputtering.**

The electrode design used for further tests described in Chapter 4 has a 12 by 13 microneedle array, yielding a total of 156 microneedles with a tip diameter of approximately 90  $\mu\text{m}$ , a base diameter of approximately 200  $\mu\text{m}$ , and a height of approximately 600  $\mu\text{m}$ . The substrate has a 1  $\text{cm}^2$  square shape, with a thickness of 0.4 mm. Figure 26 shows the final electrode.

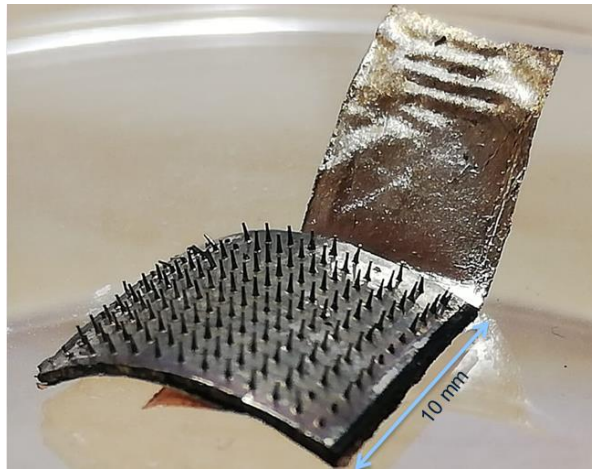


**Figure 26 Final prototype of the microneedle electrode.**

## **Chapter 3: Materials and methods**

This chapter is divided into two segments, the first one describes the final materials used to build the microneedle electrode, provides a rationale for choosing such materials, and provides their measured mechanical properties. The second segment of this chapter explains the testing methodology followed to evaluate the ability of the fabricated device to pierce the outermost layer of the skin, to evaluate the impedance of the fabricated electrode at the skin-electrode interface, and to evaluate the ability of the electrode to record biosignals.

### **3.1 Electrode structure materials**

Microneedle electrodes made from metallic materials provide the electrical conductivity needed for a low electrode-skin impedance while providing enough strength to cross the stratum corneum. The use of metals either for the backing of the electrode or the microneedle structures, make the device fabrication processes complicated and expensive as these materials are often machined from a material block [77], which requires custom made drills and tools, or by electroplating of a mold structure [78] [65], that typically requires the creation of a new microneedle mold for each fabricated array.

Silicon is another common material for microneedle fabrication, as there are many micromachining techniques for this material thanks to the microelectronics industry. Unfortunately, this material is stiff and brittle, and a silicon backing plate is therefore not able to adapt to the round shapes of the body.

From the mechanical point of view, polymers can be very flexible or hard, are inexpensive, and can be easily cast and molded at low temperatures simplifying the fabrication process. An

obvious limitation is that most polymers are not conductive, but by doping or combining them with conductive fillers these materials can become conductive enough to record biosignals.

### **3.1.1 Conductive polymers**

Conductive polymers can be classified in three categories, ionically conductive polymers, intrinsically conductive polymers, and extrinsically conductive polymers. Ionically conductive polymers, mostly used for batteries, are solid electrolytes that need to be blended or doped with other compounds to achieve similar conductivity to liquid electrolytes [79]. Intrinsically conductive polymers are conjugate polymers with delocalized pi electrons in their main chain and can be doped to achieve similar electrical conductivity to metals. These materials are hard to process and are mechanically stiff [80].

Extrinsically conducting polymers were selected to fabricate the microneedle electrode backing as the fabrication process of these polymers is low cost and significantly simple. These polymers are fabricated by adding conductive fillers into an insulating polymer matrix [80]; metal and carbon derivative powders are the two main types of fillers used to fabricate conductive polymers.

Metal powders are more conductive than carbon-based fillers. Noble metals like gold and silver powders are good conductors but they tend to be quite expensive, so they are not a feasible option for most applications and are less frequently used in polymer composites. Less expensive metals like steel, aluminum and copper are not useful because they tend to oxidize forming an electrically insulating layer on their surface [81].

Carbon derivatives like carbon black and graphite powder are an affordable alternative to metal fillers. Carbon black is incorporated in polymers for applications that require electrical

resistivity below 10  $\Omega/\text{cm}$ . Carbon black fillers are able to impart electrical conductivity to a polymer compound by creating conductive networks inside the insulating polymer matrix, where the electronic charge carriers move along conduction paths between particles mainly formed by particles touching each other or by the tunneling effect [81].

When fillers are mixed with polymers, the conductivity of the resulting material depends on the filler concentration and distribution. The fillers distributed into the polymer matrix should be above a certain concentration threshold known as percolation threshold, where the polymer shows a significant decrease in resistivity. They should be uniformly distributed in the polymer matrix to ensure a uniform conductivity on the bulk material.

### **3.1.2 Electrode backing materials**

The backing of the electrode is made of polyurethane mixed with carbon black powder to achieve a flexible material and a cost-effective fabrication process. The favorable mechanical properties of polyurethanes such as their high flexural endurance and blood compatibility make them a popular material for use in medical devices. Examples of polyurethane use in medical devices include catheters, lead insulation of pacemakers, vascular protheses, heart valves and wound dressings [82]. While the microneedle backing is not going to be implanted, it is important that it is made from a biocompatible material that will not produce allergic skin reactions.

The optimal amount of carbon black needed to mix with polyurethane for the backing of the electrode was determined by finding the percolation threshold. The conductivity of this mixture

$$\sigma = \frac{1}{\rho} = \frac{(w*h)}{R*l} \quad (6)$$

was calculated using the measured resistance  $R$  and the width  $w$ , thickness  $h$  and length  $l$  of the sample while  $\rho$  is the resistivity of the material. The resistance  $R$  was measured with a four-point resistance test on blocks of the sample materials with different concentrations of carbon black.

For this tests Cmax22 carbon black (Cabot, USA) was mixed with Max Cast polyurethane epoxy resin (MaxCast, USA) for 20 mins, which is the working time of the polyurethane/epoxy resin. Then it is let cure for 48 hours in rectangular mold cavities with 4 embedded copper wires; Figure 27 shows the sample dimensions. The current was supplied by connecting a power source to the outer wires of the sample marked as “a” and “b” in the Figure 27 and voltage was measured across the inner wires marked as “c” and “d”.

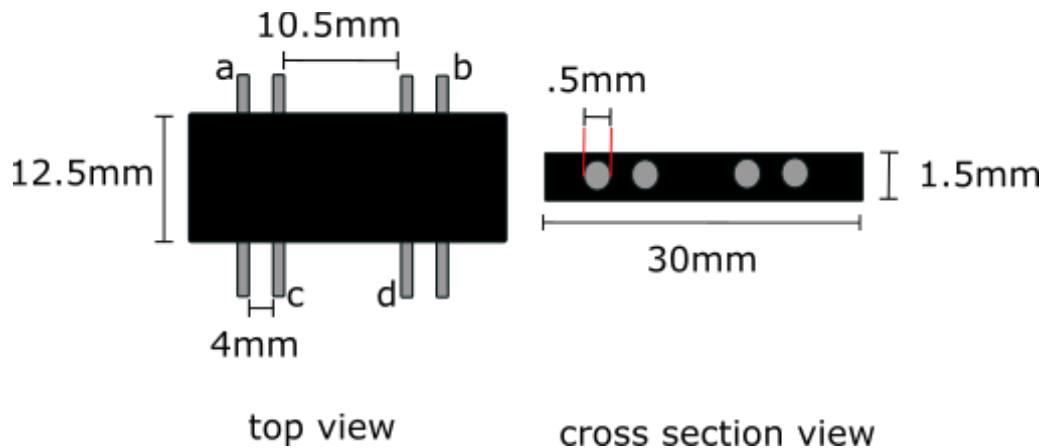


**Figure 27 Test sample dimensions for resistivity measurement of the carbon black polyurethane samples.**

The percolation threshold was crossed around 15 wt% concentration of carbon black. Figure 28 shows the conductivity of the material as a function of the carbon black concentration. A limiting factor to increase the concentration of carbon black beyond 15% is the consistency of the mixture, that at higher concentrations of carbon black becomes so viscous that is impossible to spread it over the mold. Besides the molding problem, the addition of carbon black particles makes

the carbon black very difficult to mix with the polyurethane and decreases the flexibility of the cured polymer. Hexane, a solvent often used to thin elastomers, was used to improve the dispersion of carbon black particles while mixing them with the polyurethane and reduce the viscosity of the mixture to easily spread it on the mold. The carbon black-polyurethane blend is mixed with hexane by adding 1 part of hexane for every 10 parts of the total weight of polyurethane-carbon black mixture; the hexane will evaporate once the polymer is fully cured, thus the resulting material will have a porous composition making it more flexible. Adding an excessive amount of hexane to the blend will result in a very porous material, that could potentially reduce the contact between carbon black particles, reducing the conductivity of the material. Furthermore, the increase in porosity could also embrittle the material as observed for 2 parts of hexane for 10 parts of the polyurethane-carbon black mixture.

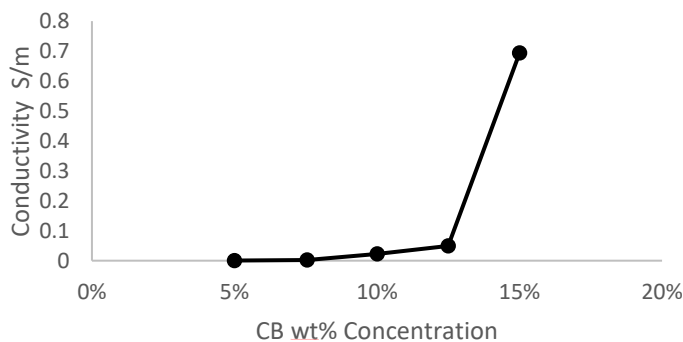


**Figure 28 Conductivity of the carbon black / hexane / polyurethane mixture as a function of the carbon black concentration in the polyurethane-carbon black mixture.**

PDMS was considered to fabricate the backing of the electrode but PDMS will not adhere to the microneedle material during the fabrication process.

### **3.1.3 Concentration of carbon black in the microneedle structures**

The ability of a microneedle array to penetrate the skin depends on three main factors. First, the geometry of the structures is important, as the sharper the tip of the needle, the easier it is to pierce the skin with less pressure. Second, the aerial density of the needles plays an important role, as the bed-of-nails effect can prevent high-density microneedle arrays from piercing the skin due to the distribution of the force. Finally, the stiffness of the material needs to be adequate to avoid needle bending when pushing the array into the skin.

As opposed to the backing of the electrode, the microneedle structures should be stiff enough to cross the first layer of the skin without bending, so the flexible polyurethane mixture used for the backing is not a feasible option. Biocompatibility is the most relevant factor to select a material for these structures, as there is always the chance that the microneedles will break when they are inside the skin. Carbon black mixed with a medical grade epoxy resin that passes the Biocompatibility ISO 10993-5 Cytotoxicity test was therefore selected to fabricate the microneedles [83].

Since the high viscosity of the biocompatible resin and carbon black mixture does not let it penetrate the mold cavities, they are not mixed before depositing into the mold. Therefore, two steps are needed to cast the structures: first, Carbon black Vulcan XC 72R powder (Cabot, USA) is pushed inside the needle-shaped cavities. Then, the 20-3401 medical grade epoxy resin (Epoxies, USA) is spread and left on top of the mold for four hours, allowing it to penetrate in between the carbon black particles, as shown in Figure 29. With this process, we expect to have the highest possible amount of carbon black in the microneedle structures, so the process to find the percolation threshold is not needed.

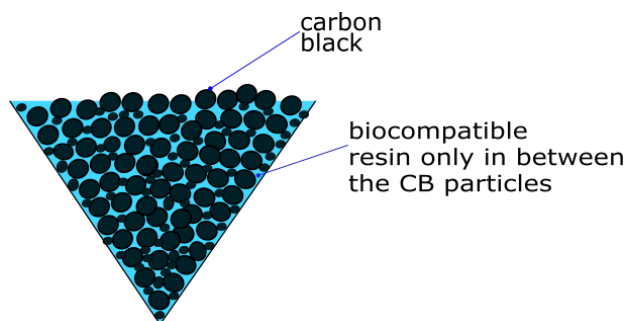


**Figure 29 Resulting microneedle material with the proposed fabrication method.**

### **3.1.4 Mechanical characterization of electrode materials**

The proposed fabrication method to achieve electrical conductivity in polymers will modify the mechanical properties of the polyurethane used in the backing, and of the biocompatible resin used for the microneedles. A high concentration of carbon black in the mixture is expected to embrittle the materials [79] and in the case of the backing material, the hexane also will modify its mechanical properties. In order to better understand these changes of the materials properties, a tensile stress test was run using a DMA 8000 Dynamic Mechanical Analyzer (Perkin Elmer, USA) with 10 N applied force at 1 N increments per minute to find the Young's modulus of these materials.

The strain-stress curves in Figure 30, show the comparison between the 20-3401 medical grade epoxy resin without carbon black and the mixture of this resin with carbon black that composes the microneedle's final material. The addition of carbon black makes the polymer stiffer but there is not much difference to the original material, as the carbon black/biocompatible resin mixture has a Young's modulus of 1.422 GPa, while the biocompatible resin alone has a modulus of 1.228 GPa. The Young's moduli were determined as the slope of the curves in Figure 30.

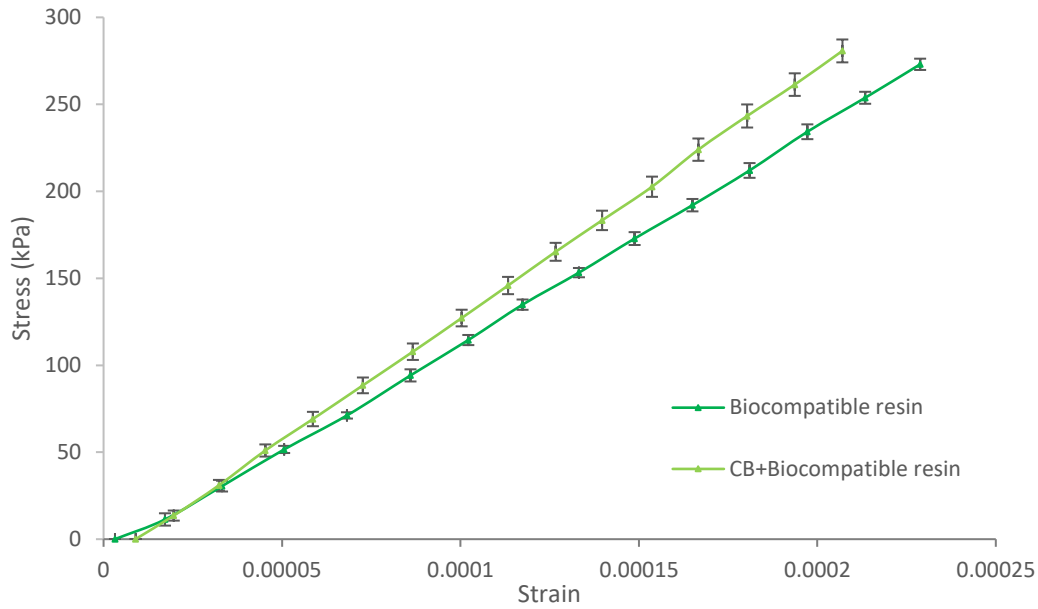


**Figure 30 Stress-strain curves for the biocompatible resin (dark green) and the carbon black/biocompatible resin mixture used to fabricate the microneedle structures (light green). The curves show the mean value from 4 different tests performed on different samples and the error bars correspond to the calculated standard error.**

The medical epoxy resin mixed with carbon black is evaluated to determine if this material is hard enough to avoid buckling of the needle when it is pressed against the skin. The critical load [84]

$$P_{cr} = \frac{\pi E_{R/Cb} I_{MN}}{0.7(l_{MN}^2)} \quad (7)$$

is calculated using the Young's modulus  $E_{R/CB}$  of the biocompatible resin and carbon black mixture, the height and the area moment of inertia of the microneedle,  $l_{mn}$  and  $I_{mn}$  respectively.

This load is calculated for the simplified system by considering the microneedle as a hinged-fixed cylindrical column as shown in Figure 31. The column is considered to be a cylinder

with the radius of the microneedle tip as the worst-case scenario to find a lower bound value for the critical load.

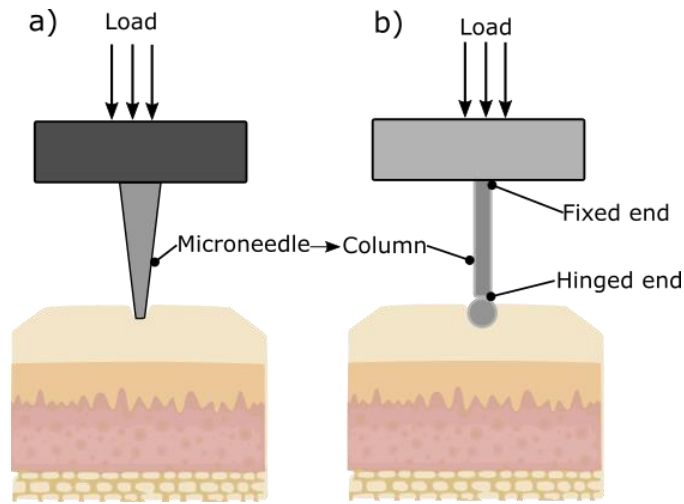


**Figure 31 (a) Microneedle insertion (b) Simplified model to approximate the critical load for the microneedle structure fabricated with the biocompatible resin and carbon black blend.**

Results of the calculated critical load and a comparison with the force needed to pierce the skin discussed in section 2.1 are shown in Table 6.

**Table 6 Comparison between critical load for buckling of the microneedle structure and the force to pierce the skin for different microneedle shapes.**

Mask diameter ( $\mu\text{m}$ )	Critical Load $P_{cr}$ (N)	Force to pierce the skin (N)
20	0.002	0.03
30	0.01	0.08
40	0.03	0.15
50	0.09	0.23
60	0.20	0.33
100	1.56	0.94

These results show that the material used for the microneedle electrode is strong enough to cross the stratum corneum when the fabricated needles have a 100  $\mu\text{m}$  tip diameter. However, for smaller tip radii, the needles will potentially buckle when they are pressed against the skin thus a different material should be used for these structures. This analytical approach does not consider that the microneedle is a tapered structure, as modeling the needle as such structure makes the computation of the critical load very complex.

To understand better the effect of adding carbon black and hexane to the polyurethane to fabricate the backing of the electrode, the stress-strain curves of these mixtures were obtained performing the tensile test previously described. Figure 32 shows the stress-strain curves for polyurethane (dark blue), polyurethane and hexane (light blue) and the final material used for the backing (purple) composed of polyurethane, carbon black and hexane. The figure shows that adding hexane to improve the mixing process of carbon black with polyurethane makes the polymer flexible, as the hexane evaporates from after the polymer is cured leaving a less dense structure. The mixture of polyurethane with carbon black and hexane is stiffer than the polyurethane as carbon black makes the material stiffer; this effect is expected and similar to the effect of mixing carbon black with the medical grade epoxy.

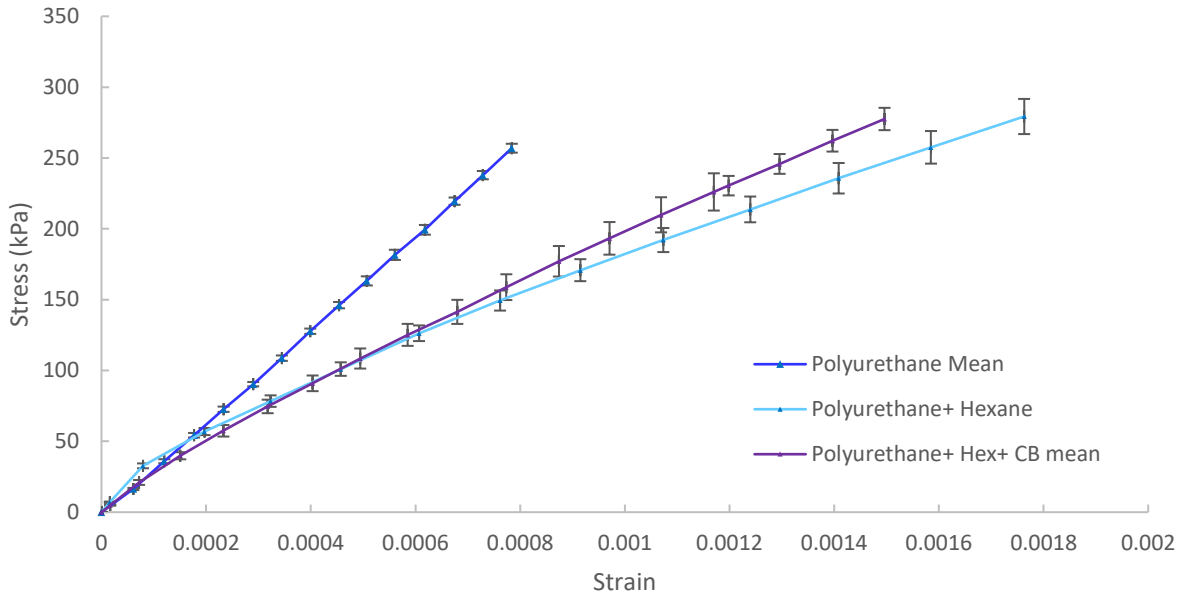


**Figure 32 Stress-strain curves comparison for polyurethane, polyurethane with hexane and polyurethane with hexane and carbon black biocompatible mixture.**

The backing of the electrode is expected to be flexible enough to bend to the round shapes of the body, but no maximum value for the material Young modulus is defined. Kim et al [59] proposed the use of a polyester substrate with a Young's modulus of 60 kPa for a sensor attached to the skin without microneedles. The argument to use such substrate is that a sensor substrate should have a Young's modulus close to that of the skin, 140-600 kPa for the epidermis and 80 kPa for the dermis [59]. According to this author, the electrode should bend and stretch as the skin does to avoid losing electrode contact on the skin wrinkles that according to this author have maximum thickness dimensions of 100  $\mu\text{m}$ . The microneedles of the proposed electrode in this thesis have an average height of around 600  $\mu\text{m}$ , that means that the wrinkles will not impede that such structures cross the stratum corneum.

Table 7 shows a comparison of the Young's modulus of the materials used to fabricate microneedle electrode backing found in the literature. The Young's modulus of the polyurethane

and carbon black mixture used to fabricate the backing of the microneedle electrode in this thesis is at least 10 times smaller than the materials proposed by other authors.

**Table 7 Materials used in the backing of microneedle electrodes.**

Author	Substrate material	Substrate material Young's modulus (PA)
Wang et al [58]	parylene	3.2 GPa
Griss et al [45]	silicon	140-180 GPa
Arai et al [77]	SU-8	2 GPa
Rent et al. [60]	polyethylene terephthalate (PET)	2 GPa
Electrode proposed in this thesis	polyurethane/carbon black blend	183 MPa

The application of the electrode should be simple, and it will most likely be applied with the hand in a clinical setting. Normally, when we bend some material sheet with the hand around a rounded part of the body we use the pinching force created by the thumb and the index fingers to bend the sheet as depicted in Figure 33.

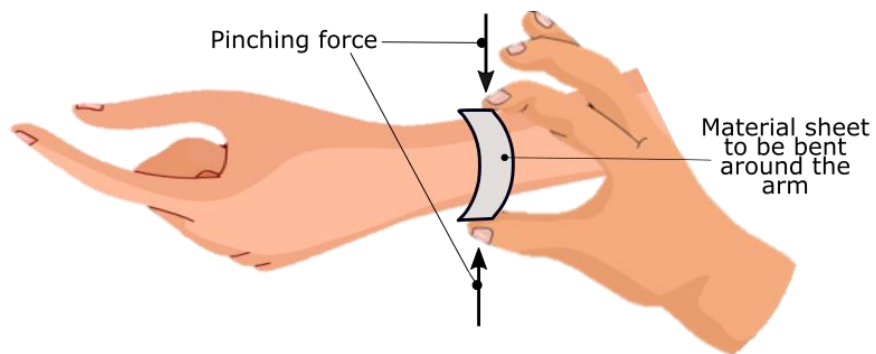


**Figure 33 Diagram of how a material sheet is bent around a body part.**

The force exerted between these fingers is approximately 80 N for males and around 50 N for females [70]. Thus, the electrode's backing should be able to easily bend (buckle) when a force with a magnitude below 50 N is applied on the edges of the electrode. Once again, to evaluate that the backing can easily bend, the critical load

$$P_{cr} = \frac{\pi E_{PU/Cb} I_{Bck}}{(l_{Bck}^2)} \quad (8)$$

was calculated using the Young's modulus of the Polyurethane/carbon black blend  $E_{PU/Cb}$ , the length of the of the electrode backing  $l_{Bck}$ , that is 1 cm long, and the area moment of inertia of the edge of the backing  $I_{Bck}$ . To calculate this load, the system was simplified and modeled as a hinged-hinged column as shown in Figure 34. The cross-sectional area of the “column” is the area of the rectangular edge of the backing of the electrode with dimensions of 0.4 mm by 1 cm.

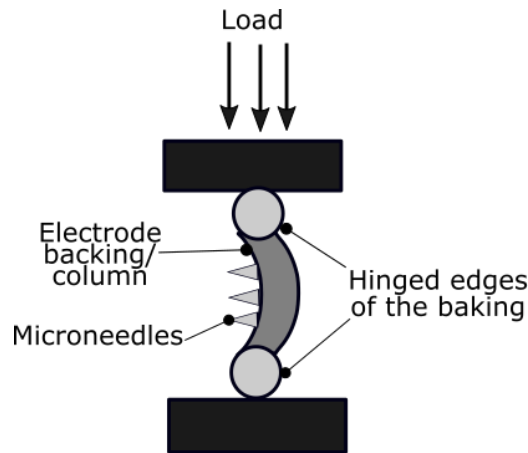


**Figure 34 Model used to approximate the critical load of the microneedle backing.**

The calculated critical load for of the backing structure fabricated with the polyurethane mixture is 0.96 N, this value is significantly lower than the 50 N maximum force exerted by the

pinching of the index and thumb fingers. These results validate that the electrode backing will easily bend when the pinching force is applied to its edges.

Finally, Table 8 shows the comparison between the microneedle’s material and the backing’s material used for the final electrode design. The desired goal of having a flexible backing material with stiff microneedle material is achieved as the Young’s modulus of the polyurethane mixture used for the backing of the electrode is 10 times smaller than the Young’s modulus of the medical grade epoxy resin and carbon black mixture used for the microneedle structures. Thus, the proposed fabrication method is suitable to manufacture a microneedle electrode with materials with different mechanical properties.

**Table 8 Young’s moduli comparison for the microneedle’s material and the backing material.**

<b>Material</b>	<b>Young modulus</b>
Biocompatible resin with carbon black	1.4 GPa
Polyurethane with carbon black and hexane	183 MPa

### **3.1.5 Metal coating selection**

Metals are widely used for electrodes as they are suitable for the reduction-oxidation reactions needed to have an ion interchange between the electrode and the electrolyte, in the case of a microneedle electrode the dermis tissue (supposed to be moist) is considered as the solid electrolyte. Furthermore, metals like gold, stainless steel and silver also have proven to be highly biocompatible [62]. When choosing a metal for an electrode coating, an important factor that comes into play is the half-cell potential created at the electrode-electrolyte interface, as the reduction of this potential lowers the noise when measuring low frequency signals like EEG. Silver is the most used metal for coating electrodes as it has 0.799 V half-cell potential, compared with a 1.680 V

potential for gold or a -1.706 V potential for an aluminum electrode. Moreover, silver can be treated with a chloride solution to produce a silver/ silver chloride electrode which helps to reduce the potential to 0.223 V [13].

## **3.2 Electrode testing methods**

### **3.2.1.1.1 Microneedle insertion tests**

Microneedle electrodes rely on the penetration of the stratum corneum to achieve a low impedance at the electrode-skin interface. Insertion tests are a common procedure to validate that microneedles can cross the stratum corneum specially for drug delivery [65][66]. Ideally, microneedle arrays should penetrate the skin by slightly pressing them against the skin surface, but researchers have found that the chance of crossing the stratum corneum improves by using a high velocity insertion method [85][86].

Microneedle skin insertion tests normally involve two main steps. First the needle or needle array is applied to the skin with a certain pressure or with a certain velocity. Then the electrode is removed, and a staining dye solution is applied to the microneedle insertion site. The dye binds to proteins found in the viable epidermis and not to the outer surface of the stratum corneum. As a result, after the dye is cleaned from the skin, the remaining dye indicates only the areas where the microneedle or microneedles arrays were able to pierce the stratum corneum. The proposed electrode design and chosen materials were assessed with an ex-vivo insertion test using porcine skin to validate that the electrode can pierce the stratum corneum.

### 3.2.1.2 Skin sample preparation

The fabricated electrode was evaluated on pig skin samples of a female Yorkshire pig skin excised from the abdomen, that were stored at  $-80^{\circ}\text{C}$  and defrosted each time a test was run. After defrosting the skin, the subcutaneous fat layer was removed with surgical scalpels and cut into 30mm x 25mm rectangular pieces with a thickness of around 1-2 mm. Each sample was stretched uniformly in radial direction with a 3D printed skin holder as shown in Figure 35. Porcine skin was used to emulate the behavior of human skin when the electrode is inserted, as the porcine skin has anatomical resemblance and similar mechanical properties to human skin [69]

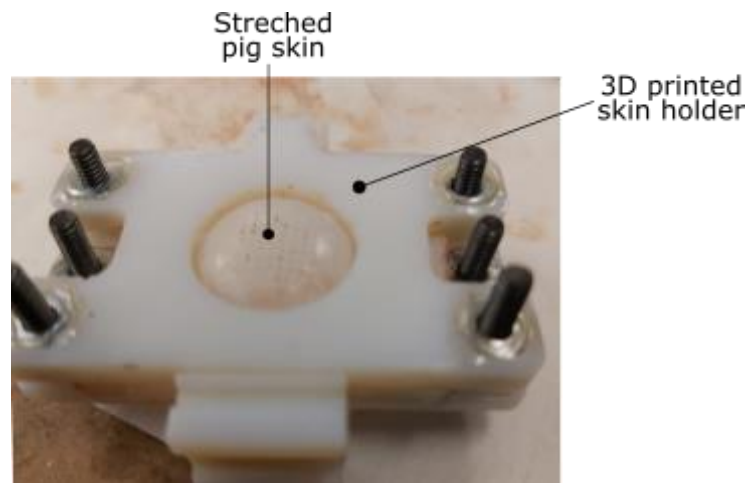


**Figure 35 Porcine skin stretched on the skin holder for insertion test.**

After the skin was prepared and stretched, the electrode is pressed against the skin. Two different methods were performed to press the electrode against the skin; for the first test only the pressure of the thumb was used to apply the electrode to the skin, and for the second test a high velocity inserter was used.

### 3.2.1.3 Insertion test with thumb pressure

In order to ensure a similar pressure distribution between the tests performed with the inserter and the tests with only the pressure of the thumb, the microneedle electrode was first attached to the syringe plastic tip cap similar to the one used to attach the electrode to the impact inserter as shown in Figure 36. An electrode array of 156 microneedles and 750  $\mu\text{m}$  center to center spacing was placed on the stretched skin together with the syringe tip cap and pressed with the thumb for 5 seconds. Similarly, the test was repeated with an electrode with 90 microneedles and a center to center spacing of 1,000  $\mu\text{m}$ .

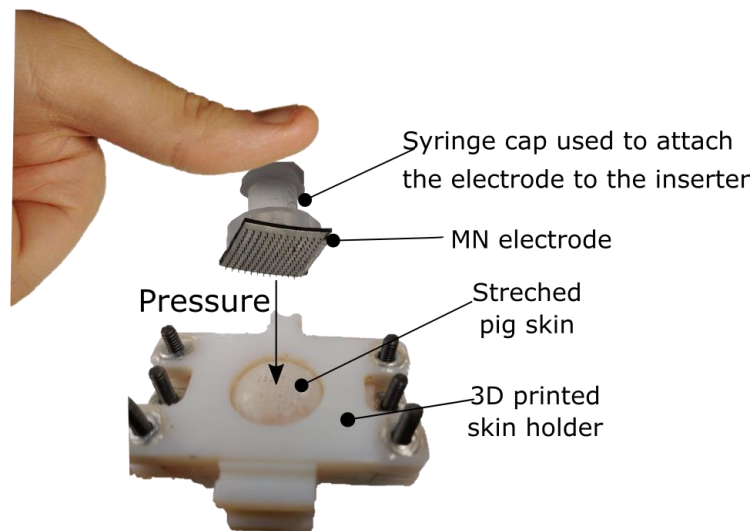
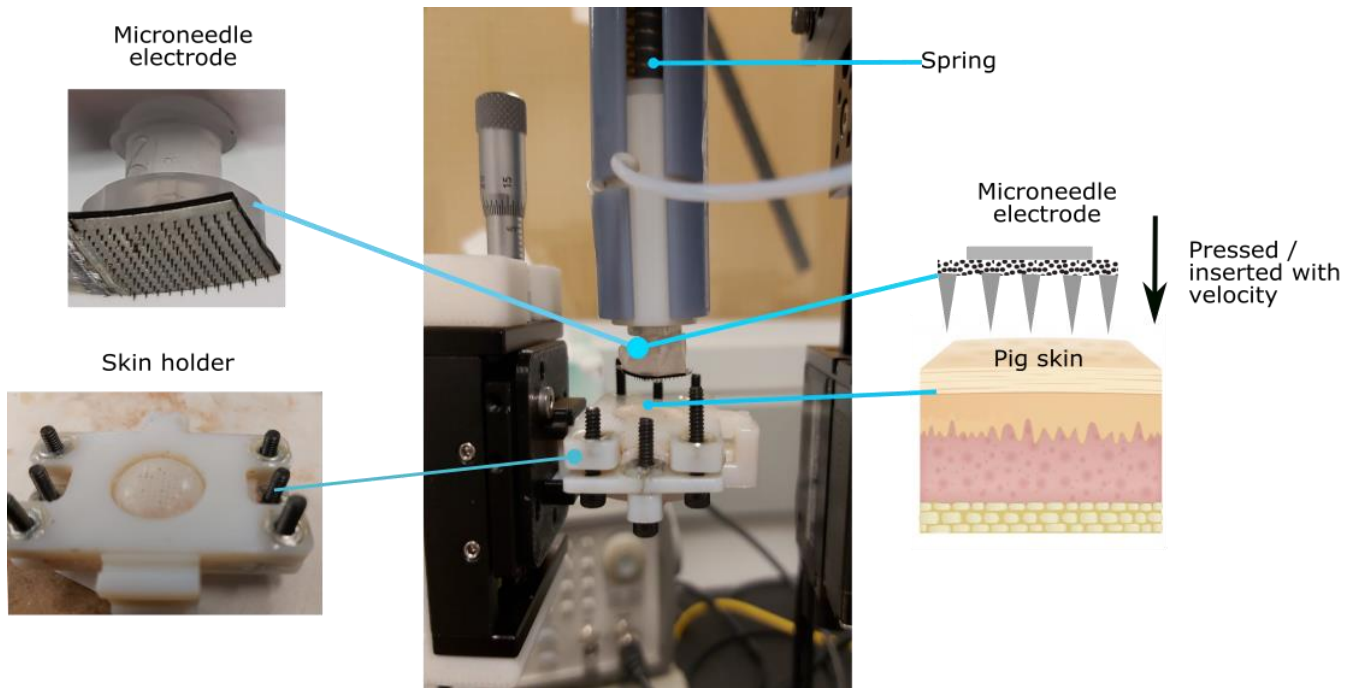


Figure 36 Insertion test set-up to apply the electrode by thumb pressure.

### 3.2.1.4 Insertion test using the high velocity impact inserter

The set-up for the insertion test with the impact inserter device previously used by [87] is shown in Figure 37. The electrode was adhered to the inserter using double sided tape and the syringe cap, used in the thumb pressure insertion test, with the microneedles facing downwards. The skin holder with the stretched skin is placed under the microneedles touching them but without any

pressure applied. Then the spring with a spring constant  $k = 343 \text{ N/m}$  is compressed by 15 mm and secured. When the spring of the inserter is released, the inserter pushes the electrode toward the skin where the electrode reaches a velocity of 2 m/s. An electrode array of 156 microneedles and 750  $\mu\text{m}$  center to center spacing was placed on the inserter and impacted on the stretched skin. Similarly, the test was repeated with an electrode with 90 microneedles with a center to center spacing of 1,000  $\mu\text{m}$ .



**Figure 37** Experimental set-up for microneedle electrode insertion test with impact inserter.

### 3.2.1.5 Dye

After inserting the microneedle electrode into a porcine skin sample, either by thumb pressure or with the inserter, the dye methylene blue is used to indicate the areas where the microneedles were able to pierce the stratum corneum. The dye is applied to the skin, covering the entire microneedle insertion site, and is left to rest on the skin for 1 minute. The dye is carefully cleaned off from the skin with a Kimtech wipe soaked in isopropanol alcohol. Methylene blue is a

dye that binds to nucleic acids (DNA and RNA biomolecules housed in the cell nucleus) and other cellular components [88]. It will only remain on the inner layers of the epidermis and dermis and will wash off from the stratum corneum as this layer is composed of flattened dead cells that have lost their nuclei [89]. As a result, after the dye is cleaned from the external surface of the skin the remaining stains will expose the areas where the microneedles were able to pierce the stratum corneum.

### **3.2.2 Short term electrode impedance test on a human subject**

When measuring biosignals, the impedance measured between the reference electrode and the recording electrode is a parameter used to evaluate the electrode-skin state. Ideally, to ensure acquisition of a signal with high quality, this impedance should be equal or less than 10 k $\Omega$  [90] for EEG recordings independent of the electrode placement. Conductive gel is applied between the conventional metal cup electrode and the skin to reduce the impedance. When the impedance is larger than this value after applying the gel, skin abrasion is performed to lower the electrode-skin impedance.

The aim of this project is to record biosignals without the use of conductive gel and without any kind of skin preparation or abrasion, so the performance of the fabricated device is evaluated with an impedance test without skin preparation. The test is performed over a frequency range from 0.5 to 200 Hz at 100 mV using a 1260A impedance analyzer (Solartron Analytical, UK). The impedance is measured between a metal cup electrode with conductive paste (Ten20, USA), placed on the left earlobe, and the fabricated electrode, placed in the Fp1 position (forehead) according to the 10-20 international system of EEG electrode placement [9]. The electrode placement for this test is shown in Figure 38.

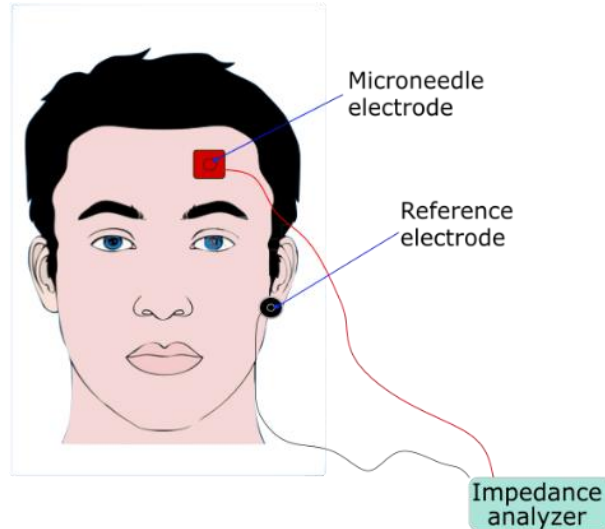


**Figure 38 Electrode placement for electrodes for short term impedance measurement.**

The measurement with the microneedle electrode is evaluated with two tests in two different days. For the first test, the electrode is applied by thumb pressure; for the second test the electrode is inserted using the impact inserter. The test is repeated on a different day with the wet electrode to compare the impedance values. The tests are run on different days to let the area of the skin, where the electrode was applied, heal by closing the holes generated by the electrode. If the tests are run one immediately after the other the moisture created in the skin after using the wet electrode could affect the measurement with the microneedle electrode. Similarly, if the microneedle electrode is first tested, and the wet electrode test is performed immediately after, the apertures in the skin created by the needles may affect the wet electrode impedance measurement.

### **3.2.3 Long term electrode impedance test on a human subject**

Baek et al, [31] have reported that when using wet electrodes for long-term measurements, the impedance at the skin-electrode interface normally tends to increase, reducing the quality of

the signals recorded. In order to evaluate the performance of the designed electrode during long term measurements, an 8-hour impedance test is performed to evaluate the stability of the device. For this test, the microneedle electrode is placed in the Fp1 position (forehead) and a reference wet electrode is placed on the left earlobe as shown in Figure 38. The impedance between both electrodes is measured every hour during 8 hours by applying a 100-mV amplitude stimulus signal at 40 Hz with a 4294A Precision impedance analyzer (Agilent Technologies, USA). Following a similar procedure to the short-term impedance test, the microneedle electrode is evaluated with both scenarios, applying it with thumb pressure and using the velocity inserter. The test is repeated on a different day with a wet electrode. Similarly to the short-term impedance test, the experiments are run on different days to let the skin heal.

### **3.3 Biosignal recordings**

#### **3.3.1 EEG evoked potential recording**

The microneedle electrode should be able to record EEG signals, but these signals do not have a well-defined morphology that would allow to differentiate the signal from noise with a simple analysis. Therefore, in order to validate that the fabricated electrode was able to record EEG signals, a visually evoked potential test was performed. During this test a subject is stimulated with a video with black and white frames changing at a fixed frequency. A response to this stimulus is reflected in the EEG signal recorded at the back of the head where the visual cortex is located. The frequency component of the stimulus signal can be identified in the frequency spectrum of the recorded EEG signal. Figure 39 shows the set up for this test.

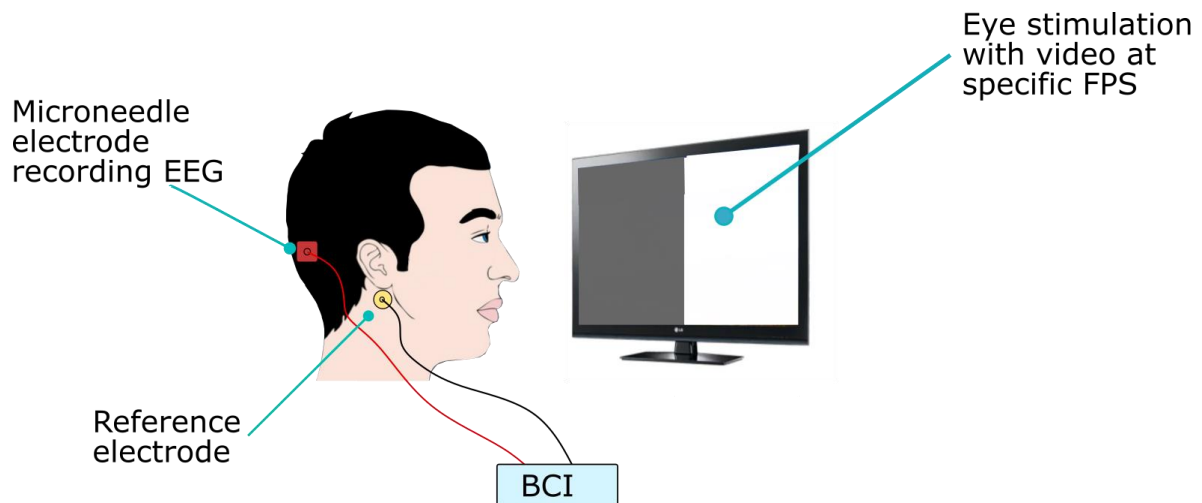


**Figure 39 Set up for EEG optically evoked potential test.**

An OpenBCI (OpenBCI, USA) acquisition development board is used to record the EEG signal. The fabricated electrode is placed at the occipital area in the O1 position according to the 10-20 placing system. A reference metal cup electrode with conductive paste is placed on the left earlobe and a second wet bias electrode is placed on the right earlobe. The eyes are stimulated at a frame rate of 5 fps, 8 fps, 20 fps and 26 fps. The recorded EEG signal recordings are processed with MATLAB to obtain the power spectrum of the signal in order to confirm whether the measured signal has a significant frequency content corresponding to the video frame rate used to stimulate the eye. An example of the frequency spectrum of the EEG signal recorded when the subject is stimulated with a 20 fps video is shown in Figure 40.

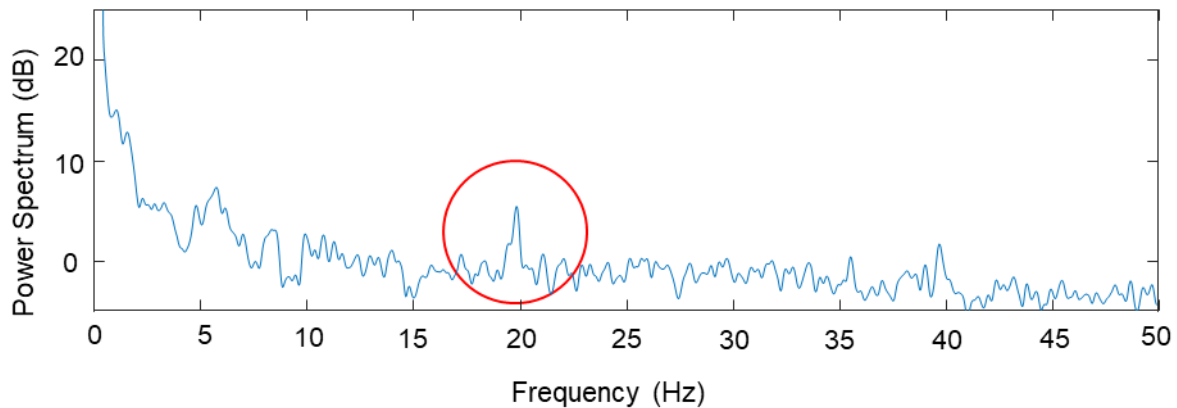


**Figure 40** Frequency spectrum of the EEG signal recorded from the occipital area of a subject stimulated with video at 20 FPS. The red circle highlights the peak produced by the stimulus signal.

The signal to noise ratio (SNR) is calculated for the recorded signals by calculating the difference between the peak power value of the frequency component of the stimulus signal and the noise floor mean 3 Hz around this peak.

For the EEG acquisition test the test was only performed by pressing the microneedle electrode onto a hairy area of the scalp with a thumb and spreading the hairs where the electrode was placed. The impact inserter device was not used as the hair might have dampened the impact of the electrode on the scalp, preventing proper inserting and anchoring.

### 3.3.2 ECG recording

The capability of the fabricated device to record a variety of biosignals is evaluated by measuring the electrocardiogram signal, which has a defined morphology composed by the P wave, QRS segment and T wave, shown in Figure 1.

The openBCI acquisition board is used to record the ECG signal using the micromachined electrode. For this test, the microspike array electrode is placed on the left wrist and a reference wet electrode is placed on the right wrist as depicted in Figure 41. This test is performed three

times, applying the microneedle electrode with the pressure of the thumb, applying the electrode with the impact inserter and as a reference, with a wet electrode instead of the microneedle electrode on the left wrist.

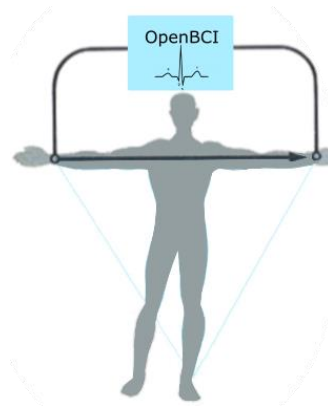


**Figure 41 Electrodes placement for ECG recording.**

The acquired signals are digitally filtered with MATLAB using a notch filter with a center frequency of 60 Hz to significantly attenuate the noise from the AC power line and a bandpass filter with a low cutoff and upper cutoff frequencies of 0.5 Hz and 50 Hz, respectively as the ECG is a low frequency signal.

The signal to noise ratio of the signals recorded with the three different methods is calculated as follows:

1. The recorded signals are cropped to a single cardiac cycle for 15 different periods, where one cycle is a time interval containing P, Q, R, S, T waves; Figure 42 shows an example of 5 periods of the cropped signal.

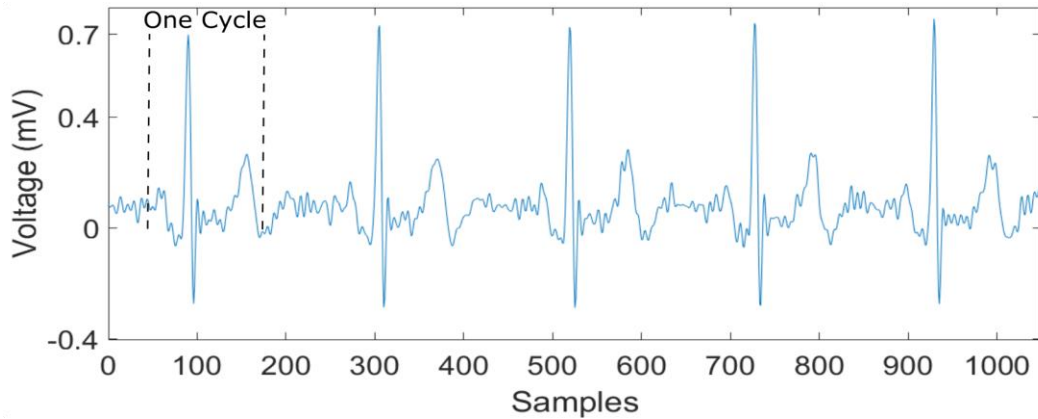


**Figure 42** Five heart cycles from the cropped signal recorded with a wet electrode.

2. The cropped signal is divided into cycles, that are aligned in time using the R peak as a reference; Figure 43 shows the superimposed cycles.

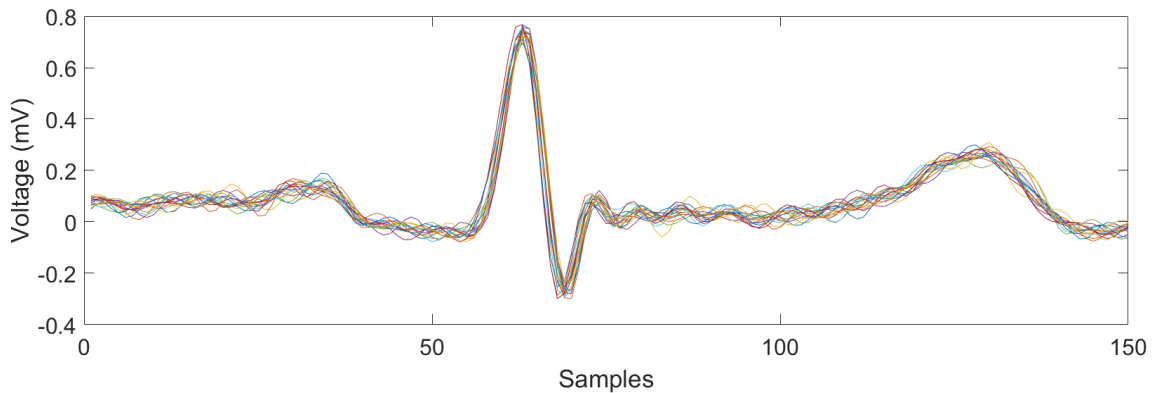


**Figure 43.** Fifteen heart cycles superimposed and aligned by the R peak from the signal recorded with a wet electrode.

3. An average cycle is obtained by calculating the mean of the data points at each time point of the 15 cycles. Figure 44 shows an example of the resulting average signal.

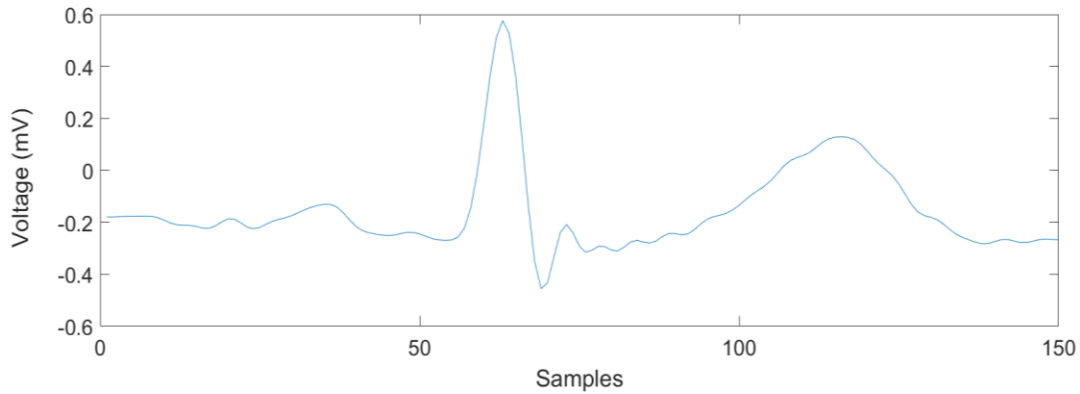


**Figure 44 Average signal from 15 heart cycles recorded with a wet electrode.**

4. The average signal is then subtracted from each original cardiac cycle to obtain the noise in the signal. Figure 45 shows an example of the resulting noise.

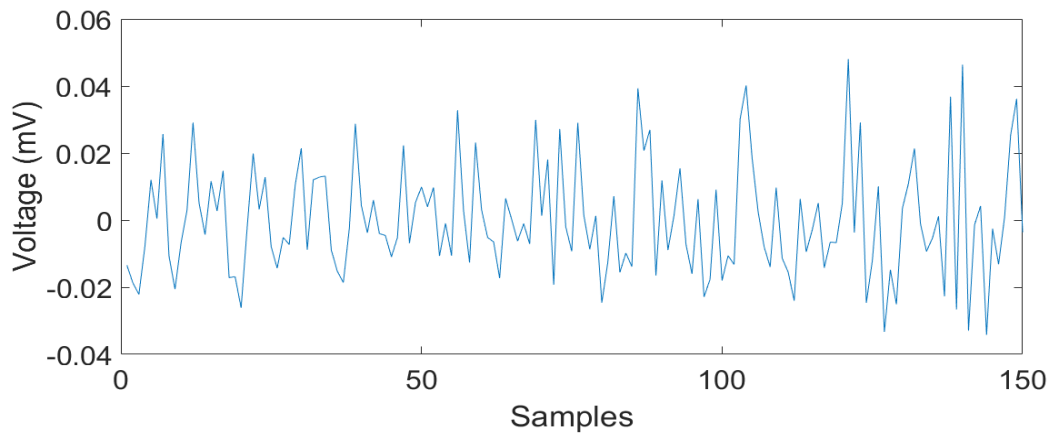


**Figure 45 Example of noise extracted from one heart cycle signal recorded with a wet electrode.**

5. The RMS value from such a noise signal is calculated and the RMS values of the different signals are used to calculate  $A_{\text{noise}}$ , the RMS value of the whole-time interval containing the 15 cycles.
6. The mean of the average signal is calculated and subtracted from this signal. The RMS value  $A_{\text{average signal}}$  is calculated from the resulting signal.

7. Finally, the signal to noise ratio

$$SNR = 20\text{Log}\left(\frac{A_{\text{Average signal}}}{A_{\text{noise}}}\right) \quad (9)$$

can be calculated.

## Chapter 4: Results

This chapter presents the results of the characterization experiments described in Section 3.2. It compares the performance of the microneedle electrode with the performance of such a standard wet electrode.

### 4.1 Skin insertion tests

#### 4.1.1 Thumb pressure insertion test

Following the testing method described in Chapter 3 Section 3.2.1.3., an electrode with 90 microneedles with a center to center spacing of 1,000  $\mu\text{m}$ , is inserted into the stretched skin sample with the pressure of a thumb. Figure 46 (a) shows that of the 90 microneedles only 5 microneedles are successfully inserted as indicated by the dye. Figure 46(b) shows the results for an electrode array of 156 microneedles with 750  $\mu\text{m}$  spacing. Only 23 of microneedles have successfully pierced the stratum corneum.

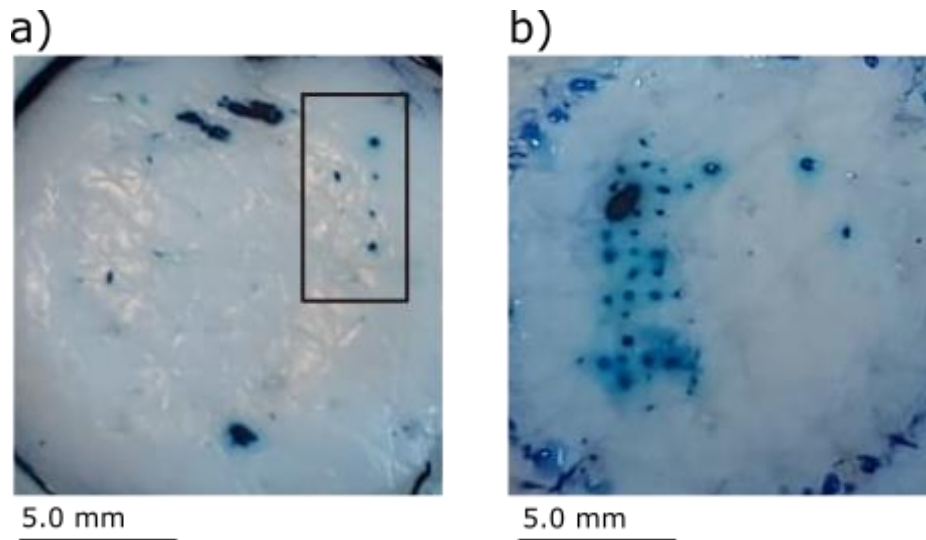


**Figure 46** Pig skin samples after insertion test pressing the microneedle electrode with the thumb. The blue dots dyed with the methylene blue are the areas where the microneedles crossed the skin (a) results with the electrode with 1000  $\mu\text{m}$  pitch (b) results with the electrode with 750  $\mu\text{m}$  pitch.

The results obtained through these tests are unexpected as the electrode with a microneedle center to center distance of 1000  $\mu\text{m}$  should penetrate the skin easier than the electrode with a center to center distance of 750  $\mu\text{m}$ , as the pressure applied to the denser array is distributed over more microneedles such that each microneedle is pressed with less force. A possible explanation to this could be a different pressure applied for both tests, as it is hard to control the exact amount of pressure applied with the thumb between tests. Most likely, a higher pressure was applied when performing the test with the electrode with a 750  $\mu\text{m}$  needles separation. Similarly, it seems that the pressure of the thumb on the electrode is not uniform across the backing area, as we can observe that the microneedles penetrated in specific areas, only in the top-right section for the electrode with 1000  $\mu\text{m}$  spacing and only in the left side for the microneedle with 750  $\mu\text{m}$  spacing. Ideally, the electrode is applied to the body by the pressure from a thumb, but the inconsistent distribution and magnitude of the force need to be addressed; this could perhaps be achieved using a load cell to apply a uniform force on the electrode backing area and a repeatable force magnitude.

Although some of the microneedles were able to cross the stratum corneum, this is not the ideal scenario as we want all the microneedles to cross the stratum corneum to increase the contact area of the electrode with the epidermis to reduce the impedance at the electrode skin interface. In order to increase the number of microneedles that cross the stratum corneum, an inserter is used.

#### **4.1.2 High velocity impact insertion test**

The insertion test is repeated with the high velocity impact inserter as described in chapter 3 section 3.2.1.4. Figure 47 (a) shows the result for the electrode with 156 microneedles and a

750  $\mu\text{m}$  center to center spacing. The pattern created by the microneedle insertion resembles a duplicated needle pattern, which may be produced by the electrode bouncing and making a second insertion into the skin. Without counting the second insertion holes, from the 156 microneedles only 115 penetrate the skin during what appears to be the initial impact.

Similarly, Figure 47 (b) shows the result for an electrode with 90 microneedles with a center to center spacing of 1,000  $\mu\text{m}$ . Only 64 successful microneedle insertions are clearly indicated by the dye.

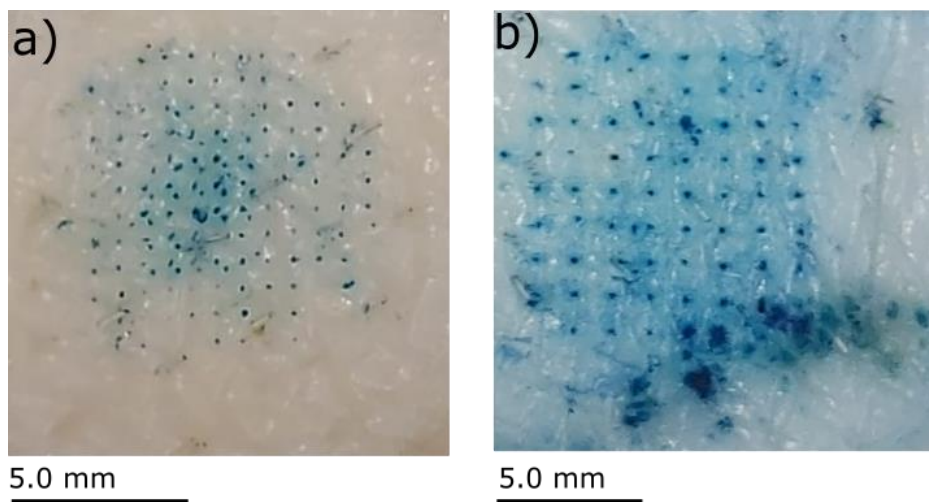


**Figure 47 Pig skin samples after insertion tests using microneedle electrodes with the high velocity impact inserter. The blue dots are the areas where the microneedles crossed the skin (a) results with the electrode with 750  $\mu\text{m}$  pitch (b) results with the electrode with 1000  $\mu\text{m}$  pitch.**

The performed insertion tests confirmed reports in the literature as they corroborate that using a high velocity impact inserter increases the number of microneedles crossing the stratum corneum. This will produce a higher contact area of the electrode with wet cells reducing the impedance at the electrode skin interface.

Apparently, the electrode bouncing and microneedle reinsertion only happened with the electrode with a microneedle center to the center separation of 750  $\mu\text{m}$ . Bouncing could have happened with the electrode with a pitch of 1000  $\mu\text{m}$ , and as this electrode theoretically needs less

pressure to pierce the skin, the needles penetrated deeper into it. If the electrode penetrates deeper, once the electrode bounces back up the needles may not get out of the skin so reinsertion does not happen. In Figure 47, we can observe that the microneedle insertion points of the electrode with a 750  $\mu\text{m}$  pitch look slightly smaller than the insertion points with the electrode with a 1000  $\mu\text{m}$  pitch. Therefore, this last electrode probably penetrated deeper into the skin.

This test also showed that even when using the impact inserter not all the microneedles of the electrode penetrated the skin. In Figure 47, we observe that all the needles at the center of the electrode penetrated while the needles at the periphery of the array that did not penetrate. This problem is most likely created by the 3D printed skin holder used to stretch the skin for these tests. As shown in Figure 48, such holder seems to create a curvature on the skin when it stretches it, and as the electrode is not able to bend when is applied with the inserter, the needles at the border of the array will not penetrate the skin. Further tests are needed with a skin holder that stretches the skin while keeping it flat for a larger skin area.

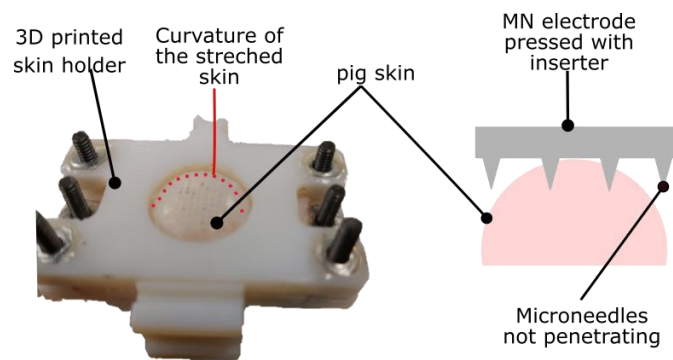


**Figure 48 Curvature of the skin created by the 3D printed skin holder and the effect of it on the microneedle insertion test.**

## 4.2 Impedance tests on a human subject

### 4.2.1 Short-term impedance test

A microneedle electrode with 156 microneedles and 750  $\mu\text{m}$  center to center distance is used to run a short-term impedance experiment as described in Chapter 3 Section 3.2.2 without any type of skin preparation. The test is performed on a human subject in two different days, first with the microneedle electrode inserted with the pressure of a thumb, then with the microneedle electrode inserted with the high velocity impact inserter. The same test is performed on the following day using a cup electrode with conductive paste (wet electrode). The results of this test are shown in Figure 49.

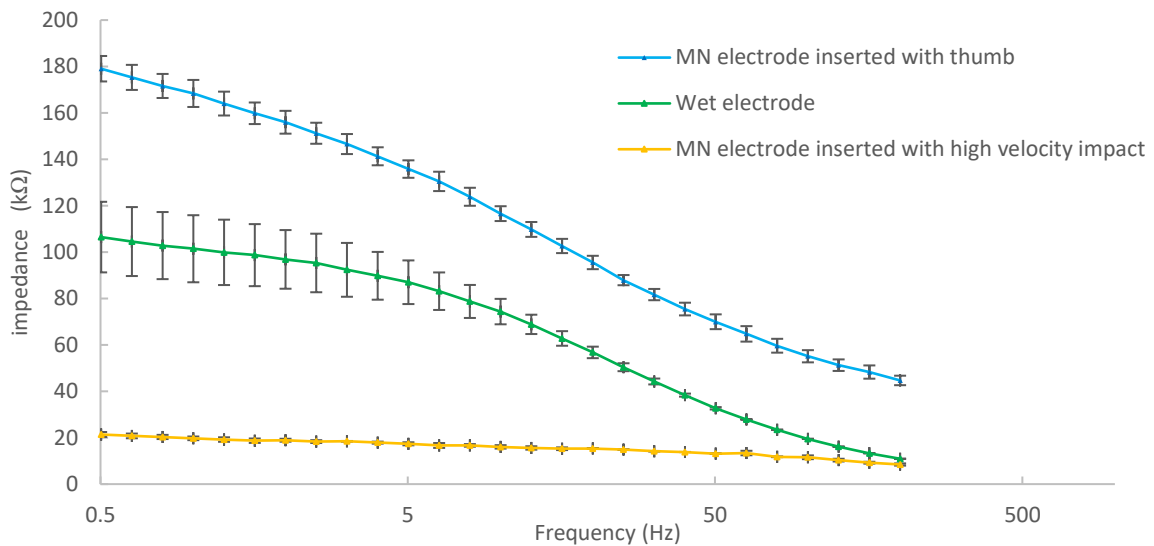


**Figure 49** Short-term impedance measurement between a reference (wet) electrode placed on the right earlobe and a wet electrode (green line), a microneedle electrode pressed with the thumb (blue line) or a microneedle electrode inserted with a high velocity inserter (yellow line) placed in the Fp1 position (left side in the forehead). The curves show the mean value from 3 different measurements and the error bars correspond to the calculated standard error.

When the microfabricated electrode is inserted with the pressure of a thumb, it has an impedance value higher but comparable to the wet electrode without performing skin abrasion. As demonstrated by the insertion tests, probably just a small amount of the total number of

microneedles are crossing the stratum corneum thus the impedance component of the skin layer still affects the impedance measurement. When inserting the microneedle electrode using the high velocity impact inserter the impedance at the electrode-skin interface is considerably reduced. Still none of the electrodes complies with the requirement of achieving an impedance lower than 10 k $\Omega$  without skin abrasion.

#### 4.2.2 Long-term impedance test

A microneedle electrode with 156 microneedles and 750  $\mu\text{m}$  center to center distance is used to run a long-term impedance experiment as described in Chapter 3 Section 3.2.3 without any type of skin preparation. The results of the three measurements are shown in Figure 50.

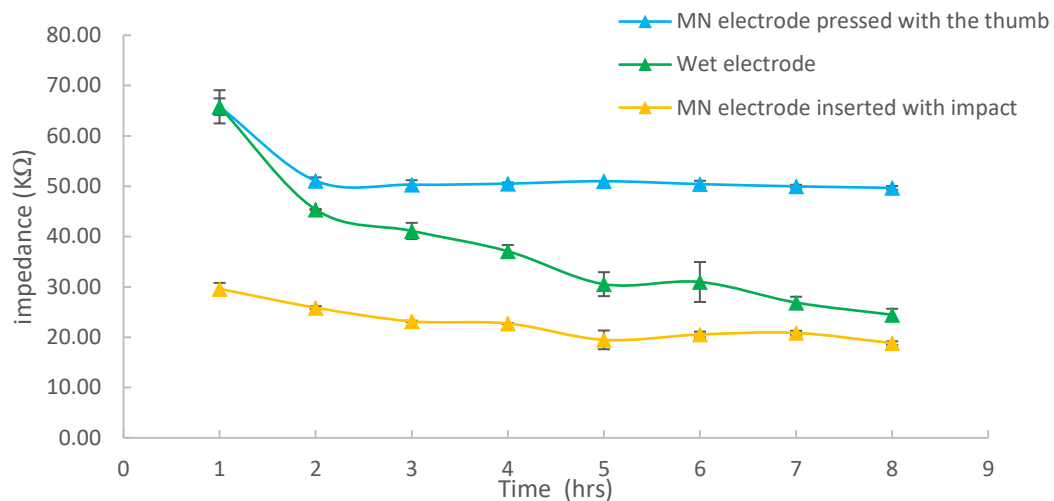


**Figure 50** Long term impedance measurement at 40 Hz between a reference electrode placed on the right earlobe and a wet electrode (green line), a microneedle electrode pressed against the skin with the thumb (blue line) or a microneedle electrode inserted with a high velocity inserter (yellow line) placed in the Fp1 position (left side in the forehead). The curves show the mean value from 2 different measurements and the error bars correspond to the calculated standard error.

The obtained results of the experiment show a gradual decrease in the impedance measured with the three electrodes in the first hour. This behavior is expected from all the electrodes right after the placement of the electrodes; this results from the accumulation of perspiration under the electrodes and generally reaches a steady state after 30 minutes [91]. Additionally, the results from

this experiment show that the microneedle electrode inserted with both methods has a more stable impedance than the wet electrode during the long-term measurements with almost not change after the first hour. As seen before, the microneedle electrode applied using the impact inserter has a better performance than the wet electrode and the microneedle electrode applied by thumb pressure.

From the literature it was expected that the wet electrode's impedance would increase over time as reported by [36][19], but during the two different experiments performed the impedance actually decreases. Nevertheless, the impedance of this electrode seems less stable over time which is not desired as these variations will affect the quality of the recording signals. These changes in impedance are most likely due to the changes of the conductive gel.

A headband and medical tape are used to keep the electrodes in place during the 8-hour measurement. Such a band and the tape could maintain the temperature higher than normal in the area where the electrode is placed, creating more sweat over time and keeping the stratum corneum and electrolytic gel moist. Such effect could explain why the wet electrode impedance decreases over time.

### **4.3 Signal acquisition tests on a human subject**

#### **4.3.1 EEG evoked potential test**

An EEG evoked potential test was performed and the results analyzed as described in Chapter 3, Section 3.3.1 and the resulting SNR for measurements of both electrodes for this test are shown in Figure 51.

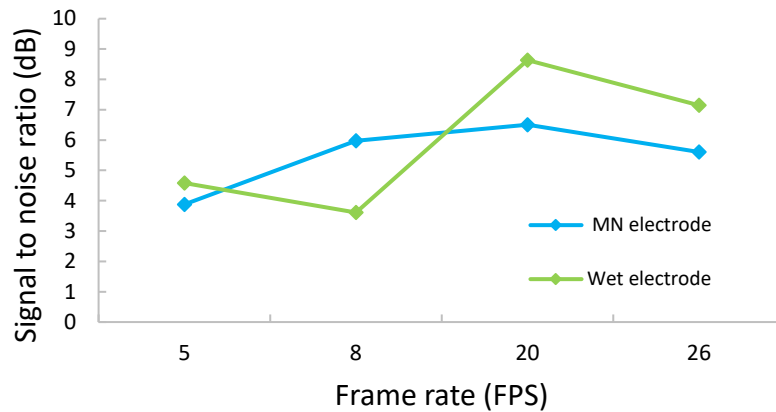


**Figure 51** Signal to noise ratio for the EEG visually evoked potential test for videos with different frame rate.

The comparison shows that the SNR for both electrodes is similar when recording on the hairy section of the scalp. For this test the microneedle electrode is only pressed against the hairy scalp after spreading the hair in the area where the microneedle was placed, as pointed out in Chapter 3. The use of the high velocity impact inserter is not likely going to make a difference for this measurement as the hair will dampen the impact. So, having a similar performance of the pressed microneedle electrode and the wet electrode is expected. This test validates that the microneedle electrode is able to record EEG signals and proves its potential to record over the hairy area of the scalp.

### 4.3.2 ECG recording test

The capability of the fabricated device to record a variety of biosignals is evaluated by measuring the electrocardiogram signal, which has a defined morphology composed by the P wave, QRS segment and T waves. The ECG recording test is executed and the recorded signals are analyzed as described in Chapter 3, Section 3.3.2. Figure 52 shows the average of the signals recorded with the three different procedures: using a wet electrode, using a microneedle electrode

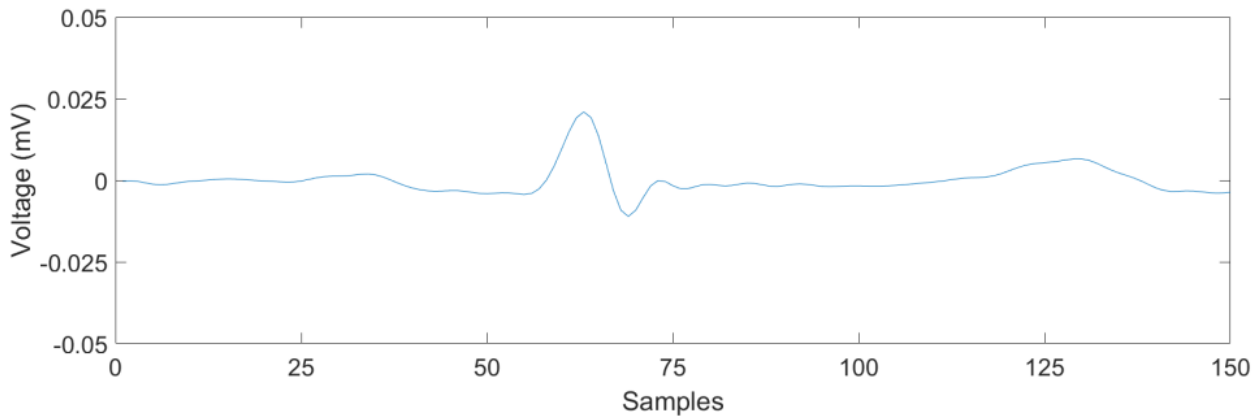
inserted with a velocity impact inserter and using the microneedle electrode inserted using only the thumb pressure. Table 9 shows the corresponding RMS voltage for these signals. It is evident that the wet electrode has a higher amplitude and a larger voltage difference between the “R” and “S” waves, almost 10 times larger than both the microneedle electrode inserted with thumb pressure and high impact inserter. Correspondingly, the RMS voltage for the wet electrode also has the highest value.

The ECG signal recorded with the microneedle electrode inserted with the thumb has a lower RMS value than the electrode inserted with a high-velocity impact. Most likely, a few microneedles from the electrode applied with an impact penetrated the stratum corneum, so this electrode is able to record the ECG signal with a higher amplitude as opposed to the ECG signal recorded with the electrode pressed with the thumb. However, not enough of the needles crossed the stratum corneum to record signals with an amplitude as high as the wet electrode.

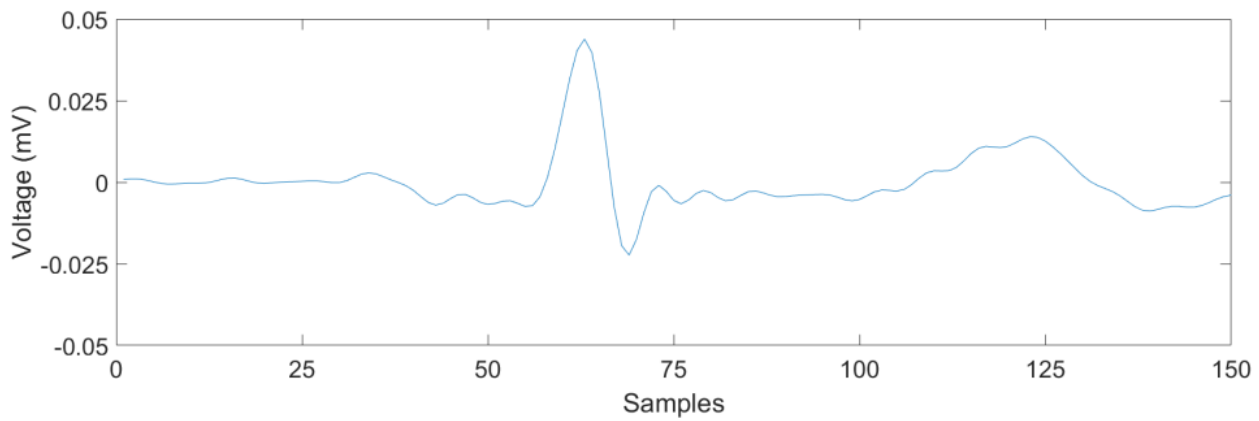
**Table 9 RMS Voltage for ECG signals recorded with wet electrode, microneedle electrode inserted with the pressure of the thumb and microneedle electrode inserted with high velocity impact**

<b>Recording method</b>	<b>Signal average RMS voltage (mV)</b>
Wet electrode	0.137
Microneedle electrode inserted with thumb pressure	0.0044
Microneedle electrode inserted with impact inserter	0.0092

(a) Microneedle electrode inserted with thumb pressure



(b) Microneedle electrode inserted with high velocity impact inserter



(c) Wet electrode

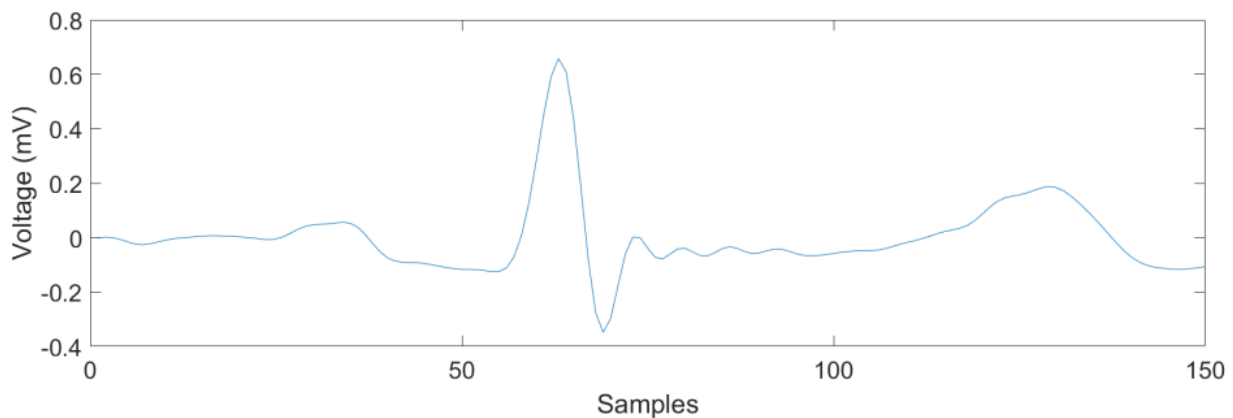


**Figure 52 ECG signal recording average (15 cycles) recorded with: (a) Microneedle electrode inserted with thumb pressure, (b) microneedle electrode inserted with high velocity inserter, (c) wet electrode.**

The signal-to-noise ratio calculated as described in Section 3.7.2 for each recording is shown in Table 10. The signal to noise ratio of the wet electrode is almost 2 times higher than the better SNR of both recordings with the microneedle electrode. This was not expected as the microneedle electrode inserted with the high velocity impact shows a lower impedance measurement on the forehead. One possible explanation could be the skin's anatomical variation between the forehead and the arms; the skin on the arms seems looser compared with the skin on the head and the tissue underneath the skin in the wrist is softer than the skull underneath the skin of the scalp. Probably not all the microneedles are penetrating the skin in the arms as the impact of the electrode is damped, thus the contact area of the electrode is reduced.

The ECG signal recorded with the microneedle electrode inserted with an impact has a signal to noise ratio 5 times higher than the signal recorded with the electrode inserted with the pressure of the thumb. Most of the noise at the electrode-tissue interface has a low amplitude and is caused mainly by the half-cell potential when no motion artifact is present. If the electrode inserted with an impact is able to record an ECG signal with a higher amplitude, this means that the signal will be less prone to the low amplitude noise. Additionally, if not a single needle crossed the stratum corneum when the electrode was pressed with the thumb, this electrode could be acting as a capacitive electrode with the stratum corneum behaving as the insulator between the electrode conductive needles surface and the moist subcorneum skin tissue. As explained before, a capacitive electrode is more prone to noise due to the high impedance of the stratum corneum and to the polarization of the electrode.

For this test the reference electrode used was a wet electrode that may add some impedance to the recording. Thus, further testing using microneedle electrodes for both, the reference and the

recording electrode, are needed to evaluate if that improves the signal to noise ratio and amplitude of the recorded signal, and the impedance at the skin-electrode interface.

Nevertheless, these tests demonstrated that the microneedle electrode is able to record ECG signals without skin preparation. An interesting test to run should be an ECG long-term recording test to evaluate if their recordings with the microneedle electrode maintain a constant signal to noise ratio and signal amplitude, and if the recordings performed with the wet electrode decrease their quality.

**Table 10 ECG signal to noise ratio comparison between wet electrode, microneedle electrode inserted with the thumb pressure, microneedle electrode inserted with the high velocity impact inserter.**

<b>Recording method</b>	<b>Signal to noise ratio (dB)</b>
Wet electrode	14.2
Microneedle electrode inserted with thumb pressure	1.4
Microneedle electrode inserted with impact inserter	7.9

## **Chapter 5: Conclusions and future work**

This chapter recapitulates the results presented in this thesis, describes the conclusions drawn from the experimental results, and proposes possible future research directions.

The objective of this thesis was to design a dry electrode able to record EEG and ECG signals. The fabrication process for such electrode should be simple and minimize the use of expensive equipment and facilities. The materials of the electrode should be biocompatible, as inexpensive as possible and, should have specific mechanical properties to allow the microneedles to pierce the stratum corneum and simultaneously allow the backing to adapt to body shape.

### **5.1 Conclusions**

#### **5.1.1 Electrode design**

This work proposed a microneedle electrode design and demonstrates that it is capable of recording electroencephalogram and electrocardiogram signals. The electrode can cross the outmost layer of the skin reducing the impedance of the skin-electrode interface without skin abrasion. The electrode design has a flexible backing that allows to improve the mechanical attachment of the device to the round shapes of the body, this may reduce the chances to have motion artifact while recording biosignals.

#### **5.1.2 Fabrication method**

This work proposed the design and a simple microfabrication process of a microneedle electrode for biosignals monitoring. The fabrication process is suitable for mass production of the device as the electrode is made based on mold casting techniques that allow to produce multiple electrodes in parallel. This process reduces the time spent in the cleanroom, as the use of this space

is only required to produce the master mold that can be reused multiple times to produce multiple PDMS molds. The PDMS mold can be reused to create many electrodes. The proposed fabrication method allows to fabricate an electrode with a stiff polymer for the microneedle structures and a flexible material for the backing.

The fabrication process used to pattern the SU-8 with microneedle structures allows to produce an array that is able to cross the stratum corneum. If the blend of carbon black and biocompatible resin is used to fabricate the electrode, the array of microneedles with a tip diameter of 100  $\mu\text{m}$  is the optimal shape to fabricate the electrode because is the only structure that will not buckle when the electrode is pressed against the skin. However, in order to avoid the use of the impact inserter and to simplify the application of the electrode, the device needs sharper microneedles. The fabrication of such structures requires a stiffer material than the proposed material in this thesis.

An alternative to increase the chances of the microneedles to cross the stratum corneum is to increase the radius of the base and the taper angle while a small tip diameter is maintained. Fabrication of such structures can be achieved by modifying the gap between the mask and the wafer. It was not possible to optimize this gap as the mask aligner used in this work does not allow to modify the separation between the mask and the wafer.

After evaluating different methods to perform the metal deposition on the electrode microneedles, it was found that a more uniform coating was achieved using a sputter deposition process. This method is simple and can be used for high-volume production. Nevertheless, the electroplating attempts showed that the electrode can be partially coated by this method. More research is necessary to optimize the electroplating process to achieve a uniform layer; this

deposition method would be preferred over sputter deposition as the set-up for electroplating is significantly less expensive than a sputter deposition tool.

### **5.1.3 Electrode materials**

The selected materials for the microneedle electrode provide the electrical properties needed to record biosignals without an electrolytic gel. The mechanical properties of the microneedle structures with a 100  $\mu\text{m}$  tip diameter are adequate to cross the stratum corneum, and the biocompatibility of these materials are supposed to avoid producing allergic reactions while the electrode is attached to the skin.

Biocompatibility was the most important parameter while choosing the microneedle material. The selected medical epoxy resin has a certification of the cytotoxicity test approval. However, as discussed in section 3.5, such resin is not suitable for structures with tip diameters smaller than 100  $\mu\text{m}$ . Further research is needed in order to find proper materials that can be cast at low temperatures to fabricate the microneedle structures with smaller radii. Table 11 shows the required minimum of Young's modulus needed to fabricate such structures.

**Table 11 Materials Young's modulus needed to fabricate microneedles with smaller radii.**

<b>Mask diameter (<math>\mu\text{m}</math>)</b>	<b>Materials Young's modulus needed to cross the SC (GPa)</b>
20	21.44
30	9.53
40	5.36
50	3.43
60	2.38
100	0.85

Ideally, the electrode should be applied without the use of an impact inserter and most likely the hand will be used in a real situation. As discussed in section 3.5, the materials used for the backing of the electrode allows to easily bend the device with the pressure applied between the thumb and the index finger, proven that the device can adapt to the rounded shapes of the body. Apart from the mechanical properties of the backing material, the 12 k $\Omega$  resistance between the surface of the microneedle and the backing needs to be reduced. The total impedance measured between two electrodes applied to the body needs to be less than 10 k $\Omega$ . Thus, further research is needed to optimize this parameter.

#### **5.1.4 Biosignal recoding performance**

This thesis demonstrated that the fabricated electrode can record EEG and ECG signals without the use of a conductive gel or skin preparation. Nevertheless, the EEG signal recording showed that the microneedle electrode can achieve a similar signal to noise ratio as a conventional wet electrode when the electrode is placed on the scalp. For the ECG signal recording, the wet

electrode performance was significantly better than the microneedle electrode. This was not expected as the impedance measurements from the forehead with the microneedle electrode inserted with a high velocity impact were lower than the wet electrode, thus signals with higher amplitude were expected when the ECG measurement was done with the microneedle electrode. One possible explanation to this discrepancy, is the anatomical differences between the skin and the structure of the forehead compared to the wrist where the electrode was attached for the ECG test. The skin on the wrist has soft tissue underneath as opposed to the forehead that has much less soft tissue but rather hard tissue (the skull) under it. The soft tissue under the skin of the wrist could dampen the impact insertion avoiding the penetration of all the needles of the electrode.

## **5.2 Suggested future work**

When the fabricated electrode is inserted into the skin with a high velocity impact, it provides a lower impedance than the wet electrode at the skin-electrode interface, when no skin preparation is performed. The impedance for high-velocity insertion is around 25 k $\Omega$  at low frequencies, which is still higher than the recommended value of 10 k $\Omega$  suggested in the polysomnography standard. This could be improved by modifying the material used to fabricate the microneedles as the resistance measured between a tip of one needle and the metal sheet attached to the back of the electrode is approximately 12 k $\Omega$  as discussed in Chapter 2. This value is relatively high compared with microneedles made out of highly conductive materials like metals, that most likely have a resistance between the tip and the backing of less than 1  $\Omega$ . However, as mentioned before fabricating microneedles from metals is quite complicated or may require expensive equipment, and it is challenging to combine metal microneedles with a flexible backing.

Thus, in order to improve the current design, it will be interesting to fabricate the electrode with different polymers that can be mixed with higher concentrations of carbon black to increase the conductivity of the electrode body and evaluate if that helps to reduce the impedance of the electrode. An alternative is the use of different types of carbon black, with larger particle dimensions that might increase the contact between particles inside the polymer blend. The use of silver particles commonly used for conductive inks is also a viable alternative, although this material will increase the cost of the device.

The silver coating connects the surface of the microneedles reducing the impedance between any point in this surface and the backside of the electrode below 12 k $\Omega$ . Thus, it will be interesting to perform further testing using electrodes with a higher microneedle density or an electrode with a larger area to optimize the electrode design

Another interesting research direction will be to treat the silver coating of the electrode to produce a silver chloride compound, this may help to increase the ion conduction at the skin electrode interface.

Ideally the microneedle electrode should be able to penetrate the outmost layer of the skin without the use of the impact inserter. Apart from the pressure and velocity used to insert the microneedle into the skin, the ability of the electrode to cross the skin can be improved using shaper microneedle structures. In this work the microneedles used for testing have a 100  $\mu\text{m}$  diameter tip, since the SU-8 mold for these was the first one to be successfully fabricated, thus they were used to develop the following electrode fabrication steps while working simultaneously to fabricate sharper microneedles with SU-8.

According to the critical load calculations discussed in section 3.5, if the biocompatible resin and carbon black blend is used to fabricate microneedles with a tip diameter smaller than

100 $\mu$ m, such structures will probably bend when they are pressed against the skin. Therefore, future research could be directed towards the fabrication of sharper microneedles using stiffer polymers. There are two aspects to consider for this research direction, one of them is the material used as the tip diameter of the needles is reduced, the material used to fabricate the structures should be stiff enough in order to avoid bending of the microneedle structures when they are pressed on the skin. The second aspect is the fabrication method as the materials selected will dictate the possible fabrication methods for the microneedle structures.

The silver deposition process of the electrode surface was performed with a sputter deposition tool after a uniform deposition by electroplating was not achieved. The use of such equipment increases the costs of the fabrication process. Mansoor et al. [76] have demonstrated that nickel deposition is possible on carbon black/polymer mixtures by electroplating. Further research could be performed to solve the uniformity problem encountered in this work. It will be interesting to investigate ways to improve the distribution of carbon black particles, as this may be the most likely cause of the non-uniform deposition. Methods to treat the surface of the electrode before metal deposition could be also investigated in order to improve the adhesion of the silver layer to the electrode surface.

### **5.3 Application of the research findings**

Although there are some challenges to overcome before the electrode prototype presented in this thesis becomes a replacement of the wet electrode, the results corroborate the potential of the device. The stable impedance of the electrode makes it a viable alternative for long term biosignal recordings, where the electrode does not need to be removed and applied multiple times. Applications for the developed electrode include brain computer interfaces and any diagnostics

procedure that requires ECG and EEG long-term recordings like sleep disorder monitoring. The proposed fabrication method provides a simple alternative to produce microneedle electrodes by mold casting with different materials for the microneedle structures and the backing. This process can be modified to fabricate electrodes with other polymers or other materials that can be cast at low temperatures.

## Bibliography

- [1] E. Kaniusas and E. Kaniusas, *Linking physiological phenomena and biosignals*. Berlin: Springer, 2012.
- [2] S. Ha, C. Kim, Y. M. Chi, and G. Cauwenberghs, “Chapter 4.3 - Low-Power Integrated Circuit Design for Wearable Biopotential Sensing,” in *Wearable Sensors*, E. Sazonov and M. R. Neuman, Eds. Oxford: Academic Press, 2014, pp. 323–352.
- [3] E. Kaniusas, *Biomedical Signals and Sensors III: Linking Electric Biosignals and Biomedical Sensors*. Cham: Springer International Publishing, 2019.
- [4] J. E. Hall, “The Normal Electrocardiogram, The Normal Electrocardiogram,” in *Guyton and Hall Textbook of Medical Physiology*, 13th ed., Philadelphia, PA: Elsevier, 2016, pp. 131–137.
- [5] A. L. Goldberger, Z. D. Goldberger, and A. Shvilkin, “ECG Leads,” in *Goldberger’s Clinical Electrocardiography*, 9th ed., Philadelphia, PA, 2018, pp. 21–31.
- [6] G. R. Müller-Putz, “Chapter 18 - Electroencephalography,” in *Handbook of Clinical Neurology*, vol. 168, N. F. Ramsey and J. del R. Millán, Eds. Elsevier, 2020, pp. 249–262.
- [7] F. Amzica and F. H. L. da Silva, *Cellular Substrates of Brain Rhythms*. Oxford University Press.
- [8] J. G. Webster, “Medical Instrumentation: Application and Design,” 1997, doi: 10.1097/00004669-197807000-00017.
- [9] O. Mecarelli, “Electrode Placement Systems and Montages,” in *Clinical Electroencephalography*, O. Mecarelli, Ed. Cham: Springer International Publishing, 2019, pp. 35–52.
- [10] O. G. Martinsen and S. Grimnes, *Bioimpedance and Bioelectricity Basics*. Academic Press, 2011.
- [11] S. Standring, “Skin and its appendages,” in *Gray’s Anatomy*, Philadelphia, PA, 2016, pp. 141-161.e1.
- [12] L. A. Geddes, “Historical evolution of circuit models for the electrode-electrolyte interface,” *Ann Biomed Eng*, vol. 25, no. 1, pp. 1–14, Jan. 1997, doi: 10.1007/BF02738534.
- [13] Y. David, W. W. von Maltzahn, M. R. Neuman, and J. D. Bronzino, *Clinical Engineering*. CRC Press, 2003.
- [14] “Chapter 6 Bioelectric and Biomagnetic Measurements | Biomedical Sensors and Instruments | Taylor & Francis Group,” *Taylor & Francis*. <https://www.taylorfrancis.com/> (accessed Nov. 18, 2019).
- [15] B. Taji, A. D. C. Chan, and S. Shirmohammadi, “Effect of Pressure on Skin-Electrode Impedance in Wearable Biomedical Measurement Devices,” *IEEE Transactions on Instrumentation and Measurement*, vol. 67, no. 8, pp. 1900–1912, Aug. 2018, doi: 10.1109/TIM.2018.2806950.
- [16] C. Assambo, A. Baba, R. Dozio, and M. J. Burke, “Determination of the parameters of the skin-electrode impedance model for ECG measurement,” in *Proceedings of the 6th WSEAS international conference on electronics, hardware, wireless and optical communications*, 2007, pp. 90–95.
- [17] W. Boucsein, “Principles of Electrodermal Phenomena,” in *Electrodermal Activity*, W. Boucsein, Ed. Boston, MA: Springer US, 2012, pp. 1–86.

- [18] H. Tam and J. G. Webster, "Minimizing Electrode Motion Artifact by Skin Abrasion," *IEEE Transactions on Biomedical Engineering*, vol. BME-24, no. 2, pp. 134–139, Mar. 1977, doi: 10.1109/TBME.1977.326117.
- [19] L.-F. Wang, J.-Q. Liu, X.-X. Yan, B. Yang, and C.-S. Yang, "A MEMS-based pyramid micro-needle electrode for long-term EEG measurement," *Microsyst Technol*, vol. 19, no. 2, pp. 269–276, Feb. 2013, doi: 10.1007/s00542-012-1638-2.
- [20] N. A. Alba, R. J. Scwabassi, M. Sun, and X. T. Cui, "Novel Hydrogel-Based Preparation-Free EEG Electrode," *IEEE Transactions on Neural Systems and Rehabilitation Engineering*, vol. 18, no. 4, pp. 415–423, Aug. 2010, doi: 10.1109/TNSRE.2010.2048579.
- [21] A. R. Mota *et al.*, "Development of a quasi-dry electrode for EEG recording," *Sensors and Actuators A: Physical*, vol. 199, pp. 310–317, Sep. 2013, doi: 10.1016/j.sna.2013.06.013.
- [22] H. Hua, W. Tang, X. Xu, D. D. Feng, and L. Shu, "Flexible Multi-Layer Semi-Dry Electrode for Scalp EEG Measurements at Hairy Sites," *Micromachines*, vol. 10, no. 8, p. 518, Aug. 2019, doi: 10.3390/mi10080518.
- [23] X. Xing *et al.*, "Assessing a novel micro-seepage electrode with flexible and elastic tips for wearable EEG acquisition," *Sensors and Actuators A: Physical*, vol. 270, pp. 262–270, Feb. 2018, doi: 10.1016/j.sna.2017.12.048.
- [24] M. A. Lopez-Gordo, D. Sanchez-Morillo, and F. P. Valle, "Dry EEG Electrodes," *Sensors (Basel)*, vol. 14, no. 7, pp. 12847–12870, Jul. 2014, doi: 10.3390/s140712847.
- [25] A. Lopez and P. C. Richardson, "Capacitive Electrocardiographic and Bioelectric Electrodes," *IEEE Transactions on Biomedical Engineering*, vol. BME-16, no. 1, pp. 99–99, Jan. 1969, doi: 10.1109/TBME.1969.4502613.
- [26] Y. M. Chi, S. R. Deiss, and G. Cauwenberghs, "Non-contact Low Power EEG/ECG Electrode for High Density Wearable Biopotential Sensor Networks," in *2009 Sixth International Workshop on Wearable and Implantable Body Sensor Networks*, Berkeley, CA, Jun. 2009, pp. 246–250, doi: 10.1109/BSN.2009.52.
- [27] T. J. Sullivan, S. R. Deiss, and G. Cauwenberghs, "A Low-Noise, Non-Contact EEG/ECG Sensor," in *2007 IEEE Biomedical Circuits and Systems Conference*, Nov. 2007, pp. 154–157, doi: 10.1109/BIOCAS.2007.4463332.
- [28] K. Vlach, J. Kijonka, F. Jurek, P. Vavra, and P. Zonca, "Capacitive biopotential electrode with a ceramic dielectric layer," *Sensors and Actuators B: Chemical*, vol. 245, pp. 988–995, Jun. 2017, doi: 10.1016/j.snb.2017.01.116.
- [29] A. Ueno, Y. Akabane, T. Kato, H. Hoshino, S. Kataoka, and Y. Ishiyama, "Capacitive Sensing of Electrocardiographic Potential Through Cloth From the Dorsal Surface of the Body in a Supine Position: A Preliminary Study," *IEEE Transactions on Biomedical Engineering*, vol. 54, no. 4, pp. 759–766, Apr. 2007, doi: 10.1109/TBME.2006.889201.
- [30] E. Spinelli and M. Haberman, "Insulating electrodes: a review on biopotential front ends for dielectric skin–electrode interfaces," *Physiol. Meas.*, vol. 31, no. 10, pp. S183–S198, Sep. 2010, doi: 10.1088/0967-3334/31/10/S03.
- [31] J.-Y. Baek, J.-H. An, J.-M. Choi, K.-S. Park, and S.-H. Lee, "Flexible polymeric dry electrodes for the long-term monitoring of ECG," *Sensors and Actuators A: Physical*, vol. 143, no. 2, pp. 423–429, May 2008, doi: 10.1016/j.sna.2007.11.019.
- [32] H.-L. Peng, J.-Q. Liu, Y.-Z. Dong, B. Yang, X. Chen, and C.-S. Yang, "Parylene-based flexible dry electrode for biopotential recording," *Sensors and Actuators B: Chemical*, vol. 231, pp. 1–11, Aug. 2016, doi: 10.1016/j.snb.2016.02.061.

- [33] C. T. Lin, L. D. Liao, Y. H. Liu, I. J. Wang, B. S. Lin, and J. Y. Chang, “Novel Dry Polymer Foam Electrodes for Long-Term EEG Measurement,” *IEEE Transactions on Biomedical Engineering*, vol. 58, no. 5, pp. 1200–1207, May 2011, doi: 10.1109/TBME.2010.2102353.
- [34] “g.SAHARASYS,” *g.tec medical engineering*. <https://www.gtec.at/product/gsahasys/> (accessed Feb. 17, 2020).
- [35] R. Matthews *et al.*, “Real time workload classification from an ambulatory wireless EEG system using hybrid EEG electrodes,” in *2008 30th Annual International Conference of the IEEE Engineering in Medicine and Biology Society*, Aug. 2008, pp. 5871–5875, doi: 10.1109/IEMBS.2008.4650550.
- [36] L.-D. Liao, I.-J. Wang, S.-F. Chen, J.-Y. Chang, and C.-T. Lin, “Design, Fabrication and Experimental Validation of a Novel Dry-Contact Sensor for Measuring Electroencephalography Signals without Skin Preparation,” *Sensors*, vol. 11, no. 6, pp. 5819–5834, Jun. 2011, doi: 10.3390/s110605819.
- [37] L. F. Wang, J. Q. Liu, B. Yang, and C. S. Yang, “PDMS-Based Low Cost Flexible Dry Electrode for Long-Term EEG Measurement,” *IEEE Sensors Journal*, vol. 12, no. 9, pp. 2898–2904, Sep. 2012, doi: 10.1109/JSEN.2012.2204339.
- [38] Y.-H. Yu, S.-W. Lu, L.-D. Liao, and C.-T. Lin, “Design, Fabrication, and Experimental Validation of Novel Flexible Silicon-Based Dry Sensors for Electroencephalography Signal Measurements,” *IEEE Journal of Translational Engineering in Health and Medicine*, vol. 2, pp. 1–7, 2014, doi: 10.1109/JTEHM.2014.2367518.
- [39] C. Grozea, C. D. Voinescu, and S. Fazli, “Bristle-sensors—low-cost flexible passive dry EEG electrodes for neurofeedback and BCI applications,” *J. Neural Eng.*, vol. 8, no. 2, p. 025008, 2011, doi: 10.1088/1741-2560/8/2/025008.
- [40] S. Kaushik *et al.*, “Lack of Pain Associated with Microfabricated Microneedles:,” *Anesthesia and Analgesia*, vol. 92, no. 2, pp. 502–504, Feb. 2001, doi: 10.1213/0000539-200102000-00041.
- [41] S. Henry, D. V. McAllister, M. G. Allen, and M. R. Prausnitz, “Microfabricated microneedles: A novel approach to transdermal drug delivery,” *Journal of Pharmaceutical Sciences*, vol. 87, no. 8, pp. 922–925, 1998, doi: 10.1021/js980042+.
- [42] M. R. Prausnitz, “Microneedles for transdermal drug delivery,” *Advanced Drug Delivery Reviews*, vol. 56, no. 5, pp. 581–587, Mar. 2004, doi: 10.1016/j.addr.2003.10.023.
- [43] A. T. Satti, J. Park, J. Park, H. Kim, and S. Cho, “Fabrication of Parylene-Coated Microneedle Array Electrode for Wearable ECG Device,” *Sensors*, vol. 20, no. 18, Art. no. 18, Jan. 2020, doi: 10.3390/s20185183.
- [44] L.-S. Hsu, S.-W. Tung, C.-H. Kuo, and Y.-J. Yang, “Developing Barbed Microtip-Based Electrode Arrays for Biopotential Measurement,” *Sensors*, vol. 14, no. 7, pp. 12370–12386, Jul. 2014, doi: 10.3390/s140712370.
- [45] P. Griss, P. Enoksson, and G. Stemme, “Micromachined barbed spikes for mechanical chip attachment,” *Sensors and Actuators A: Physical*, vol. 95, no. 2, pp. 94–99, Jan. 2002, doi: 10.1016/S0924-4247(01)00719-1.
- [46] C. O’Mahony, F. Pini, A. Blake, C. Webster, J. O’Brien, and K. G. McCarthy, “Microneedle-based electrodes with integrated through-silicon via for biopotential recording,” *Sensors and Actuators A: Physical*, vol. 186, pp. 130–136, Oct. 2012, doi: 10.1016/j.sna.2012.04.037.
- [47] N. S. Dias, J. P. Carmo, A. F. da Silva, P. M. Mendes, and J. H. Correia, “New dry electrodes based on iridium oxide (IrO) for non-invasive biopotential recordings and stimulation,”

- Sensors and Actuators A: Physical*, vol. 164, no. 1, pp. 28–34, Nov. 2010, doi: 10.1016/j.sna.2010.09.016.
- [48] N. Wilke, C. Hibert, J. O'Brien, and A. Morrissey, "Silicon microneedle electrode array with temperature monitoring for electroporation," *Sensors and Actuators A: Physical*, vol. 123–124, pp. 319–325, Sep. 2005, doi: 10.1016/j.sna.2005.05.017.
- [49] P. Griss, H. K. Tolvanen-Laakso, P. Merilainen, and G. Stemme, "Characterization of micromachined spiked biopotential electrodes," *IEEE Transactions on Biomedical Engineering*, vol. 49, no. 6, pp. 597–604, Jun. 2002, doi: 10.1109/TBME.2002.1001974.
- [50] H. Tachikawa, N. Takano, K. Nishiyabu, N. Miki, and Y. Ami, "Effect of Tension and Curvature of Skin on Insertion Characteristics of Microneedle Array," *Journal of Solid Mechanics and Materials Engineering*, vol. 4, no. 3, pp. 470–480, 2010, doi: 10.1299/jmmp.4.470.
- [51] P. Salvo, R. Raedt, E. Carrette, D. Schaubroeck, J. Vanfleteren, and L. Cardon, "A 3D printed dry electrode for ECG/EEG recording," *Sensors and Actuators A: Physical*, vol. 174, pp. 96–102, Feb. 2012, doi: 10.1016/j.sna.2011.12.017.
- [52] H.-L. Peng *et al.*, "Flexible dry electrode based on carbon nanotube/polymer hybrid micropillars for biopotential recording," *Sensors and Actuators A: Physical*, vol. 235, pp. 48–56, Nov. 2015, doi: 10.1016/j.sna.2015.09.024.
- [53] K. Chen, L. Ren, Z. Chen, C. Pan, W. Zhou, and L. Jiang, "Fabrication of Micro-Needle Electrodes for Bio-Signal Recording by a Magnetization-Induced Self-Assembly Method," *Sensors*, vol. 16, no. 9, p. 1533, Sep. 2016, doi: 10.3390/s16091533.
- [54] W. Zhou, W. Ling, W. Liu, Y. Peng, and J. Peng, "Laser direct micromilling of copper-based bioelectrode with surface microstructure array," *Optics and Lasers in Engineering*, vol. 73, pp. 7–15, Oct. 2015, doi: 10.1016/j.optlaseng.2015.03.011.
- [55] Y. Nishinaka, R. Jun, G. S. Prihandana, and N. Miki, "Fabrication of Polymer Microneedle Electrodes Coated with Nanoporous Parylene," *Japanese Journal of Applied Physics*, vol. 52, no. 6S, p. 06GL10, Jun. 2013, doi: 10.7567/JJAP.52.06GL10.
- [56] M. Arai, Y. Nishinaka, and N. Miki, "Electroencephalogram measurement using polymer-based dry microneedle electrode," *Jpn. J. Appl. Phys.*, vol. 54, no. 6S1, p. 06FP14, May 2015, doi: 10.7567/JJAP.54.06FP14.
- [57] R. Wang, W. Zhao, W. Wang, and Z. Li, "A Flexible Microneedle Electrode Array With Solid Silicon Needles," *Journal of Microelectromechanical Systems*, vol. 21, no. 5, pp. 1084–1089, Oct. 2012, doi: 10.1109/JMEMS.2012.2203790.
- [58] R. Wang, X. Jiang, W. Wang, and Z. Li, "A microneedle electrode array on flexible substrate for long-term EEG monitoring," *Sensors and Actuators B: Chemical*, vol. 244, pp. 750–758, Jun. 2017, doi: 10.1016/j.snb.2017.01.052.
- [59] D.-H. Kim *et al.*, "Epidermal Electronics," *Science*, vol. 333, no. 6044, pp. 838–843, Aug. 2011, doi: 10.1126/science.1206157.
- [60] L. Ren *et al.*, "Fabrication of Flexible Microneedle Array Electrodes for Wearable Bio-Signal Recording," *Sensors (Basel)*, vol. 18, no. 4, Apr. 2018, doi: 10.3390/s18041191.
- [61] M. Arai, Y. Kudo, and N. Miki, "Electroencephalogram measurement from the hairy part of the scalp using polymer-based dry microneedle electrodes," in *2015 37th Annual International Conference of the IEEE Engineering in Medicine and Biology Society (EMBC)*, Aug. 2015, pp. 3165–3168, doi: 10.1109/EMBC.2015.7319064.

- [62] W. C. Ng *et al.*, “Micro-spike EEG electrode and the vacuum-casting technology for mass production,” *Journal of Materials Processing Technology*, vol. 209, no. 9, pp. 4434–4438, May 2009, doi: 10.1016/j.jmatprotec.2008.10.051.
- [63] S. Indermun *et al.*, “Current advances in the fabrication of microneedles for transdermal delivery,” *Journal of Controlled Release*, vol. 185, pp. 130–138, Jul. 2014, doi: 10.1016/j.jconrel.2014.04.052.
- [64] P. Griss, P. Enoksson, H. K. Tolvanen-Laakso, P. Merilainen, S. Ollmar, and G. Stemme, “Micromachined electrodes for biopotential measurements,” *Journal of Microelectromechanical Systems*, vol. 10, no. 1, pp. 10–16, Mar. 2001, doi: 10.1109/84.911086.
- [65] K. Kim *et al.*, “A tapered hollow metallic microneedle array using backside exposure of SU-8,” *J. Micromech. Microeng.*, vol. 14, no. 4, p. 597, 2004, doi: 10.1088/0960-1317/14/4/021.
- [66] W. Demtröder, “Interference, Diffraction and Scattering,” in *Electrodynamics and Optics*, W. Demtröder, Ed. Cham: Springer International Publishing, 2019, pp. 285–330.
- [67] W.-C. Yang, Y.-S. Huang, B.-Y. Shew, and C.-C. Fu, “Study on diffraction effect and microstructure profile fabricated by one-step backside lithography,” *J. Micromech. Microeng.*, vol. 23, no. 3, p. 035004, 2013, doi: 10.1088/0960-1317/23/3/035004.
- [68] S. P. Davis, B. J. Landis, Z. H. Adams, M. G. Allen, and M. R. Prausnitz, “Insertion of microneedles into skin: measurement and prediction of insertion force and needle fracture force,” *Journal of Biomechanics*, vol. 37, no. 8, pp. 1155–1163, Aug. 2004, doi: 10.1016/j.jbiomech.2003.12.010.
- [69] J.-H. Park, M. G. Allen, and M. R. Prausnitz, “Biodegradable polymer microneedles: Fabrication, mechanics and transdermal drug delivery,” *Journal of Controlled Release*, vol. 104, no. 1, pp. 51–66, May 2005, doi: 10.1016/j.jconrel.2005.02.002.
- [70] H. Brorson, C.-O. Werner, and K.-G. Thorngren, “Normal pinch strength,” *Acta Orthopaedica Scandinavica*, vol. 60, no. 1, pp. 66–68, Jan. 1989, doi: 10.3109/17453678909150096.
- [71] D. C. Duffy, J. C. McDonald, O. J. A. Schueller, and G. M. Whitesides, “Rapid Prototyping of Microfluidic Systems in Poly(dimethylsiloxane),” *Anal. Chem.*, vol. 70, no. 23, pp. 4974–4984, Dec. 1998, doi: 10.1021/ac980656z.
- [72] J. C. McDonald *et al.*, “Fabrication of microfluidic systems in poly(dimethylsiloxane),” *ELECTROPHORESIS*, vol. 21, no. 1, pp. 27–40, 2000, doi: 10.1002/(SICI)1522-2683(20000101)21:1<27::AID-ELPS27>3.0.CO;2-C.
- [73] D. Qin, Y. Xia, and G. M. Whitesides, “Soft lithography for micro- and nanoscale patterning,” *Nature Protocols; London*, vol. 5, no. 3, pp. 491–502, 2010, doi: <http://dx.doi.org/10.1038/nprot.2009.234>.
- [74] B. Mustin and B. Stoeber, “Low cost integration of 3D-electrode structures into microfluidic devices by replica molding,” *Lab Chip*, vol. 12, no. 22, pp. 4702–4708, Oct. 2012, doi: 10.1039/C2LC40728K.
- [75] M. J. Madou, “Physical and Chemical Vapor Deposition—Thin Film Properties and Surface Micromachining,” *Manufacturing Techniques for Microfabrication and Nanotechnology*, Jun. 13, 2011. <http://www.taylorfrancis.com/> (accessed Nov. 17, 2020).
- [76] I. Mansoor, Y. Liu, U. O. Häfeli, and B. Stoeber, “Fabrication of hollow microneedle arrays using electrodeposition of metal onto solvent cast conductive polymer structures,” in *2013 Transducers Eurosensors XXVII: The 17th International Conference on Solid-State Sensors*,

- Actuators and Microsystems (TRANSDUCERS EUROSENSORS XXVII)*, Jun. 2013, pp. 373–376, doi: 10.1109/Transducers.2013.6626780.
- [77] M. Arai, Y. Kudo, and N. Miki, “Polymer-based candle-shaped microneedle electrodes for electroencephalography on hairy skin,” *Jpn. J. Appl. Phys.*, vol. 55, no. 6S1, p. 06GP16, Jun. 2016, doi: 10.7567/JJAP.55.06GP16.
- [78] S. P. Davis, M. R. Prausnitz, and M. G. Allen, “Fabrication and characterization of laser micromachined hollow microneedles,” in *TRANSDUCERS '03. 12th International Conference on Solid-State Sensors, Actuators and Microsystems. Digest of Technical Papers (Cat. No.03TH8664)*, Jun. 2003, vol. 2, pp. 1435–1438 vol.2, doi: 10.1109/SENSOR.2003.1217045.
- [79] J. M. Margolis, *Conductive polymers and plastics*. 2011.
- [80] M. Rahaman, D. Khastgir, and A. K. Aldalbah, Eds., *Carbon-Containing Polymer Composites*. Singapore: Springer Singapore, 2019.
- [81] R. Rothon, *Fillers for polymer applications*. New York, NY: Springer Berlin Heidelberg, 2017.
- [82] N. K. Lamba, *Polyurethanes in Biomedical Applications*. Routledge, 2017.
- [83] EPOXIES, “20-3401MEDICAL, OPTICAL AND SEMICONDUCTOR GRADE EPOXY RESIN TECHNICAL BULLETIN.” Accessed: Oct. 21, 2020. [Online]. Available: [https://www.epoxies.com/\\_resources/common/userfiles/file/20-3401.pdf](https://www.epoxies.com/_resources/common/userfiles/file/20-3401.pdf)[https://www.epoxies.com/\\_resources/common/userfiles/file/20-3401.pdf](https://www.epoxies.com/_resources/common/userfiles/file/20-3401.pdf)
- [84] S. P. Timoshenko and J. M. Gere, “Theory of Elastic Stability (2nd Edition),” [Online]. Available: <https://app.knovel.com/hotlink/toc/id:kpTESE0003/theory-elastic-stability/theory-elastic-stability>.
- [85] F. J. Verbaan *et al.*, “Improved piercing of microneedle arrays in dermatomed human skin by an impact insertion method,” *Journal of Controlled Release*, vol. 128, no. 1, pp. 80–88, May 2008, doi: 10.1016/j.jconrel.2008.02.009.
- [86] K. van der Maaden, E. Sekerdag, W. Jiskoot, and J. Bouwstra, “Impact-Insertion Applicator Improves Reliability of Skin Penetration by Solid Microneedle Arrays,” *AAPS J*, vol. 16, no. 4, pp. 681–684, Jul. 2014, doi: 10.1208/s12248-014-9606-7.
- [87] P. Shrestha and B. Stoeber, “Imaging fluid injections into soft biological tissue to extract permeability model parameters,” *Physics of Fluids*, vol. 32, no. 1, p. 011905, Jan. 2020, doi: 10.1063/1.5131488.
- [88] M. R. Ven Murthy and L. Carrier-Malhotra, “Progressive Unfolding of the Conformational States of Transfer RNA and Ribosomal 5S RNA by Methylene Blue Binding,” in *Protein-Dye Interactions: Developments and Applications*, M. A. Vijayalakshmi and O. Bertrand, Eds. Dordrecht: Springer Netherlands, 1989, pp. 316–330.
- [89] E. Touitou, B. W. Barry, and B. W. Barry, “Stratum Corneum Bypassed or Removed,” *Enhancement in Drug Delivery*, Nov. 27, 2006. <http://www.taylorfrancis.com/> (accessed Oct. 21, 2020).
- [90] S. R. Sinha *et al.*, “American Clinical Neurophysiology Society Guideline 1: Minimum Technical Requirements for Performing Clinical Electroencephalography,” *The Neurodiagnostic Journal*, vol. 56, no. 4, pp. 235–244, Oct. 2016, doi: 10.1080/21646821.2016.1245527.
- [91] L. A. (Leslie A. Geddes, 1921-, and L. E. Baker, *Principles of applied biomedical instrumentation*. Wiley, 1975.